Climate Change 2013: The Physical Science Basis

Technical Summary

Coordinating Lead Authors: Thomas Stocker (Switzerland), Qin Dahe (China), Gian-Kasper Plattner (Switzerland)

Lead Authors: Lisa Alexander (Australia), Simon Allen (Switzerland), Nathaniel Bindoff (Australia), Francois-Marie Breon (France), John Church (Australia), Ulrich Cubasch (Germany), Seita Emori (Japan), Piers Forster (United Kingdom), Pierre Friedlingstein (United Kingdom), Nathan Gillett (Canada), Jonathan Gregory (United Kingdom), Dennis Hartmann (USA), Eystein Jansen (Norway), Ben Kirtman (USA), Reto Knutti (Switzerland), Krishna Kumar Kanikicharla (India), Peter Lemke (Germany), Jochem Marotzke (Germany), Valerie Masson-Delmotte (France), Gerald Meehl (USA), Igor Mokhov (Russia), Shilong Piao (China), Venkatachalam Ramaswamy (USA), David Randall (USA), Monika Rhein (Germany), Maisa Rojas (Chile), Christopher Sabine (USA), Drew Shindell (USA), Lynne Talley (USA), David Vaughan (United Kingdom), Shang-Ping Xie (USA)

Contributing Authors (list to be updated): Olivier Boucher (France), Philippe Ciais (France), Peter Clark (USA), Matthew Collins (United Kingdom), Joey Comiso (USA), Gregory Flato (Canada), Jens Hesselbjerg Christensen (Denmark), Albert Klein Tank (Netherlands), Gunnar Myhre (Norway), Scott Power (Australia), Stephen Rintoul (Germany), Matilde Rusticucci (Argentina), Michael Schulz (Germany), Peter Stott (United Kingdom), Donald Wuebbles (USA)

Review Editors: Sylvie Joussaume (France), Joyce Penner (USA), Fredolin Tangang (Malaysia)

Date of Draft: 5 October 2012

Notes: TSU Compiled Version

Table of Contents

TS.1 Introduction

"*Climate Change 2013: The Physical Science Basis*" is the contribution of Working Group I to the Fifth Assessment Report of the Intergovernmental Panel on Climate Change. This comprehensive assessment of the physical aspects of climate change puts a focus on those elements that are relevant to understand past, document current, and project future climate change. The assessment builds on the IPCC Fourth Assessment Report (AR4)[1] and the recent Special Report on Managing the Risk of Extreme Events and Disasters to Advance Climate Change Adaptation (SREX)[2] and is presented in 14 chapters. The chapters cover direct and proxy observations of changes in all components of the climate system, they assess the current knowledge of various processes within, and interactions among, climate system components, which determine the sensitivity and response of the system to changes in forcing, and they quantify the link between the changes in atmospheric constituents, and hence radiative forcing[3], and the consequent detection and attribution of climate change. Projections of changes in all climate system components are based on model simulations forced by a new set of scenarios. The report also provides a comprehensive assessment of past and future sea level change in a dedicated chapter. Regional climate change information is presented in the form of an Atlas of Global and Regional Climate Projections.

The primary purpose of this Technical Summary is to provide the link between the complete assessment of the multiple lines of independent evidence presented in the 14 chapters of the main report and the highly condensed summary prepared as the WGI Summary for Policymakers. The Technical Summary thus serves as a starting point for those readers who seek the full information on more specific topics covered by this assessment. This is facilitated by including pointers to the chapters and sections where the full assessment can be found. Policy-relevant topics, which cut across many chapters and involve many interlinked processes in the climate system, are presented here as Thematic Focus Elements, allowing rapid access of this information.

An integral element of this report is the use of uncertainty language which permits a traceable account of the assessment. The degree of certainty in key findings in this assessment is expressed as a level of confidence which results from the type, amount, quality, and consistency of evidence and the degree of agreement in the scientific studies considered[4]. Confidence is expressed qualitatively. Quantified measures of uncertainty in a finding are expressed probabilistically and are based on a combination of statistical analyses of observations or model results, or both, and expert judgment.

The Technical Summary is structured into four main sections presenting the assessment results following the storyline of the WGI contribution to AR5: Section TS.2 covers the assessment of observations of changes in the climate system; Section TS.3 summarizes the information on the different drivers, natural and anthropogenic, expressed in terms of radiative forcing; Section TS.4 presents the assessment of the quantitative understanding of observed climate change; and Section TS.5 summarizes the assessment results for projections of future climate change over the 21st century and beyond from regional to global scale. Section TS.6 combines and lists remaining key uncertainties in the WGI assessment from Sections TS.2–TS.5. The overall nine Thematic Focus Elements (TFEs) are dispersed throughout the four main TS sections, are visually distinct from the main text, and should allow stand-alone reading.

---

[1] IPCC, 2007: *Climate Change 2007: The Physical Science Basis*. Contribution of Working Group I to the Fourth Assessment Report of the Intergovernmental Panel on Climate Change [Solomon, S., D. Qin, M. Manning, Z. Chen, M. Marquis, K.B. Averyt, M. Tignor and H.L. Miller (eds.)]. Cambridge University Press, Cambridge, United Kingdom and New York, NY, USA, 996 pp.

[2] IPCC, 2012: *Managing the Risks of Extreme Events and Disasters to Advance Climate Change Adaptation*. A Special Report of Working Groups I and II of the Intergovernmental Panel on Climate Change [Field, C.B., V. Barros, T.F. Stocker, D. Qin, D.J. Dokken, K.L. Ebi, M.D. Mastrandrea, K.J. Mach, G.-K. Plattner, S.K. Allen, M. Tignor, and P.M. Midgley (eds.)]. Cambridge University Press, Cambridge, UK, and New York, NY, USA, 582 pp.

[3] Radiative Forcing is defined as the change in net irradiance at the tropopause since 1750 after allowing for stratospheric temperatures to readjust to radiative equilibrium, while holding surface and tropospheric temperatures and state variables fixed at the unperturbed values. Positive forcing tends to warm the surface while negative forcing tends to cool it. In this report, radiative forcing values are expressed in watts per square metre (W m^{-2}). (see Glossary)

[4] Mastrandrea, M.D., C.B. Field, T.F. Stocker, O. Edenhofer, K.L. Ebi, D.J. Frame, H. Held, E. Kriegler, K.J. Mach, P.R. Matschoss, G.-K. Plattner, G.W. Yohe, and F.W. Zwiers, 2010: *Guidance Note for Lead Authors of the IPCC Fifth Assessment Report on Consistent Treatment of Uncertainties*. Intergovernmental Panel on Climate Change (IPCC).

TS.2 Observation of Changes in the Climate System

TS.2.1 Introduction

The assessment of observational evidence for climate change is summarized in this section. Substantial advancements in the availability, acquisition, quality and analysis of observational data sets in atmosphere, land surface, ocean, and cryosphere have occurred since the AR4. Many aspects of the climate system are showing evidence of a changing climate.

TS.2.2 Changes in Temperature

TS.2.2.1 Surface Temperatures

Globally averaged near surface temperatures have increased since the beginning of the 20th century. This warming is *virtually certain* and has been particularly marked since the 1970s. Several independently analyzed data records of global and regional land surface air temperature obtained from station observations support this conclusion. It is *virtually certain* that the global average sea surface temperatures have increased since the beginning of the 20th century. Intercomparisons of new data records obtained by different measurement methods, including satellite data, have resulted in better understanding of errors and biases in the records. (Figure TS.1) {2.4}

[INSERT FIGURE TS.1 HERE]

Figure TS.1: Multiple complementary indicators of a changing global climate. Each line represents an independently-derived estimate of change in the climate element. All publicly-available, documented, datasets known to the authors have been used in this latest version. In each panel all datasets have been normalized to a common period of record. A full detailing of which source datasets go into which panel is given in the Appendix to Chapter 2. {FAQ 2.1, Figure 1}

The global combined land and ocean temperature data show an increase of about 0.8°C over the period 1901–2010 and about 0.5°C over the period 1979–2010. The warming from 1886–1905 (early-industrial) to 1986–2005 (reference period for the modeling chapters and the Atlas in Annex 1) is 0.66°C ± 0.06°C (5–95% confidence interval). {2.4.3}

It is *likely* that effects of urban heat-islands and land use change have not raised the centennial global land surface air temperature trends by more than 10% of the observed trend. This is an average value; in some regions that have rapidly developed urban heat island and land use change impacts on regional trends have been substantially larger {2.4.3}.

This 20th century warming has reversed the long-term cooling trends attributed to orbital forcing prevailing in mid-to high latitudes of the Northern Hemisphere throughout the last 2000 years (*high confidence*) {5.5.1}. It is *very likely* that in the Northern Hemisphere, the 1981–2010 CE period was the warmest of the last 800 years, and there is *medium confidence* that is was the warmest in the last 1300 years {5.3.5}. In contrast to the late 20th century there is *high confidence* that the Medieval Climate Anomaly was not characterized by a pattern of higher temperatures that were consistent across seasons and regions. Internal variability as well as solar and volcanic forcing may have significantly influenced the patterns of temperature difference between the Medieval Climate Anomaly and the Little Ice Age (see Glossary). {5.3.5, 5.5.1}

TS.2.2.2 Troposphere and Stratosphere

Based upon multiple independent analyses of measurements from radiosondes and satellite sensors it is *virtually certain* that globally the troposphere has warmed since the mid 20th century. There is at most *medium confidence* in the rate of change and its vertical structure. While it is *virtually certain* that globally the lower stratosphere has cooled since the mid 20th century and the whole stratosphere since 1979, there is only *low confidence* in the cooling rate and vertical structure. {2.4.4}

TS.2.2.3 Ocean

It is *virtually certain* that the upper ocean has warmed since 1971, when observations covering most of the global upper ocean became available (Figure TS.1). Confidence in this assessment is *high* based on the high level of agreement between independent observations of subsurface temperature {3.2}, sea surface temperature {2.2.2}, and sea level rise, which is known to include a substantial component due to thermal expansion {3.7, 13}. Largest warming is found near the sea surface (>0.1°C per decade in the upper 75 m), decreasing to about 0.015°C per decade by 700 m, for the time period 1971 to 2010. The surface intensification of the warming signal increased the thermal stratification of the upper ocean by about 4% (between 0 and 200 m depth) over that time period. Instrumental biases in historical upper ocean temperature measurements have been identified and mitigated, reducing a spurious decadal variation in temperature and upper ocean heat content present in analyses included in AR4 {3.2.2, Figure 3.1, FAQ3.1}

It is *likely* that the deep ocean has warmed below 3000-m depth since the 1990s. The global ocean has warmed at a rate of <0.01°C per decade below 4000 m over this time interval. It is *very likely* that the Southern Ocean has warmed throughout the full ocean depth since the 1990s, at a rate of about 0.03°C per decade. Warming of the global ocean below 4000 m and the Southern Ocean below 1000 m combined amount to a heating rate of 48 [21 to 75] TW between 1992 and 2005. Sparse sampling of the deep ocean means that there is less confidence in estimates of heat content change there than in the upper ocean. {3.2.4, Figure 3.3}

TS.2.3 Changes in Energy Budget and Heat Content

Earth has been in radiative imbalance, with more energy from the sun entering than exiting the top of the atmosphere, since at least circa 1970. It is *virtually certain* that Earth has gained substantial energy from 1971–2010—an estimated first-difference change of 273 [194 to 353] ZJ (1 ZJ = 10^{21} J), with a rate of 213 TW from a linear fit over that time period {Box 3.1, Figure 1}. From 1993–2010 the estimated energy gain from a first difference is 163 [125 to 200] ZJ with a linear rate estimate of 27 TW. Ocean warming dominates the total energy change inventory, accounting for roughly 90% on average from 1971–2010. Melting ice—including Arctic sea ice, ice sheets, and glaciers and warming of the continents and atmosphere—account for the remainder. The ocean component of the 1993–2010 rate of energy gain is 257 TW, equivalent to a global mean net air-sea heat flux of 0.71 W m^{-2}, and that for 1971–2010 is 199 TW, implying a mean net air-sea heat flux of 0.55 W m^{-2} {Box 3.1}. Uncertainties in currently available surface flux products are too large to allow detection of the very small change in global mean net heat flux expected from observed ocean heat content changes {3.4}.

TS.2.4 Changes in Circulation and Modes of Variability

Large variability on interannual to decadal time scales and remaining differences between data sets hamper robust conclusions on long-term changes in large-scale atmospheric circulation. *Confidence is high* that several trends found from the 1950s or earlier to the 1990s reported in AR4 (e.g., an increase in the mid-latitude westerly winds and the North Atlantic Oscillation (NAO) index or a weakening of the Pacific Walker circulation) have been largely offset by more recent changes. {2.7} There is *medium confidence* that wind stress over the Southern Ocean has increased since the early 1980s, based on agreement between atmospheric reanalyses, satellite observations and island station data. {3.4} It is *likely* that, in a zonal mean sense, circulation features have moved poleward (widening of the tropical belt, poleward shift of storm tracks and jet streams, contraction of the polar vortex) since the 1970s. {2.7}

It is very likely, that the subtropical gyres in the North Pacific and South Pacific have expanded and strengthened since 1993. It is about as likely as not that this reflects a decadal oscillation linked to changes in wind forcing, including changes in winds associated with the modes of climate variability as the El Niño-Southern Oscillation (ENSO), NAO, and the Southern Annular Mode (SAM). {3.6} As found in AR4, there is no evidence for a long-term trend in the Atlantic Meridional Overturning Circulation (AMOC). There is also no evidence for trends in the transports of the Indonesian Throughflow, the Antarctic circumpolar Current or the exchange between the Atlantic and the Nordic Seas. {3.6, Figures 3.10, 3.11}

Observed changes in water mass properties likely reflect the combined effect of long-term trends (e.g., warming of the surface ocean and changes in the hydrological cycles) and variability associated to climate modes. Strong variability in the temperature and salinity of the source water masses of North Atlantic Deep

Water is observed, but there is no evidence of long-term trends in formation rates and transports. The observed weakening in the formation rate of Labrador Sea Water from 1997 to 2005 is likely associated with the NAO. A freshening trend in the dense overflow waters, highlighted in AR4, reversed in the mid 1990s. Warming and lower oxygen observed in the North Pacific Intermediate Water since the 1950s likely reflects a reduction in ventilation. {3.5, Figure 3.9}

TS.2.5 Changes in the Water Cycle and Cryosphere

TS.2.5.1 Atmosphere and Surface Fluxes

Confidence in global precipitation change over land *is low* prior to 1950 and *medium* afterwards because of incomplete data coverage. When virtually all the land area is filled in using a reconstruction method, the resulting time series shows little change in land-based precipitation since 1900. This is different from AR4, which reported that global precipitation averaged over land areas has increased, with most of the increase occurring in the early to mid 20th century. {2.5.1}

The mid-latitudes and higher latitudes of the Northern Hemisphere do show an overall increase in precipitation from 1900–2010, however *confidence is low* because of much uncertainty in the data records for the early 20th century. Insufficient evidence exists to define a long-term temporal change of precipitation averaged across the mid-latitudes of the Southern Hemisphere. Precipitation in the tropics has *likely* increased over the last decade, reversing the drying trend that occurred from the mid-1970s to mid-1990s reported in AR4.

As reported in AR4, there is *very high confidence* that absolute moistening of the atmosphere near the surface has been widespread across the globe since the 1970s. However, during recent years this has abated over land, coincident with greater warming over land relative to the oceans {2.5.5}. As a result, fairly widespread decreases in relative humidity near the surface have been observed over the land areas recently. Radiosonde, GPS and satellite observations indicate increases in tropospheric water vapour at continental scales, which are consistent with the observed increase in atmospheric temperature aloft. It is *very likely* that tropospheric specific humidity has increased since the 1970s. Because tropospheric temperatures have also increased, significant trends in tropospheric relative humidity have not been observed {2.5.6}.

While trends of cloud cover are consistent between independent data sets in certain regions, substantial ambiguity and therefore low confidence remains in the observations of global-scale cloud variability and trends. {2.5.7}

TS.2.5.2 Ocean

Sea surface salinities are governed by evaporation and precipitation. It is *very likely* that the mean regional pattern of sea surface salinity has been enhanced since the 1960s: saline surface waters in the evaporation-dominated mid-latitudes have become more saline, while the relatively fresh surface waters in rainfall-dominated tropical and polar regions have become fresher. Similarly, it is *very likely* that the interbasin contrast between saline Atlantic and fresh Pacific surface waters has increased {3.3}. These patterns are *very likely* caused by an intensification of the water cycle as the lower atmosphere has warmed, reflecting the expected and observed increased water vapour content of the warmer air {2.5}. A similar conclusion was reached in AR4. The more recent studies, based on expanded data sets and new analysis approaches, have substantially increased the level of confidence in the inferred change in the global water cycle {3.3.2, Figure 3.4, FAQ 3.3}. Uncertainties in currently available surface flux products cannot yet be reliably used to identify trends in the regional or global distribution of evaporation or precipitation over the oceans on the timescale of the observed salinity changes since the 1960s {3.4}.

TS.2.5.3 Runoff

The most recent and most comprehensive analyses of river runoff which include newly assembled observational records do not support the AR4 conclusion that global runoff increased during the 20th century. Average runoff has not changed in the majority of rivers, but year-to-year variability has increased. {2.5.2}

TS.2.5.4 Sea Ice

The strong and significant decrease in Arctic sea ice extent (ocean area where ice concentrations are at least 15%, and total Arctic sea ice area reported in AR4 has continued (Figure TS.1), and has been accompanied by many other changes in the characteristics of the Arctic sea ice cover (robust evidence, high agreement). The overall trend in sea ice extent over the period 1979–2011 has been –3.9% per decade with larger changes occurring in summer and autumn. The largest changes are the decline in the coverage of perennial ice (the summer minimum extent; –12.2% per decade) and of ice more than 2 years old (–15.6 % per decade). There is robust evidence for a decline in perennial and multiyear sea ice coverage and decreases in ice thickness, and in ice volume. The overall mean winter thickness decreased by 48% to only 1.89 m between 1980 and 2009. With decreases in both concentration and thickness, sea ice has less resistance to wind forcing, and the rate of drift has also increased. Other significant changes to the Arctic Ocean sea ice include lengthening in the duration of the period of surface melt on perennial sea ice of 6 days per decade over the period 1979–2010, and a nearly two month lengthening of the ice-free season in the region from the East Siberian Sea to the western Beaufort Sea over the period 1979–2011. {4.2.4, FAQ 4.2}

In Antarctica, there was a small but significant increase in total sea ice extent of 1.4% per decade between 1979 and 2011, and a greater increase in sea ice area, due to an increase in concentration. Robust evidence shows strong regional differences within this total, with some regions increasing in extent/area and some decreasing. There are also contrasting regions around the Antarctic where, over the period of satellite observations, the ice-free season has lengthened, and others where it has shortened. Decadal trends in ice drift show acceleration of the Ross Sea Gyre and deceleration of the Weddell Gyre. Available data are inadequate to assess the status of change of many other characteristics of Antarctic sea ice (e.g., thickness and volume). {4.2.3, FAQ 4.2}

TS.2.5.5 Glaciers and Ice Sheets

The time series of measured changes in glacier length and area, as well as estimates of volume and mass change give robust evidence in high agreement that globally, glaciers continue to shrink and lose mass (Figure TS.1). There are, however, notable regional exceptions to these trends in all three characteristics (length, area, mass changes) resulting from regionally-specific climatic conditions (e.g., increased precipitation), or from glacier-specific characteristics unrelated to climate (e.g., surge-type, calving, or debris-covered). The number of regional-scale estimates of glacier change have grown with newly available data sets (e.g., from satellite remote sensing) and methods (e.g., gravimetry) becoming available, but results still show some spread due to methodological limitations and uncertainties. {4.3.3}

Between 2003–2009 or 2005–2009, respectively, global glacier ice loss was estimated with various methods to be within 251± 65 Gt yr^{-1} to 371 ± 50 Gt yr^{-1} (or 210 ± 65 Gt yr^{-1} to 262 ± 67 Gt yr^{-1} if glaciers around the periphery of the ice sheets are excluded). There is thus robust evidence and high agreement that, globally, mass loss from glaciers is ongoing, but there is less agreement about the actual rate. Glacier area changes averaged over entire mountain ranges varied between 0 and –1% yr^{-1} from the 1960s to 2000, and are regionally higher (–1 to –2% yr^{-1}) for the past two decades. Several hundred glaciers globally have completely disappeared in the past 30 years (robust evidence, high agreement). Estimates from different methods that yield long time series, indicate steady increases in ice loss from glaciers since about 1985 with a slight decline in the most recent years. Two estimates indicate that in the 1920s to 1940s, ice loss from glaciers in the Arctic, mainly from the Greenland peripheral glaciers was higher than today (medium evidence, medium agreement). {4.3.4, Table 4.5}

There is robust evidence in high agreement that the Greenland Ice Sheet has lost mass since the early 1990s, and that the rate of loss has increased. The average ice loss from Greenland was 123 ± 22 Gt yr^{-1} over the period 1993–2010, and 228 ± 54 Gt yr^{-1} in the period 2005–2010. Melt has increased with warming temperature and discharge has increased with increased glacier speed, particularly in southeast, central west and northwest Greenland. {4.4.2, Figure 4.15}

The Antarctic Ice Sheet is also *very likely* currently losing mass (robust evidence, high agreement). The average ice loss from Antarctica was 65 ± 33 Gt yr^{-1} over the period 1993–2010, and 112 ± 58 Gt yr^{-1} over

the period 2005–2010. The largest ice losses from Antarctica have occurred on the northern Antarctic Peninsula and from the Amundsen Sea sector of West Antarctica. In the last two decades, East Antarctica is *likely* to have experienced a small gain in mass. As in AR4, reconstructions of snowfall, now covering the period 1979–2011, do not suggest any change in total snowfall in Antarctica. {4.4.2, Figure 4.16}

Ice shelves in the Antarctic Peninsula are *very likely* continuing a long-term trend of retreat and partial collapse that began decades ago, and is *very likely* due to climate warming. Similarly, a progressive weakening of the floating parts of glaciers is *likely* taking place in Greenland. In the Antarctic, many floating ice shelves are *virtually certain* to be thinning in areas of rapid glacier changes due to enhanced oceanic thermal forcing. Many ice shelves in East Antarctica, especially the large ice shelves in the Ross and Weddell seas, however, are *likely* stable at present. {4.4.2}

TS.2.5.6 Snow Cover and Permafrost

Both satellite and in-situ observations show significant reductions in the Northern Hemisphere snow cover extent (SCE) over the past 90 years, with most reduction occurring in the 1980s. Snow cover decreased most in spring when the average extent decreased by around 8% (7 million km^2) over the period 1970–2010 compared with the period 1922–1970. Because of earlier spring snowmelt, the duration of the Northern Hemisphere snow season has declined by 5.3 days per decade since the 1972/1973 winter. Since AR4, the rate of reductions in June SCE—both absolute and relative—has surpassed the rate of reduction of March-April SCE. These trends in spring SCE are *very likely* linked to rising temperature. In addition to reductions in SCE, there is some evidence that the reflectivity (albedo) of the snow itself may also be changing in response to human activities. In the Southern Hemisphere, very few long records exist; satellite records of snow water equivalent date from 1979, but show no trends. {4.5.2, 4.5.4, Figure 4.19, 4.20}

There is robust evidence with high agreement that permafrost temperatures have increased by up to 3°C during the past three decades over major permafrost regions of the Northern Hemisphere in response to increased air temperature and changing snow cover. However, in some regions, permafrost temperatures show little change, or even slight decreases. Generally, the temperature increase for colder permafrost has been greater than for warmer permafrost. Significant permafrost degradation has occurred in the Russian European North (robust evidence, high agreement), where taliks (layers of year-round unfrozen ground) have developed in the discontinuous permafrost zone; permafrost with thickness of 10 to 15 m completely thawed in some regions over the period 1975–2005; the southern limit of the Northern Hemisphere permafrost boundary moved north by about 80 km; and the boundary of the continuous permafrost moved north by 15–50 km. {4.6.2}

The thickness of the active layer (that portion of the soil above permafrost that thaws in summer and re-freezes in winter) has increased by up to 90 cm since the 1980s, although this change varies from a few centimeters to tens of centimeters. In some areas, especially in northern North America, the active layer thickness shows large inter-annual variations and no significant trend. {4.6.4}

TFE.1: Water Cycle Change

The water cycle describes the continuous movement of water through the climate system in its liquid, solid and vapour forms, and storage in the reservoirs of ocean, cryosphere, land surface and atmosphere {FAQ 12.2, Figure 1}. In the atmosphere, water occurs primarily as a gas, water vapour, but it also occurs as ice and liquid water in clouds. The ocean is primarily liquid water, but the ocean is partly covered by ice in Polar Regions. Terrestrial water in liquid form appears as surface water (lakes, rivers), soil moisture and groundwater. Solid terrestrial water occurs in ice sheets, glaciers, snow and ice on the surface and permafrost. The movement of water in the climate system is essential to life on land, since much of the water that falls on land as precipitation and supplies the soil moisture and river flow has been evaporated from the ocean and transported to land by the atmosphere. Water that falls as snow in winter can provide soil moisture in springtime and river flow in summer and is essential to both natural and human systems. The movement of fresh water between the atmosphere and the ocean can also influence oceanic salinity, which is an important driver of the density and circulation of the ocean. The latent heat contained in water vapour in the

atmosphere is critical to driving the circulation of the atmosphere on scales ranging from individual thunderstorms to the global circulation of the atmosphere. {12.4.5, FAQ3.3}

Observations of Water Cycle Change

Because the saturation vapour pressure of air increases with temperature, it is expected that the amount of water vapour suspended in air will increase with a warming climate. Observations from surface stations, radiosondes, GPS, and satellite measurements indicate increases in tropospheric water vapour at large spatial scales. It is *very likely* that tropospheric specific humidity has increased since the 1970s. The magnitude of the observed global change in water vapour of about 3.5% in the past 40 years is consistent with the observed temperature change of about 0.5°C during the same period, and the relative humidity has stayed approximately constant. The water vapour change can be attributed to human influence with *medium confidence.* {2.5.6}

Changes in precipitation are harder to measure with the existing records, both because of the greater difficulty in sampling precipitation and also because we expect that precipitation will have a smaller fractional change than the water vapour content of air as the climate warms. When virtually all the land area is filled in using a reconstruction method, the resulting time series shows little change in land-based precipitation since 1900. At present there is *medium confidence* that there has been a significant human influence on global scale changes in precipitation patterns, including reductions in tropical latitudes and increases in northern hemisphere mid to high latitudes. Changes in the extremes of precipitation, and other climate extremes related to the water cycle are comprehensively discussed in TFE.9 {2.5.1}

Although direct trends in precipitation and evaporation are difficult to measure with the available records, measurements of oceanic surface salinity, which is strongly dependent on the difference between evaporation and precipitation, show significant trends. It is *very likely* that the mean regional pattern of sea surface salinity has been enhanced since the 1960s: Saline surface waters in the mid-latitudes have become more saline, while the relatively fresh surface waters in tropical and Polar Regions have become fresher. Also, the inter-basin contrast between saline Atlantic and fresh Pacific surface waters has *very likely* increased. These patterns are *very likely* caused by an intensification of the water cycle as the lower atmosphere has warmed, reflecting the expected and observed increased water vapour content of the warmer air. {3.3.4, FAQ3.3}

In most regions analyzed, it is *likely* that decreasing numbers of snowfall events are occurring where increased winter temperatures have been observed. Both satellite and in-situ observations show significant reductions in the Northern Hemisphere snow cover extent over the past 90 years, with most reduction occurring in the 1980s. Snow cover decreased most in spring when the average extent decreased by around 8% (7 million km^2) over the period 1970–2010 compared with the period 1922–1970. Because of earlier spring snowmelt, the duration of the Northern Hemisphere snow season has declined by 5.3 days per decade since the 1972/1973 winter. It is *likely* that there has been an anthropogenic component to these observed reductions in snow cover and permafrost since 1970. It is *likely* that glaciers have diminished significantly due to human influence since the 1960s. {4.5.2}

The most recent and most comprehensive analyses of river runoff do not support the AR4 conclusion that global runoff has increased during the 20th century. New results also indicate that the AR4 conclusions regarding global increasing trends in droughts since the 1970s are no longer supported.{2.6.2, 2.5.2}

Projections of Future Changes

Changes in the water cycle are projected to occur in a warming climate (TFE.1, Figure 1, see also TS 4.6, TS 5.6). Global-scale precipitation is projected to gradually increase in the 21st century. It is *virtually certain*, that precipitation increase will be much smaller, approximately 2% K^{-1}, than the rate of lower tropospheric water vapour increase (~7% K^{-1}), due to global energetic constraints. It is *virtually certain* that changes of average precipitation in a much warmer world will not be uniform, with some regions experiencing increases, and others with decreases or not much change at all. The high latitudes are *very likely* to experience greater amounts of precipitation due to the additional water carrying capacity of the warmer troposphere. Many mid-latitude arid and semi-arid regions will *likely* experience less precipitation and many

moist mid-latitude regions will *likely* experience more precipitation. The largest precipitation changes over northern Eurasia and North America are projected to occur during the winter. {12.4.5}

[INSERT TFE.1, FIGURE 1 HERE]

TFE.1, Figure 1: Annual mean changes in precipitation (P), evaporation (E), relative humidity, soil moisture, runoff, and E-P, for 2081–2100 relative to 1986–2005 under the RCP8.5 scenario (see Box TS.4). {Figures 12.25–12.27}

Regional to global-scale projections of soil moisture and drought remain relatively uncertain compared to other aspects of the water cycle. Nonetheless, drying in the Mediterranean, south western U.S. and south African regions are consistent with projected changes in Hadley circulation, so drying in these regions as global temperatures increase is *likely*. Decreases in runoff are *likely* in southern Europe, the Middle East, and south western U.S. The CMIP5 models project consistent increases in high latitude runoff, consistent with AR4 (see Box TS.4), but confidence in this projection is tempered by large biases in their simulation of present-day snow cover. {12.4.5}

TS.2.6 Changes in Sea Level

Changes in sea level represent an integration of many aspects of climate change, and thus occur over a broad range of temporal and spatial scales. The primary contributors to sea-level change are the expansion of the ocean as it warms and the transfer to the ocean of water currently stored on land, particularly from glaciers and ice sheets. Anthropogenic processes such as water impoundment (dams, reservoirs) and ground water depletion also affect sea level. Regional mean sea level change can be significantly different from the global mean change. {13}

Paleo sea level records indicate sea level has varied considerably in the past. During the middle Pliocene (3.3 to 3 million years ago), there is *medium confidence* that global mean surface temperatures were approximately 2°C–3.5°C warmer than for the pre-industrial climate and multiple lines of evidence provide *medium confidence* that global mean sea level was 10 ± 10 m above present values. Direct geological evidence, together with ice sheet simulations, suggest that, for the central estimate, most of the variation in ice volume occurred in the Greenland and West Antarctic ice sheets with only a slightly reduced East Antarctic ice sheet compared to today. {5.3}

During glacial cycles of the last five hundred thousand years, sea level varied from more than 100 m below present day sea level to meters higher. During the last interglaciation, there is *high confidence* that global mean sea level (GMSL) was more than 6 m higher than current values and less than 10 m above current values. Of this sea level rise, there is *medium confidence* that contributions from thermosteric and glacier changes are less than 1 m, and about 2 m can be attributed to melting of the Greenland ice sheet, indicating that at least 3 to 4 m of sea level rise from mass loss in Antarctica. For the time interval in which global mean sea level was above present, the maximum 1000-year average rate of global mean sea level rise *very likely* exceeded 2.0 m kyr^{-1}, *likely* exceeded 4.1 m kyr^{-1}, and was *unlikely* to have exceeded 5.8 m kyr^{-1}. Faster rates lasting less than a millennium cannot be ruled out. Because these periods give only a limited analogy for future anthropogenic climate change, they do not provide upper bounds for global mean sea level rise during the 21st century. {5.6, 13.2}

It is *very likely* that the rate of global mean sea level rise has increased during the last two centuries. Paleo sea level data from many locations around the globe indicate low rates of sea level change during the late Holocene (order tenths of mm yr^{-1}) and modern rates (order mm yr^{-1}) during the 20th century. Long tide-gauge records and reconstructions of global averaged sea level extending back to the 19th century confirm this acceleration. {3.7, 5.6, 13.2}

It is *virtually certain* that global mean sea level has risen at a mean rate between 1.4 to 2.0 mm yr^{-1} during the 20th century, and between 2.7 and 3.7 mm yr^{-1} since 1993. This assessment is based on high agreement among multiple analyses using different methods, and, since 1993, from independent observing systems (tide gauges and altimetry) (see also TFE.2, Figure 1). As a result, there is *high confidence* that this change in

observed rate of sea level rise is real and not an artefact of the different sampling or instruments {3.7.1}. It is *likely* that a rate comparable to that since 1993 occurred between 1930 and 1950, as individual tide gauges around the world and all reconstructions of GMSL show higher rates of sea level rise during this period {3.7}. High agreement between studies with and without corrections for land motion suggests that it is *very unlikely* that estimates of the global average rate of sea level change are significantly affected by land motion {3.7}.

It is *very likely* that the rate of mean sea level rise along Northern European coastlines has accelerated since the early 1800s and that the increased rate of sea level rise has continued into the 20th century, as the signal has been observed in multiple long tide gauge records and by different groups using different analysis techniques. Many more long (>60 year) tide gauge records around the world show the increased rate of sea level rise since 1900. Two out of three reconstructions of GMSL from tide gauge data extending back to 1900 or earlier indicate acceleration. Estimates range from 0.000 to 0.013 [–0.002 to 0.019] mm yr^{-2}, so it is *likely* that GMSL rise has accelerated since the early 1900s. {3.7, 13.2}

It is *very likely* that the warming in the upper 700 m has been contributing an average of 0.6 [0.4 to 0.8] mm yr^{-1} of sea level change since 1971. It is *likely* that warming between 700 m and 2000 m has been contributing an additional 0.1 mm yr^{-1} [0 to 0.2] of sea level rise since 1971, and that warming below 2000 m has been contributing another 0.15 [0.05 to 0.25] mm yr^{-1} of sea level rise since the early 1990s. {3.7}

The mass loss of the Greenland ice sheet since the early 1990s is equivalent to a sea level rise of 0.34 mm yr^{-1} for 1993–2010, and 0.63 mm yr^{-1} for 2005–2010 {4.4.2.2, Figure 4.15}. Between 1993 and 2010, the Antarctic Ice sheet contributed 0.18mm yr^{-1}, and 0.31mm yr^{-1} for 2005–2010 {4.4.2.3}. Global glacier loss is equivalent to a sea level rise of 0.58–0.72 mm yr^{-1} for the period 2003–2009 {4.3.4}.

It is *virtually certain* that the ocean mass has increased at a rate between [0.8 to 1.6] mm yr^{-1} since 2005, based on high agreement between GRACE estimates over the same 6-year period and from the closure of the sea level balance equation based on multiple independent observations (altimetry, GRACE, Argo). Direct observations of ocean mass change are not available for earlier periods. {3.7}

Regional rates of sea level change are often higher or lower than the global mean on interdecadal periods. The regional rates are known globally to high precision using satellite altimetry since 1993, and results have shown a persistent pattern of change, with rates in the Warm Pool of the western Pacific up to three times larger than GMSL, while rates over much of the Eastern Pacific from 1993–2010 are near zero or negative. {3.7, FAQ 13.1}

The current understanding of recent sea level change using both observations and models is summarized in TFE.2.

TFE.2: Sea Level Change: Scientific Understanding and Uncertainties

Global mean sea level varied between glacial and interglacial periods, due to changes in continental ice volume. After the Last Glacial Maximum, global mean sea levels reached close to present day values several thousand years ago. Since then, it is *very likely* that the rate of global mean sea level rise has increased from low rates of sea level change during the late Holocene (order tenths of mm yr^{-1}) to modern rates (order mm yr^{-1}) during the 20th century. TFE.2, Figure 1.{3.7, 5.6, 13.2}

[INSERT TFE.2, FIGURE 1 HERE]

TFE.2, Figure 1: Observed and modelled global-mean sea level. (a) Observed GMSL from satellites (light blue dashed) and estimated from tide gauges (dark blue solid) and the sum of contributions (red). The shading indicates 5-95% confidence limits. The mean sea level from the sum of modeled thermal expansion, glaciers and land water storage is in black. (b) The projected sea level rise relative to the 1986–2005 average (black and coloured lines for the four scenarios, with shading indicating the likely range). Also shown is the observed sea level from (a), set to have the same value as the projections over 1993 to 2001. (c) Observed sea level (blue - tide gauges; red - altimeter) and modeled sea level (black, the sum of ocean thermal expansion, glaciers and land water storage, and black dashed also including a small long-term contributions from ice sheets, the possible underestimate in modelled thermal expansion from not

including preindustrial volcanic forcing, and from greater mass loss from glaciers during the 1930's due to unforced climate variability). {Figures 13.4, 13.5}

Ocean thermal expansion and glacier mass loss are *very likely* the dominant contributors to global mean sea level rise during the 20th century. {13.3}

It is *very likely* that warming of the ocean has contributed 0.8 [0.5 to 1.1] mm yr^{-1} of sea level change since 1971, with the majority of the contribution coming from the upper 700 m. The model-mean rate of ocean thermal expansion for 1971–2010 is close to observations, but for 1993–2010, the model-mean rate exceeds that observed. Following the major volcanic eruptions in 1963, 1982 and 1991, the modelled rate of expansion is substantially larger than the 20th century average, as the ocean recovers from the cooling caused by the volcanic forcing. {3.7, 13.3}

Observations, combined with improved methods of analysis, indicate the global glacier contribution to sea level was 0.86 [0.64 to 1.07] mm yr^{-1} sea level equivalent during 1971–2009. Confidence in global glacier mass balance models used for projections of global changes arises from the ability of the models of the well-observed glaciers to reproduce time series of historical changes of those glaciers using observed climate input. A simulation using observed climate data shows a larger rate of glacier mass loss during the 1930s than the simulations using AOGCM input, possibly a result of an episode of warming in Greenland associated with unforced regional climate variability. {4.3, 13.3}

Observations indicate that the Greenland Ice Sheet is *very likely* to be experiencing a net loss of mass due to increased surface melting and run off, and increased ice outflow. The rate of loss is *likely* to have increased over the last two decades. Regional climate models indicate that Greenland ice-sheet surface mass balance showed no significant trend from the 1960s to the 1980s, but melting and consequent runoff has increased since the early 1990s. This tendency is related to pronounced regional warming, which may be attributed to a combination of anomalous regional variability in recent years and anthropogenic climate change. While there is not yet sufficient evidence to evaluate how realistically AOGCMs simulate anthropogenic regional climate change in Greenland, we have confidence in projections of future warming in Greenland because of the qualitative agreement of models in predicting amplified warming at high northern latitudes for well-understood physical reasons, and we have confidence in projections of increasing surface melting in surface mass balance models. {4.4.2, 13.3}

The Antarctic Ice Sheet is also *likely* to be in a state of net mass loss and its contribution to sea level is also *likely* to be increasing through time. Acceleration in ice outflow has been observed since the 1990s, especially in the Amundsen Sea sector of West Antarctica. Interannual variability in accumulation is large and as a result no significant trend is present in accumulation since 1979 in either models or observations, although East Antarctica may have experienced a small gain in mass over the last two decades. Surface melting is currently negligible in Antarctica. {4.4.2, 13.3}

Model-based estimates of climate-related changes in water storage on land (as snow cover, surface water, soil moisture and ground water) do not show significant long-term trends for the past decades. However, human-induced changes (reservoir impoundment and groundwater depletion) have each contributed at least several tenths of mm yr^{-1} SLE. Reservoir impoundment exceeded groundwater depletion for the majority of the 20th century but the rate of groundwater depletion has increased and now exceeds the rate of impoundment. Their combined net contribution for the 20th century is estimated to be small. {13.3}

The observed GMSL rise for 1993–2010 is consistent with the sum of the observationally estimated contributions (TFE.2, Figure 1a). The closure of the observational budget for recent periods within uncertainties represents a significant advance since the AR4 in physical understanding of the causes of past GMSL change, and provides an improved basis for critical evaluation of models of these contributions in order to assess their reliability for making projections. The sum of modelled ocean thermal expansion and glacier contributions and land-water storage agrees with the observed rise since 1993 (TFE.2, Figure 1a) with a residual of 0.2 [–0.6 to 1.1] mm yr^{-1} that is consistent with the sum of the observed ice-sheet contributions of 0.42 ± 0.11 mm yr^{-1} over 1993–2009 and 0.73 ± 0.26 mm yr^{-1} over 2005–2009. The

projected change of global mean sea level from 1996 (TFE.2, Figure 1b) also agrees with the observed rise and the sum of contributions. {4.3.4, 13.3}

The observational budget cannot be rigorously assessed for 1901–1990 or 1971–2010 because there is insufficient observational information. However, the sum of modelled ocean thermal expansion and glacier contributions and the estimated change in land water storage (which is relatively small) accounts for about 70% of the observed rate of GMSL rise for 1901–1990, and over 80% for 1971–2010 (TFE.2, Figure 1c). The residual of 0.5 [–0.1 to 1.0] mm yr^{-1} for 1901–1990 is also consistent with zero, but is potentially explained by a small long-term contributions from ice sheets, the possible underestimate in modelled thermal expansion from not including preindustrial volcanic forcing, or from greater mass loss from glaciers during the 1930's due to unforced climate variability, as described above. The sum of these four additional terms captures much of the trend in the residual time series (TFE.2, Figure 1c). The evidence now available gives a clearer account than in previous IPCC assessments of 20th century sea level change. {13.3}

It is now clear that the observed increases in ice flow from the Antarctic and Greenland Ice Sheets come from ocean ice shelf interactions. If increasing ice-sheet outflow explains half the contribution from Greenland during 1993–2010 and all of that from Antarctica, it would amount to about 6 mm, which is about 10% of the GMSL rise during that period, and about 3% of the GMSL rise during 1901–2010. Thus, this contribution has been relatively small up to now. When calibrated appropriately, recently improved dynamical ice-sheet models can reproduce the observed rapid changes in ice-sheet outflow for individual glacier systems (e.g., Pine Island Glacier in Antarctica). However, models of ice sheet response to global warming and particularly ice sheet-ocean interactions are incomplete and the omission of ice-sheet models, especially of dynamics, from the model budget of the past means that we cannot place the same level of confidence in them as in other contributions and is a reason for uncertainty in projections. {13.3, 13.4}

Using the same methods as for simulating past GMSL change (and including estimates of ice sheet dynamical contributions from the literature), it is *virtually certain* that the rate of global mean sea level rise during the 21st century will exceed the rate observed during the 20th century for all RCP scenarios (see Box TS.4). For the period 2081 to 2100, compared to 1986 to 2005, global mean sea level rise is *likely* to be in the range 0.29–0.55 m for RCP2.6, 0.36–0.63 m for RCP4.5, 0.37–0.64 m for RCP6.0, and 0.48–0.82 m (0.56–0.96 m by 2100 with a rate of rise 8 to 15 mm yr^{-1}over the last decade of the 21st century) for RCP8.5. We have *medium confidence* in these ranges because we have only *medium confidence* in the *likely* range of projections from models of ice-sheet dynamics and because there is no consensus about the reliability of semi-empirical models that give higher projections than process-based models. As a result, larger values cannot be excluded but current scientific understanding is insufficient for evaluating the probability of higher values. {13.5}

TS.2.7 Changes in Extremes

Extreme weather and climate events can be defined as those that occur above or below threshold values near the upper or lower ends of the range of observed values of a given variable. Definitions of thresholds vary, but values with less than a 5%, 1% or even lower chance of occurrence during a specified reference period (generally 1961–1990) are often used. A comprehensive discussion of observed changes, their causes, and projected changes in extremes is provided in TFE.9. {2.6, Box 2.4}

TS.2.7.1 Atmosphere

Recent analyses of extreme events generally support the AR4 and SREX conclusions. It is *very likely* that the overall number of cold days and nights has decreased and the overall number of warm days and nights has increased on the global scale between 1951 and 2010 (with warming trends between 2.48 ± 0.64 and 5.75 ± 1.33 days per decade dependent on index). Globally, there is *medium confidence* that the length of warm spells, including heat waves, has increased since the middle of the 20th century. {2.6.1, Table 2.11}

Consistent with AR4 conclusions, there have been statistically significant trends in the number of heavy precipitation events (e.g., 95th percentile) in some regions. It is *likely* that the number of heavy precipitation events has increased in more regions than it has decreased since 1950. *Confidence* is *highest* for North

America where the most consistent trends towards heavier precipitation events are found. {2.6.2, Figure 2.33a}

New results indicate that the AR4 conclusions regarding global increasing trends in hydrological droughts since the 1970s are no longer supported. There is *low confidence* in observed large-scale trends in dryness (lack of rainfall), due to lack of direct observations, dependencies of inferred trends on the index choice and geographical inconsistencies in the trends. There continues to be a lack of evidence and thus *low confidence* regarding the sign of trend in the magnitude and/or frequency of floods on a global scale. {2.6.2, Figure 2.33b, c}

Recent re-assessments of tropical cyclone data do not support the AR4 conclusions of an increase in the most intense tropical cyclones or an upward trend in the potential destructiveness of all storms since the 1970s. There is *low confidence* that any reported long-term changes are robust, after accounting for past changes in observing capabilities. However, over the satellite era (since 1979) increases in the intensity of the strongest storms in the Atlantic appear robust. There is still insufficient evidence to determine whether robust global trends exist in small-scale severe weather events such as hail or tornadoes. {2.6.2, 2.6.3}

TS.2.7.2 Oceans

Mean significant wave height has *likely* increased since the 1950s over much of the mid-latitude North Atlantic and North Pacific, with winter season trends of 8 to 20 cm per decade, although confidence is limited by the lack of observations. Mean significant wave height likely increased by up to 2.5–5% per decade over much of the Southern Ocean since the mid-1980s, with the strongest changes between 80°E–160°W. {3.4, Figures 3.6–3.8}. It is *likely* that extreme sea levels have increased since 1970, and this is mainly attributable to rising mean sea level {3.7.4, 3.7.5, Figure 3.14}.

TS.2.8 Changes in Carbon and other Biogeochemical Cycles

TS.2.8.1 CO_2

Between 1750 and 2010, CO_2 emissions from fossil fuel combustion and cement production are estimated from energy and fuel use statistics to have released 365 ± 30 PgC[5]. In 2000–2009, average fossil fuel and cement manufacturing emissions were 7.7 ± 0.5 PgC yr^{-1}, with an average growth rate of 2.9% yr^{-1} (see also Figure TS.2). This rate of increase of fossil fuel emissions is higher than during the 1990's (1.0% yr^{-1}). In 2012, fossil fuel emissions were 9.4 ± 0.8 PgC. {6.3.1, Table 6.1, Figure 6.8}

[INSERT FIGURE TS.2 HERE]
Figure TS.2: Anthropogenic emissions of carbon dioxide from the indicated fuel or activity. {Figure 6.8}

Land use change (mainly deforestation), derived from land cover data and modelling, is estimated to have released 180 ± 80 PgC. Land use change emissions between 2000 and 2009 are dominated by tropical deforestation, and are estimated at 0.9 ± 0.5 PgC yr^{-1}, with possibly a small decrease from the 1990s due to lower reported forest loss during this decade. This estimate includes gross deforestation emissions of around 3 PgC yr^{-1} compensated by 2 PgC yr^{-1} of forest regrowth in some regions; mainly abandoned agricultural land. {6.3.2, Table 6.2, Figure 6.10}

Of the 545 ± 85 PgC released to the atmosphere from fossil fuel and land use emissions, 240 ± 10 PgC accumulated in the atmosphere, as estimated with very high accuracy from the observed increase of atmospheric CO_2 concentration from 278 ± 3 ppm[6] in 1750 to 390.7 ppm in January 2011. Atmospheric CO_2 concentrations grew by 4.0 ± 0.2 PgC yr^{-1} in the first decade of the 21st century. The distribution of

[5] 1 Petagram of carbon = 1 PgC = 10^{15} grams of carbon = 1 Gigatonne of carbon = 1 GtC. This corresponds to 3.67 $GtCO_2$.

[6] ppm (parts per million) or ppb (parts per billion, 1 billion = 1,000 million) is the ratio of the number of greenhouse gas molecules to the total number of molecules of dry air. For example, 300 ppm means 300 molecules of a greenhouse gas per million molecules of dry air.

observed atmospheric CO_2 increases with latitude clearly shows that the increases are driven by anthropogenic emissions which primarily occur in the industrialized countries north of the equator; based on annual average concentrations, stations in the Northern Hemisphere show slightly higher concentrations than stations in the Southern Hemisphere. An independent line of evidence for the anthropogenic origin of the observed atmospheric CO_2 increase comes from the observed consistent decrease in atmospheric O_2 content and a decrease in the isotopic ratio of CO_2 ($^{13}C/^{12}C$) in the atmosphere (see Figure TS.3). {6.1.3}

The remaining amount of carbon released by fossil fuel and land-use emissions has been re-absorbed by the ocean and terrestrial ecosystems. Based on high agreement between estimates using different approaches (e.g., oceanic carbon, nutrient, or tracer data), there is *very high confidence* that the global ocean inventory of anthropogenic carbon (C_{ant}) increased from 1994 to 2010. The C_{ant} inventory was estimated to be between 93–137 PgC in 1994, and 155 [125 to 185] PgC in 2010. The 2010 inventory corresponds to an annual global uptake rate of 2.3 [1.7 to 2.9] PgC yr^{-1}, in agreement with carbon uptake rates calculated from atmospheric O_2/N_2 measurements (2.5 [1.8 to 3.2] PgC yr^{-1}) (see Figure TS.3). {3.8.1, Figures 3.15, 3.16}

[INSERT FIGURE TS.3 HERE]

Figure TS.3: Atmospheric concentration of CO_2, oxygen, $^{13}C/^{12}C$ stable isotope ratio in CO_2, CH_4 and N_2O, and oceanic surface observations of pCO_2 and pH, recorded over the last decades at representative stations in the northern and the southern hemisphere from the observatories and time series stations. MLO: Mauna Loa Observatory; SPO: South Pole; HOT: Hawaii ocean Time series station; MHD: Mace Head; CGO: Cape Grim; ALT: Alert. {Figure 6.3 and FAQ 3.2, Figure 1}

Regional observations of the C_{ant} storage rate are in broad agreement with the expected storage rate resulting from the increase in atmospheric CO_2 concentrations, but with significant spatial and temporal variations. {3.8.1}. Analyses of the limited oxygen observations available since 1960 show *high agreement* that oxygen concentrations have decreased over much of the open ocean thermocline since the 1960s. {3.8.3}

Natural terrestrial ecosystems (those not affected by land use change) are estimated by difference from changes in other reservoirs to have accumulated 165 ± 60 PgC between 1750 and 2010. The gain of carbon by natural terrestrial ecosystems is estimated to take place mainly through the uptake of CO_2 by enhanced photosynthesis at higher CO_2 levels and nitrogen (N) deposition, longer growing seasons in high latitudes, the expansion and recovery of forests from past land use, and improved forest management. Natural carbon sinks vary regionally due to physical, biological and chemical processes acting on different time scales. An excess of atmospheric CO_2 absorbed by land ecosystems gets stored as organic matter in diverse carbon pools, from short lived (leaves, fine roots) to long-lived (stems, soil carbon). {6.3, Table 6.1, Figure 6.8}

TS.2.8.2 Carbon and Ocean Acidification

There is *very high confidence* that oceanic uptake of anthropogenic CO_2 has resulted in gradual acidification of seawater and decreasing pH (i.e., anthropogenic ocean acidification) in surface waters (Figure TS.3). The observed pH trends range between –0.015 and –0.024 per decade. In the ocean interior, pH can also be modified by natural physical and biological processes over decadal time scales. {3.8.2, Table 3.2, Box 3.2, Figures 3.17, 3.18, FAQ 3.2}. .

TS.2.8.3 CH_4

Since preindustrial times, the concentration of CH_4 increased by a factor of 2.5, from about 730 ppb in 1750 to 1790 ppb by the end of 2009 (Figure TS.3). The global growth rate of CH_4 has decreased from 12 ± 2 ppb yr^{-1} during 1983–1989, down to 2 ± 4 ppb yr^{-1} during the years 2000-2009, causing nearly-stable annual global CH_4 concentrations between 1999 and 2006. The reasons for this near stabilization are still debated but different lines of evidence include: reduced emissions from the gas industry in the countries of the former Soviet union, reduced global fossil fuel related emissions, compensation between increasing anthropogenic emissions and decreasing wetland emissions, reduced emissions from rice paddies, and changes in OH concentrations. Since 2007, atmospheric CH_4 is increasing again. A possible cause relies on positive trends in tropical wetland emissions with some contribution of northern high latitudes in 2007, due to anomalies of precipitation and temperature in these regions. {6.3.3, Table 6.7, Figure 6.17}

The single most dominant CH_4 source for annual magnitude and interannual variations is CH_4 emissions from natural wetlands, from the tropics and high northern latitudes [range of 160–210 $TgCH_4\,yr^{-1}$ for 2000–2009]. Overall for 2000-2009, anthropogenic CH_4 sources amount to 338 $TgCH_4\,yr^{-1}$ ([278–344] including ruminant animals, sewage and waste, fossil fuel related emissions, and rice-paddies agriculture. Anthropogenic emissions are dominant over natural sources with emissions of 206 $TgCH_4\,yr^{-1}$ [202–368]. Methane is mainly destroyed in the atmosphere by reaction with OH radicals. The different approaches agree now that OH changes remained within 5% in the period 2000–2009. {6.3.3, Table 6.7}

TS.2.8.4 Nitrogen

The radiative properties of the atmosphere are strongly influenced by the abundance of the long-lived greenhouse gases like nitrous oxide (N_2O). Since preindustrial times, the concentration of N_2O has increased by a factor of 1.2 (see also Figure TS.3). Changes in the nitrogen cycle, in addition to interactions with CO_2 sources and sinks, affect emissions of N_2O both on land and from the ocean. {6.4.6}

TS.3 Drivers of Climate Change

TS.3.1 Introduction

Human activities have changed and continue to change the Earth surfaces and the atmospheric composition. Some of these changes have a direct or indirect impact on the energy balance of the Earth and are thus drivers of climate change. Radiative forcing (RF) is a measure of the net change in the energy balance of the Earth system in response to some external perturbation (see Box TS.1). The RF concept is valuable for comparing the influence on global mean temperature of most individual agent affecting Earth's radiation balance. The quantitative values provided in AR5 are consistent with those in previous IPCC reports, though there have been some important revisions (Figure TS.4). Adjusted forcing (AF) is used to quantify the impact of some forcing agents that involve rapid adjustments of some components of the atmosphere and surface that are assumed constant in the RF concept (see Box TS.1). RF and AF are estimated from the change between 1750 and 2010 if other time periods are not explicitly stated, and we refer to this as the industrial era. Uncertainties are given associated with the best estimates of RF and AF, with values representing the 5 to 95% (90%) confidence range. {8.1}

In addition to the global mean RF or AF, their spatial distribution and temporal evolution of forcing, as well as climate feedbacks, play a role in determining the eventual impact of various drivers on climate {8.1}. Land surface changes may also impact the local and regional climate through processes that are not radiative in nature {8.3}.

[START BOX TS.1 HERE]

Box TS.1: Radiative Forcing and Adjusted Forcing

Radiative Forcing (RF) and Adjusted Forcing (AF) are used to quantify the energy imbalance that occurs as a result of an externally imposed change. They are expressed in Watts per square meter ($W\,m^{-2}$). RF is defined in AR5, as in previous IPCC assessments, as the change in net irradiance at the tropopause after allowing for stratospheric temperatures to readjust to radiative equilibrium, while holding other state variables such as tropospheric temperatures, water vapor and cloud cover fixed at the unperturbed values. {8.1.1, see Glossary}

Although the RF concept has proved very valuable, it also has some limitation as the impact of rapid adjustments of the Earth's surface and troposphere are not evaluated. This led to the definition of the AF. Whereas in the RF concept, all surface and tropospheric conditions are kept fixed, the AF definition allows all variables to adjust to perturbations except for ocean temperature and sea ice cover. In particular, the impact of aerosols on cloud microphysics and life cycle are rapid adjustments and occur on a time scale much shorter than adjustments of the ocean (even the upper layer) to forcings. The AF and RF values are

significantly different for the anthropogenic aerosols, due to their influence on clouds and on snow cover. For other components that drive the Earth energy balance, such as greenhouse gases, AF and RF are fairly similar. In cases where RF and AF differ substantially, AF has been shown to be a better indicator of the global mean temperature response and is therefore emphasized in AR5. {8.1}

[END BOX TS.1 HERE]

TS.3.2 Radiative Forcing from Greenhouse Gases

Human activity leads to change in the atmospheric composition either directly (emissions of gases, land use changes) or indirectly (atmospheric chemistry). Anthropogenic emissions have driven the changes in WMGHG concentrations during the industrial era (see Section TS.2.8 and TFE.7). As historical well-mixed greenhouse gas (WMGHG) concentrations since the preindustrial are well known based on direct measurements in ice core records, the computation of RF due to concentration changes provides tightly constrained values (Figure TS.4). There hasn't been significant change in our understanding of WMGHG radiative impact, so that the changes in RF estimates relative to AR4 are due essentially to concentration increases. Due to high-quality observations, it is *virtually certain* that increasing atmospheric burdens of most WMGHGs, especially CO_2, resulted in a further increase in their radiative forcing from 2005 to 2010. Based on concentration changes, the RF of all WMGHG in 2009 is 2.83 ± 0.28 W m^{-2}. This is an increase since AR4 of 0.20 ± 0.02 W m^{-2}, with nearly all of the increase due to the increase in the abundance of CO_2 since 2005. The industrial era RF for CO_2 alone is 1.82 ± 0.18 W m^{-2}. Over the last 15 years, CO_2 has been the dominant contributor to the increase in RF from the WMGHGs, with RF of CO_2 having an average growth rate slightly less than 0.3 ± 0.03 W m^{-2} per decade {5.2, 8.3}. The uncertainty in the WMGHG RF is due in part to its radiative properties but mostly to the full accounting of atmospheric radiative transfer including clouds. The best estimate for WMGHG AF is the same as RF, but the uncertainty range is twice as large due to the poorly constrained impacts on the water cycle. {8.3.2, 6.3; Table 6.1, Figure 6.8}

[INSERT FIGURE TS.4 HERE]

Figure TS.4: Radiative forcing (RF) and Adjusted forcing (AF) of climate change during the industrial era. Top: Forcing by concentration between 1750 and 2010 with associated uncertainty range (solid bars are RF, hatched bars are AF, green diamonds and associated uncertainties are those assessed in AR4). Bottom: Probability Density Functions for both the AR and AF, for the aerosol, WMGHG and total. The green line shows the AR4 estimate for the total anthropogenic RF and shall be compared to the black line which is the same for AR5. ArI=Aerosol Radiative Forcing through interaction with radiation, AcI=Aerosol Radiative Forcing through effects on clouds. {Figure 8.17}

After a decade of near stability, the recent increase of CH_4 concentration led to an enhanced contribution to the RF compared to AR4 by 2% to 0.48 ± 0.05 W m^{-2}. It is *likely* that the RF from methane is now larger than that of all halocarbons combined. {8.3}

N_2O has increased by 6% since AR4 and has a RF of 0.17 ± 0.02 W m^{-2}. N_2O concentrations continue to rise while those of CFC-12, the third largest WMGHG contributor to RF for several decades, are falling due to phase-out of this chemical under the Montreal Protocol. There is *high confidence* that N_2O is now the third largest WMGHG contributor to RF. The RF from halocarbons is very similar to the value in AR4, with a reduced RF from CFCs but increases in many of their replacements. Four of the halocarbons (CFC-11, CFC-12, CFC-113, and HCFC-22) account for 85% of the total halocarbon RF. The former three compounds have declining RF over the last five years but are more than compensated for by the increased RF from HCFC-22. There is *high confidence* that the growth rate in RF from all WMGHG is weaker over the last decade than in the 1970s and 1980s owing to a small increase in the non-CO_2 RF. {8.3}

Short-lived GHGs also contribute to anthropogenic forcing. Observations indicate that ozone (O_3) has *likely* been increasing at many undisturbed (background) locations in the 1990s. These increases have continued mainly over Asia and flattened over Europe during the last decade. The total RF due to changes in ozone is 0.30 ± 0.20 W m^{-2}, with RF due to tropospheric ozone of 0.40 ± 0.20 W m^{-2} and due to stratospheric ozone of –0.10 ± 0.15 W m^{-2}. Ozone is not emitted directly into the atmosphere; instead it is formed by photochemical reactions. In the troposphere these reactions involve precursor species such as oxides of

nitrogen and organic compounds that are emitted into the atmosphere from a variety of natural and anthropogenic sources. Tropospheric ozone RF is largely attributed to increases in emissions of methane, carbon monoxide, volatile organics and nitrogen oxides, while stratospheric RF results primarily from ozone depletion by halocarbons. However, there is now strong evidence for substantial links between the changes in tropospheric and stratospheric ozone. There is strong evidence that tropospheric ozone also has a detrimental impact on vegetation physiology, and therefore on its CO_2 uptake. This reduced uptake leads to an indirect increase in the atmospheric CO_2 concentration. Thus a fraction of the CO_2 RF, the value of which is well known, should be attributed to ozone rather than direct emission, but there is a *low confidence* on the quantitative estimates. RF for stratospheric water vapour produced from CH_4 oxidation is 0.07 ± 0.05 W m^{-2}. Recent observations indicate a reduction in the stratospheric water vapour abundance, but this is not linked to CH_4 oxidation and is therefore not treated as a RF mechanism. Changes in water vapor in the troposphere are regarded as a feedback rather than a forcing. {FAQ 8.1, 8.2, 8.3}

TS.3.3 Radiative Forcing from Anthropogenic Aerosols

Anthropogenic aerosols are responsible for a radiative forcing of climate through their interaction with radiation (RFari) and through their effects on clouds (RFaci) (Figure TS.4). There has been progress since AR4 on observing and modeling climate-relevant aerosols properties (including their size distribution, hygroscopicity, chemical composition, mixing state, optical and cloud nucleation properties) and their atmospheric distribution. Nevertheless, *confidence* in assessments of long-term trends of global aerosol optical depth and other global properties of aerosols remains *low* due to difficulties in measurement and lack of observations of some relevant parameters, high spatial and temporal variability and the relatively short observational records that exist. The anthropogenic RFari is given a best estimate of -0.40 ± 0.30 W m^{-2} using evidence from aerosol models and some constraints from observations. This does not include the contribution of mineral dust because the respective natural and anthropogenic contributions are too uncertain. The RFari is caused by multiple aerosol types. Sulphate aerosol is responsible for an RFari of -0.4 ± 0.2 W m^{-2}. Black carbon (BC) aerosol has an RFari 0.3 ± 0.2 W m^{-2} (fossil and bio fuel sources only) and 0.4 ± 0.2 W m^{-2} (fossil fuel and biomass burning including a possible small fraction from vegetation feedbacks). Organic carbon aerosol from fossil and bio fuel sources has an RFari -0.04 ± 0.04 W m^{-2}. Biomass burning aerosol has an RFari -0.0 ± 0.1 W m^{-2}. Secondary organic aerosol has an RFari -0.08 ± 0.20 W m^{-2} and nitrate aerosol has an RFari of -0.13 ± 0.10 W m^{-2}. Finally mineral aerosol has an RFari of -0.1 ± 0.2 W m^{-2} but this may include a natural component or a climate feedback effect. {7.3}

Improved understanding of aerosol-cloud interactions has led to a reduction in the magnitude of global aerosol-cloud forcings estimate. The total adjusted forcing due to aerosols (AFari+aci, excluding the effect of absorbing aerosol on snow and ice) is assessed to be -0.9 ± 0.6 W m^{-2}. The AFari+aci estimate includes rapid adjustments, such as changes to the cloud lifetime and aerosol microphysical effects on mixed-phase, ice and convective clouds. This range was obtained by giving equal weight to satellite-based studies and estimates from climate models and inverse studies grouped together, and includes a small correction term to be in line with a 1750 reference period. It is consistent with multiple lines of evidence suggesting less negative estimates for aerosol-cloud interactions than in AR4. {7.4, 7.5, Figure 7.19}

The RF from absorbing aerosol on snow and ice is assessed to be +0.04 [0.02 to 0.09] W m^{-2}. Unlike in the previous IPCC assessment, this estimate includes the effects on sea-ice, accounts for more physical processes, and incorporates evidence from both models and observations. This RF causes a 2–4 times larger global mean surface temperature change per unit forcing than CO_2 and represents a significant forcing mechanism in the Arctic and over Tibet. {7.3, 7.5}

Despite the large uncertainty range, there is a *high confidence* that aerosols have offset a substantial portion of WMGHG forcing. There is limited, if any, evidence and no agreement that the small-scale impact of aerosols on cloud microphysical structure translates into a significant regional impact in terms of precipitation amount (beyond orographic locations) but there is medium evidence and agreement for an effect on timing and intensity of precipitation. {7.4}

TS.3.4 Radiative Forcing from Land Surface Changes and Contrails

There is strong evidence that anthropogenic land use change has increased the land surface albedo, which leads to a RF of –0.15 ± 0.1 W m^{-2} (Figure TS.4). There is still a large spread of quantitative estimates due to different assumptions for the albedo of the natural and managed surfaces. In addition, the time evolution of the land use change, and in particular how much was already completed in the reference year 1750, are still debated. Additionally, land use change causes other modifications that are not radiative but impact the surface temperature, including modifications in the surface roughness, latent heat flux, river runoff, and irrigation. These are more uncertain and they are difficult to quantify, but tend to offset the impact of albedo changes. As a consequence, there is low agreement on the sign of the net change in global mean temperature as a result of land use change. Land use change, and in particular deforestation, also has significant impacts on WMGHG concentrations, which would affect the attribution of RF to activities but not the total RF due to WMGHG concentration changes. {8.3}

Persistent contrails from aviation contribute a RF of 0.02 ± 0.01 W m^{-2} for year 2010, and the combined contrail and contrail-cirrus AF from aviation is assessed to be 0.05 (0.02 to 0.15) W m^{-2}. This forcing can be much larger regionally but is *very unlikely* to produce observable regional effects on either the mean or diurnal range of surface temperature. {7.2.5}

TS.3.5 Radiative Forcing from Natural Drivers of Climate Change

Solar and volcanic forcings are the two dominant natural contributors to climate change during the industrial era (Figure TS.4). Satellite observations of total solar irradiance (TSI) changes since 1978 spanning 3 solar cycle minimums show a RF of –0.04 ± 0.02 W m^{-2}. There is some diversity in the estimated trends of the composites of various satellite data, although they agree on a downward trend in TSI over this time period, which is therefore *very likely*. Secular trends of TSI before the start of satellite observations rely on a number of indirect proxies. The best estimate of RF from TSI changes over the industrial era is 0.04 ± 0.06 W m^{-2}, which includes greater RF up to 1980 and then a small downward trend. This RF estimate is substantially weaker than the AR4 estimate due to the addition of the latest solar cycle and inconsistencies in how solar RF was estimated in earlier IPCC assessments. The recent solar minimum was unusually low and long-lasting and several projections indicate lower TSI for the forthcoming decades. However, current abilities to project solar irradiance are extremely limited so that there is *very low confidence* concerning future solar forcing. {8.4}

Cosmic rays enhance aerosol nucleation and cloud condensation nuclei production in the free troposphere, but the effect is too weak to have any climatic influence during a solar cycle or over the last century (*high confidence*). Changes in solar activity affect the flux of galactic cosmic rays impinging upon the Earth's atmosphere, which has been hypothesized to affect climate through changes in cloudiness. However, no robust association between changes in cosmic rays and cloudiness has been identified. In the event that such an association exists, it is *very unlikely* to be due to cosmic ray-induced nucleation of new aerosol particles. {7.3, 7.4.5}

The RF of stratospheric aerosols is now well understood and has a large impact on the overall RF for a few years after major volcanic eruptions. While volcanic eruptions inject both mineral particles (called ash or tephra) and sulphate aerosol precursors into the atmosphere, it is the sulphate aerosols, because of their small size and long lifetimes that are responsible for radiative forcing important for climate. The emissions of CO_2 from volcanic eruptions are at least 100 times smaller than anthropogenic emissions, and inconsequential for climate on century time scales. Large tropical volcanic eruptions have played an important role in driving annual to decadal scale climate change during the industrial era due to their sometimes very large RF. There has not been any major volcanic eruption since Mt. Pinatubo in 1991, which caused a one-year RF of –3.4 W m^{-2}, but several smaller eruptions have caused a variable RF down to about –0.1 ± 0.03 W m^{-2} during the 2000 to 2010 period. The smaller eruptions have led to better understanding of the dependence of the amount of material and time of the year of high-latitude injections to produce climate impact. {8.4}

TS.3.6 Synthesis of Forcings; Spatial and Temporal evolution

A synthesis of the industrial era forcing finds that among the forcing agents, there is a *very high confidence* only for the WMGHG RF. Five forcing agents are given a confidence level of *'high'* and three '*medium'*, while an additional three are assigned either '*low*' with two effects newly assessed in this report assigned a

confidence level of *'very low'*. Relative to AR4, the confidence level has been elevated for six forcing agents due to improved evidence and understanding. {8.5}

The time evolution of the total anthropogenic RF shows a continuous increase from 1750, primarily since about 1860. There is a *very high confidence* that there has been a strong increase in the total anthropogenic RF increase rate since 1960, fueled primarily by the continuous increase in WMGHG concentration. There is still low agreement on the magnitude of the aerosol AF, which is the primary factor for the uncertainty in the total anthropogenic forcing. There is robust evidence and agreement that natural forcing is a small fraction of the WMGHG forcing. {8.5}

Forcing can also be attributed to emissions rather than to the resulting concentration changes (Figure TS.5). Changes in carbon dioxide are the largest single contributor to historical RF from either the perspective of changes in the atmospheric concentration of CO_2 or the impact of changes in net emissions of CO_2. The relative importance of other forcing agents varies with the perspective chosen, however. In particular, methane emissions have a much larger forcing (~1.0 W m^{-2} over the industrial era) than methane concentration increases (~0.5 W m^{-2}) due to several indirect effects through atmospheric chemistry. In addition, carbon monoxide emissions have a clear positive forcing, while nitrogen oxides emissions appear to cause a net negative forcing but uncertainties are large. Emissions of ozone-depleting halocarbons *likely* cause a net positive forcing as their direct radiative effect is larger than the impact of the stratospheric ozone depletion that they induce. {8.5}

[INSERT FIGURE TS.5 HERE]

Figure TS.5: Radiative forcing of climate change during the industrial era shown by emitted components from 1750 to 2010. The horizontal bars indicate the overall uncertainty, while the vertical bars are for the individual components. CFCs= Chlorofluorocarbons, HCFCs= Hydrochlorofluorocarbons, HFCs=Hydrofluorocarbons, PFCs= Perfluorocarbons, NMVOC= Non Methane Volatile Organic Compounds, BC= Black Carbon, RFaci= Aerosol Radiative Forcing through effects on clouds. {Figure 8.17}

Although the WMGHG show a fairly homogeneous forcing, other agents such as aerosols, ozone and land-use changes are highly heterogeneous spatially. Industrial era RFari showed maximum values over eastern North America and Europe during the early 20th century, with large values extending to East and Southeast Asia, South America and central Africa by 1980. Since then, however, the magnitude has decreased over eastern North America and Europe due to pollution control and the peak forcing has shifted to South and East Asia primarily as a result of economic growth and the resulting increase in emissions in those areas. Aerosol AF shows similar behaviour for locations with maximum negative forcing, but also shows substantial positive forcing over some deserts and the Arctic. In contrast, the whole atmosphere ozone forcing increased throughout the 20th century, and has peak positive amplitudes around 15°N–30°N but negative values over Antarctica. Land-use forcing by albedo changes has been strongest in industrialized and biomass burning regions. These inhomogeneous forcing agents can have a substantial influence on the hydrologic cycle. {8.6}

Over the 21st century, there is *very high confidence* that the anthropogenic radiative forcing will increase. Simple model estimates of the RF resulting from the Representative Concentration Pathways (RCPs, see Box TS.4) show anthropogenic RF relative to 1750 increasing to 3.0–4.8 W m^{-2} in 2050, and 2.7–8.4 W m^{-2} at 2100. In the near-term, the RCPs are quite similar to one another, with RF at 2030 ranging only from 2.9 to 3.3 W m^{-2} (additional 2010 to 2030 RF of 0.7 to 1.1 W m^{-2}) but show highly diverging values for the second half of the 21st century driven largely by CO_2. Results based on the RCP scenarios show a strong reduction in the aerosols and a substantial weakening of the negative total aerosol AF. Nitrate aerosols are an exception to this reduction with a substantial increase which is a robust feature among available models. The divergence across the RCPs indicates that, although a certain amount of future climate change is already 'in the system' due to the current radiative imbalance caused by historical emissions and the long lifetime of some emission sources, societal choices can still have a very large effect on future radiative forcing, and hence on climate change. {8.5, 8.6}

TS.3.7 Climate Feedbacks

Feedbacks will also play an important role in driving future climate change. Indeed, climate change may induce modification in the carbon, water and geochemical cycles which may reinforce (positive feedback) of dampen (negative feedback) the expected temperature increase. Water vapor and lapse rate feedbacks are now fairly well quantified, while cloud feedbacks have larger uncertainties (see TFE.6). In addition, the new Coupled Model Intercomparison Project Phase 5 (CMIP5) models consistently estimate a positive carbon-cycle feedback, i.e. reduced natural sinks or increased natural CO_2 sources in response to future climate change. In particular, carbon sinks in tropical land ecosystems are vulnerable to climate change. A key update since AR4 is the introduction of nutrient dynamics in some of the CMIP5 land carbon models, in particular the limitations on plant growth imposed by nitrogen availability. The net effect of accounting for the nitrogen cycle is a smaller predicted land sink for a given trajectory of anthropogenic CO_2 emissions (see TFE.7). {6.4, Figures 6.19–6.20, Box 6.1}. Models and ecosystem warming experiments show high agreement that wetland CH_4 emissions will increase per unit area in a warmer climate, but wetland areal extent may increase or decrease depending on regional changes in temperature and precipitation affecting wetland hydrology, so that there is limited confidence in quantitative projections of wetland CH_4 emissions. Although it is poorly constrained, the global release of CH_4 from hydrates to the atmosphere is *likely* to be low due to the under-saturated state of the ocean, long-ventilation time of the ocean, and slow propagation of warming through the seafloor. Release from thawing permafrost is *likely* to provide a positive feedback, but there is limited confidence in quantitative projections of its strength. {6.4}

Aerosol-climate feedbacks occur mainly through changes in the source strength of natural aerosols or changes in the sink efficiency of natural and anthropogenic aerosols; a limited number of modelling studies have bracketed the feedback parameter within ±0.2 W m^{-2} K^{-1} with a *low confidence*. There is *medium confidence* for a weak feedback involving dimethyl sulfide (DMS), cloud condensation nuclei (CCN)-, and cloud albedo due to a weak sensitivity of CCN population to changes in DMS emissions. Although the limited evidence is for a rather weak aerosol-climate feedback at the global scale during the 21st century, regional effects on the aerosol may be important. {7.3}

TS.3.8 Emission Metrics

Different metrics can be used to quantify and communicate the relative and absolute contributions to climate change of emissions of different substances, and of emissions from regions/countries or sources/sectors. They account for the radiative efficiency of the various substances, and their lifetime in the atmosphere. Up to AR4, the most common metric has been the global warming potential (GWP) that integrates RF out to a particular time horizon. There is now increasing focus on the Global Temperature change Potential (GTP), which is based on the change in global mean surface temperature at a chosen point in time. Both the GWP and the GTP use a time horizon (Figure TS.6a), the choice of which is highly subjective. Short-lived species, such as black carbon, or intermediate lifetime species, such as methane, show a significant contribution for short time horizons, but their impacts become progressively less for longer time horizons (Figure TS.6a). Analysis of the impact of current emissions (one-year pulse of year 2010 emissions) shows that non-CO_2 impacts are comparable in magnitude to those from CO_2 emissions over a timescale of 10–20 years, but that over timescales of 50–100 years, emissions of CO_2 dominate (Figure TS.6a). {8.7}

[INSERT FIGURE TS.6 HERE]

Figure TS.6: Global anthropogenic present-day emissions weighted by GWP and GTP for the chosen time horizons (top). Effective amount of year 2010 (single-year pulse) emissions using the Global Warming Potential (GWP), which is the global mean radiative forcing integrated over the indicated number of years relative to the forcing from CO_2 emissions, and the Global Temperature Potential (GTP) which estimates the impact on global mean temperature based on the temporal evolution of both radiative forcing and climate response relative to the impact of CO_2 emissions. The Absolute GTP (AGTP) as a function of time multiplied by the present-day emissions of all compounds from the indicated sector is used to estimate global mean temperature response (bottom; AGTP is the same as GTP, except is not normalized by the impact of CO_2 emissions). The effects of aerosols on clouds (and in the case of black carbon, on surface albedo) and aviation-induced cirrus are not included. {Figure 8.31, Figure 8.32}

One may imagine and define a large number of other metrics, down the driver-response-impact chain. No single metric can accurately compare all consequences (i.e., responses in climate parameters over time) of different emissions, and the choice of metric therefore depends strongly on the particular impact being

investigated. It is important to note that the metrics do not define policies or goals, but facilitate analysis and implementation of multi-component policies to meet particular goals. {8.7}

The GWP has received much criticism and there are serious limitations and inconsistencies related to the treatment of indirect effects and feedbacks. The uncertainty in the GWP increases with time horizon and for GWP_{100} the uncertainty is larger than 50%. Several studies also point out that this metric is not well suited for target based policies. {8.7}

With these emission metrics, past and current emissions can be attributed to various activities, which makes it possible to quantify the impact of various activities on climate. Such activity-based accounting can provide more policy-relevant information since these activities are more directly affected by particular societal choices than overall emissions. A single-year's worth of emissions (a pulse) if often used to quantify the impact on future climate. From this perspective and with the GTP metric, power generation and industry have the largest contributions to warming over the next 25–100 years (Figure TS.6b). Livestock, household burning of biofuel and fossil fuel for cooking and heating, and agriculture are also large contributors to warming, especially over shorter time horizons, due to their impact on methane and black carbon emissions. Another useful perspective is to examine the effect of sustained current emissions. Since emitted substances are removed according to their residence time, short-lived species remain at nearly constant values while long-lived gases accumulate in this analysis. In both cases, those sectors with the greatest long-term warming impacts (power and industry) lead to near-term cooling, while the relative importance of other sectors varies with time and perspective. As with RF or AF, uncertainties in aerosol impacts are large, and in particular attribution of aerosol indirect effects to individual components is poorly constrained and therefore not included. {8.7}

TS.4 Understanding the Climate System and its Recent Changes

TS.4.1 Introduction

Evidence of the effects of human influence on the climate system has continued to accumulate and strengthen since the AR4. The consistency of observed and modeled changes across the climate system, including regional temperatures, the water cycle, global energy budget, cryosphere and oceans (including aspects of ocean acidification), point to global climate change resulting primarily from anthropogenic increases in greenhouse gas concentrations. {10}

TS.4.2 Surface Temperature

Several advances since the AR4 have increased confidence in the attribution of surface temperature trends to human influence. The role of observational uncertainty has been more thoroughly investigated, and found to make a comparable contribution to uncertainties to internal climate variability. Attribution analyses carried out using CMIP5 (see Box TS.4) simulations confirm that greenhouse gases have been the dominant driver of observed warming. Compared to CMIP3, these simulations have a more complete set of forcings, better account for indirect aerosol effects, and include more simulations of the response to individual forcings, allowing their effects to be separated. Observed global mean temperature anomalies in recent years lie well outside the range of temperature anomalies in CMIP5 simulations with natural forcing only, but are consistent with the ensemble mean of CMIP5 simulations including both anthropogenic and natural forcing (Figure TS.7) {Figure 10.10} even though some individual models overestimate the warming trend, while others underestimate it. Simulations with greenhouse gas changes only, and no aerosol changes, generally exhibit stronger warming than has been observed. {Figures 10.1, 10.2} The pattern of observed warming over the period 1951–2010, characterized by warming over most of the globe with the most intense warming over the Northern Hemisphere continents is, at most locations, consistent with the mean pattern of trends in CMIP5 simulations including anthropogenic and natural forcings and inconsistent with the simulated pattern of trends in response to natural forcings only (Figure TS.7). A number of studies have investigated the effects of Atlantic Multidecadal Variability on global mean temperature. Even though some models appear to underestimate this variability, this does not compromise attribution of global-scale temperature changes (*high confidence*). Including the past ten years of data in attribution analyses helps to constrain the magnitude of greenhouse-gas-attributable warming, and does not compromise attribution results {10.3}.

[INSERT FIGURE TS.7 HERE]

Figure TS.7: Four observational estimates of global mean temperature (black lines) from HadCRUT4, GISTEMP, and NOAA NCDC, JMA, compared to model simulations [both CMIP3 – thin blue lines and CMIP5 models – thin yellow lines] with greenhouse gas forcings only (bottom panel), natural forcings only (middle panel) and anthropogenic and natural forcings (upper panel). Thick red and blue lines are averages across all available CMIP3 and CMIP5 simulations respectively. Ensemble members are shown by thin yellow lines for CMIP5, thin blue lines for CMIP3. All simulated and observed data were masked using the HadCRUT4 coverage, and global average anomalies are shown with respect to 1880–1919, where all data are first calculated as anomalies relative to 1961–1990 in each grid box. Inset to middle panel shows the four observational datasets distinguished by different colours. {Figure 10.1}

Quantification of the contributions of anthropogenic and natural forcing using multi-signal detection and attribution analyses show it is *extremely likely* that human activities (with *very high confidence*) have caused most (at least 50%) of the observed increase in global average temperatures since 1951. Detection and attribution analyses show that the greenhouse gas warming contribution of 0.6°C–1.4°C was *very likely* greater than the observed warming of 0.6°C over the period 1951–2010. The response to aerosols and other anthropogenic forcings appears to be less clearly detectable using CMIP5 models than it was using CMIP3 models, but they probably contributed a net cooling over this period (Figure TS.8). Such analyses also indicate a trend of less than 0.1°C was attributable to combined forcing from solar irradiance variations and volcanic eruptions over this period. Taken together with other evidence this indicates that it is *extremely unlikely* that the contribution from solar forcing to the warming since 1950 was larger than that from greenhouse gases. Better understanding of pre-instrumental data shows that observed warming over this period is far outside the range of internal climate variability estimated from such records, and it is also far outside the range of variability simulated in climate models. Based on the surface temperature record, we therefore assess that it is *virtually certain* that warming since 1950 cannot be explained by internal variability alone. {10.3}

[INSERT FIGURE TS.8 HERE]

Figure TS.8: Estimated contributions from greenhouse gas (red), other anthropogenic (green) and natural (blue) components to observed global surface temperature changes a) from HadCRUT4 showing 5 to 95% uncertainty limits on scaling factors estimated using 8 climate models and a multi-model average (multi) and based on an analysis over the 1951–2010 period and b) The corresponding estimated contributions of forced changes to temperature trends over the 1951–2010 period. {Figure 10.4}

The instrumental record shows a pronounced warming during the first half of the 20th century. Consistent with AR4, we conclude that it is *very likely* that early 20th century warming is due in part to external forcing. It remains difficult to quantify the contributions to this early century warming from internal variability, natural forcing and anthropogenic forcing, due to forcing and response uncertainties and incomplete observational coverage. {10.3}

TFE.3: Comparing Projections of Temperature Change with Observations Over the Last Two Decades

Results of projected changes in CO_2, global mean surface temperature and global mean sea level from previous IPCC assessment reports are quantitatively compared with the best available observational estimates. The comparison between the four reports highlights the evolution in our understanding of how the climate system responds to changes in both natural and anthropogenic forcing and provides an assessment of how the projections compare with observational estimates. TFE.3, Figure 1, for example, shows the projected and observed estimates of: (i) CO_2 changes (top panel), (ii) global mean surface temperature anomaly relative to 1961–1990 (middle panel) and (iii) global mean sea level relative to 1990 (bottom panel). {2.4, 3.7, 6.3, 13.3}

[INSERT TFE.3, FIGURE 1 HERE]

TFE.3, Figure 1: [PLACEHOLDER FOR FINAL DRAFT: Observational datasets will be updated as soon as they become available] (top) Observed globally and annually averaged carbon dioxide concentrations in parts per million (ppm) since 1990 compared with projections from the previous IPCC assessments. Observed global annual CO_2 concentrations are shown in black (based on NOAA Earth System Research Laboratory measurements). The uncertainty of the observed values is 0.1 ppm. The shading shows the largest model projected range of global annual CO_2 concentrations from 1990 to 2015 from FAR (Scenario D and business-as-usual), SAR (IS92c and IS92e), TAR (B2 and A1p), and AR4 (B2 and A1B). (middle) Estimated changes in the observed globally and annually averaged surface temperature (in °C) since 1990 compared with the range of projections from the previous IPCC assessments. Values are aligned to match the average observed value at 1990. Observed global annual temperature change, relative to 1961–1990, is shown as black squares (NASA, NOAA, and UK Hadley Centre reanalyses). Whiskers indicate the 90% uncertainty range from measurement and sampling, bias and coverage (see Supplementary Material for Chapter 1 for methods). The coloured shading shows the projected range of global annual mean near surface temperature change from 1990 to 2015 for models used in FAR (Scenario D and business-as-usual), SAR (IS92c/1.5 and IS92e/4.5), TAR (full range of TAR Figure 9.13(b) based on the GFDL_R15_a and DOE PCM parameter settings), and AR4 (A1B and A1T). The 90% uncertainty estimate due to observational uncertainty and internal variability based on the HadCRUT4 temperature data for 1951–1980 is depicted by the grey shading. Moreover, the publication years of the assessment reports and the scenario design are shown. (bottom) Estimated changes in the observed global annual sea level since 1990. Estimated changes in global annual sea level anomalies from tide gauge data (black error bars showing 1σ uncertainty) and based on annual averages from TOPEX and Jason satellites (blue dots) starting in 1992 (the values have been aligned to fit the 1993 value of the tide gauge data). The shading shows the largest model projected range of global annual sea level rise from 1990 to 2015 for FAR (Scenario D and business-as-usual), SAR (IS92c and IS92e), TAR (A2 and A1FI) and based on the CMIP3 model results available at the time of AR4 using the SRES A1B scenario. Additional details and references for data given in Chapter 1 {1.3.1, 1.3.2}. {Figure 1.4, Figure 1.6, Figure 1.11}

CO_2 Changes

From 1990–2011 the observed concentrations of atmospheric CO_2 have steadily increased. Considering the period 1990–2011, the observed CO_2 concentration changes lie within the envelope of the scenarios used in the four assessment reports. As the most recent assessment, AR4 has the narrowest scenario range and the observed concentration follows this closely except perhaps in the early part of the record (1990–2000). During 2002–2011, atmospheric CO_2 concentrations increased at a rate of 1.9 to 2.1 ppm yr^{-1}. {6.3, Table 6.1}

Global Mean Temperature Anomaly

Relative to the 1961–1990 mean, the global mean surface temperature anomaly has been positive and larger than 0.25°C since 2001. Overall the observed temperature record lies within the total range of uncertainty (i.e., the combined effects of scenario uncertainty, observational uncertainty and uncertainty due to natural variability; area enclosed in grey—it should be noted that global mean temperature has relative large natural variability). Mount Pinatubo erupted in 1991 (FAQ 11.2 for discussion of how volcanoes impact the climate system) leading to a brief period of relative global mean cooling during the early 1990's. The FAR, SAR and TAR did not include the effects of volcanic eruptions and thus failed to include the cooling associated with the Pinatubo eruption. AR4, however, did include the effects from volcanoes and did simulate successfully the associated cooling. During 1995–2000 the global mean temperature anomaly was quite variable—a significant fraction of this variability was due to the large El Niño in 1997–1998 and the strong back-to-back La Niña's in 1999–2001. The projections associated with these assessment reports do not attempt to capture the actual evolution of these El Niño and La Niña events, but includes them as uncertainty due to natural variability as encompassed by the grey regions (TFE.3, Figure 1). From 2000–2011 the observational estimates have largely been on the low end of the range given by the scenarios alone. While the trend in global mean temperature since 1998 is not significantly different from zero, it is also consistent with natural variability superposed on the long-term anthropogenic warming trends projected by climate models. {2.4.3, Figure 2.21}

Global Mean Sea Level

Based on both tide gauge and satellite altimetry data, relative to 1990, the global mean sea level has continued to rise. While the increase is fairly steady, both observational records show short periods of either

no change or a slight decrease. The observed estimates lie within the envelope of all the projections except perhaps in the 1990s. The sea level rise uncertainty due to scenario-related uncertainty is smallest for the most recent assessment (AR4) and observed estimates lie well within this scenario-related uncertainty. It is *virtually certain* that over the 20th century the mean rate of sea level increase was between 1.4 to 2.0 mm yr^{-1} and between 2.7 and 3.7 mm yr^{-1} since 1993 (see TFE.2). {3.7.2, 3.7.4, Figures 3.12–3.14, 13.3}

TS.4.3 Atmospheric Temperature

A number of studies since the AR4 have investigated the consistency of simulated and observed trends in free tropospheric temperatures (see section TS.2). Despite the considerable observational uncertainties, there is *high confidence* that most, though not all, CMIP3 and CMIP5 models overestimate the warming trend in the tropical troposphere during the satellite period 1979–2011. The cause of this bias remains elusive. Nonetheless, analysis of both radiosonde and satellite datasets, combined with CMIP5 and CMIP3 simulations continues to find that observed tropospheric warming is inconsistent with internal variability and simulations of the response to natural forcings alone. Over the period 1961–2010 CMIP5 models simulate tropospheric warming driven by greenhouse gas changes, with only a small offsetting cooling due to the combined effects of changes in reflecting and absorbing aerosols and tropospheric ozone. We conclude, consistent with the AR4, that it is *likely* that the warming of the troposphere is attributable to anthropogenic forcings dominated by greenhouse gases. {2.4, 9.4, 10.3}

CMIP5 simulations including greenhouse gas, ozone and natural forcing changes broadly reproduce the observed evolution of lower stratospheric temperature, with some tendency to underestimate the observed cooling trend over the satellite era (see Section TS.2). New attribution studies of stratospheric temperature, considering the responses to natural forcings, greenhouse gases and ozone-depleting substances, demonstrate that it is *very likely* that the cooling of the lower stratosphere is primarily attributable to ozone depleting substances. CMIP5 models simulate only a very weak cooling of the lower stratospheric in response to historical greenhouse gas changes {Figure 10.8}, and the influence of greenhouse gases on lower stratospheric temperature has not been formally detected. Considering both regions together, we conclude, consistent with AR4, that the pattern of tropospheric warming and stratospheric cooling observed since 1960 is *very likely* due to the influence of anthropogenic forcings. {2.4, 9.4, 10.3}

TS.4.4 Oceans

The observed upper-ocean warming during the late 20th and early 21st centuries and its causes has been assessed more completely using updated observations and more simulations {Box 3.1, 10.4.1, see Section TS.2}. The long term trends and variability in the observations are most consistent with simulations of the response to both anthropogenic forcing and volcanic forcing. The anthropogenic fingerprint in observed upper-ocean warming, consisting of global mean and basin-scale pattern changes has also been detected. This result is robust to a number of observational, model and methodological or structural uncertainties {10.4.1}. It is *very likely* that more than half of the rise in ocean temperatures observed since the 1970s is caused by external forcing. This ocean warming is also causing thermal expansion and it is *extremely likely* that there is an anthropogenic influence on the global steric sea level rise for this period {10.4.3}.

Observed surface salinity changes also suggest an amplification in the global water cycle has occurred {3.3, FAQ 3.3, Figure 3.4, Figure 10.14b, 10.3.2, 10.4.2}. The long term trends show that there is a strong positive correlation between the mean climate of the surface salinity and the temporal changes of surface salinity from 1950 to 2000, suggesting an enhancement of the climatological salinity pattern—so fresh areas gets fresher and salty areas gets saltier {3.3, FAQ3.3, 10.4.2}. For the period 1950–2000 the observations of surface salinity amplification, (as a function of global temperature increase per degree surface warming), is $16 \pm 10\%$ K^{-1} and is about twice the simulated surface salinity change in CMIP3 models. However, the inferred water flux in the same models show an increase of the hydrological cycle to be about $8 \pm 5\%$ K^{-1} consistent with the pattern of temporal change in observations and with the response expected from the Clausius-Clapeyron equation {Figure 9.9, 9.4.1, 10.4.2}. Salinity changes taken from the simulations with only natural forcings do not match the observations at all, thus excluding the hypothesis that observed trends are can be explained by just solar or volcanic variations. It is *likely* (*high confidence*) that observed changes

in ocean surface and sub-surface salinity are due in part to anthropogenic increases in greenhouse gases {10.4.2}.

Global analyses of oxygen data from the 1960's to 1990's extend the spatial coverage from local to global scales. The observations of decreased oxygen (see Figure TS.3) {3.8.3} and increased surface temperatures {10.3.2}, increased ocean heat content {10.4.1} and observed increased ocean stratification {3.2.2}, when taken together with the physical understanding from simulations of oxygen change forced by increasing greenhouse gases, suggest it is *as likely as not* that the observed oxygen decreases can be attributed to human influences {3.2.2, 3.8.3, 10.3.2, 10.4.1, 10.4.4}.

TFE.4: The Changing Energy Budget of the Global Climate System

A fundamental aspect of the Earth's climate system is its global energy budget, which is dependent on many phenomena of the system. The ocean has stored over 90% of the increase in energy in the climate system over recent decades {Box 3.1}, resulting in ocean thermal expansion and hence sea level rise {3.7, 9, 13.4}.

The rate of storage of energy in the Earth system must be equal to the net downward radiative flux at the top of the atmosphere (TOA), this flux being the difference between radiative forcing, due to changes imposed on the system, and the radiative response of the system. There are also significant transfers of energy between components of the climate system and from one location to another.

The focus here is on the Earth's global energy budget since 1970, when better global observational data coverage is available.

The radiative forcing of the climate system has increased as a result of increases in well-mixed (long-lived) greenhouse gas concentrations, changes in short-lived greenhouse gases (tropospheric and stratospheric ozone and stratospheric water vapour), and an increase in solar irradiance {Box 13.1}, (TFE.4, Figure 1a). Simultaneously, the radiative forcing of the climate system has decreased as a result of changes in tropospheric aerosols, which reflect sunlight and furthermore enhance the brightness of clouds; of stratospheric aerosols arising from volcanic eruptions (two major eruptions since 1970, El Chichón in Mexico in 1982 and Mt Pinatubo in the Philippines in 1991, and other smaller eruptions) and for several years reflecting more incoming solar radiation; and of an increase in the surface albedo from land use change. Black carbon, including that on snow and ice, is a small positive radiative forcing but is not included here. The integrated effect of these changes in radiative forcing has been an energy gain of the climate system since 1970 {Box 13.1}, (TFE.4, Figure 1a).

[INSERT TFE.4, FIGURE 1 HERE]

TFE.4, Figure 1: The Earth's energy budget from 1970 through 2010. (a) The cumulative energy flux into the Earth system from changes in well-mixed greenhouse gases, short-lived greenhouse gases, solar forcing, surface albedo caused by land use, volcanic forcing, and tropospheric aerosol forcing are shown by the coloured lines; these contributions are added to give the total energy changes (dashed black line). (b) The cumulative total energy change from (a), with an expanded scale, is balanced by the energy absorbed in the melting of ice; the warming of the atmosphere, the land, and the ocean; and the increase in outgoing radiation inferred from the temperature change of a warming Earth. These terms are represented by the time-varying thicknesses of the coloured regions. The residuals in the cumulative energy budget are indicated by the difference between the red lines and the horizontal zero line. {Box 13.1, Figure 1}

As the climate system warms, energy is lost to space through increased outgoing radiation. This radiative response by the system is predominantly due to increased thermal grey-body radiation, but is modified by climate feedbacks, such as changes in water vapour, surface albedo and cloud, which affect both outgoing long-wave and reflected shortwave radiation. The TOA fluxes have been measured by the Earth Radiation Budget Experiment (ERBE) satellites from 1985 to 1999 and the Cloud and the Earth's Radiant Energy System (CERES) satellites from March 2000 to the present. The TOA radiative flux measurements are highly precise, allowing identification of changes in the Earth's net energy budget from year to year within the ERBE and CERES missions, but the absolute calibration of the instruments is not sufficiently accurate to

allow determination of the absolute TOA energy flux or to provide continuity across missions. Figure TFE4.1b relates the cumulative total energy change of the Earth system to the change in energy storage and the cumulative outgoing radiation. Calculation of the latter is based on the observed globally averaged surface temperature ΔT, which is multiplied by the climate feedback parameter α, which in turn, is related to the equilibrium climate sensitivity {9.7.2}. The mid-range value for α, 1.23 W m^{-2} ºC^{-1}, is equivalent to a radiative forcing for a doubled CO_2 concentration of 3.7 W m^{-2} combined with an equilibrium climate sensitivity of 3.0°C (assessed in Box 12.1 to be the most likely value). Following Box 12.1, the climate feedback parameter α is *likely* to be in the range from 0.82 W m^{-2} ºC^{-1} (corresponding to an equilibrium climate sensitivity of 4.5°C) to 1.85 W m^{-2} °C^{-1} (corresponding to an equilibrium climate sensitivity of 2.0ºC).

If radiative forcing was fixed, the climate system would eventually warm sufficiently that the radiative response would balance the radiative forcing, and there would be no further change in energy storage in the climate system. However, the forcing is increasing, and the ocean's large capacity to store heat means the climate system is not in radiative equilibrium, and has stored energy {Box 13.1, Box 3.1}, (TFE.4, Figure 1b). This storage provides strong evidence of a changing climate. The majority of this additional heat is in the upper 750 m of the ocean, but there is also warming in the deep and abyssal ocean {Box 3.1}. The associated thermal expansion of the ocean has contributed about 40% of the observed sea level rise since 1970 {Section 13.4.2}. A small amount of additional heat has been used to warm the continents, warm and melt glacial and sea ice, and warm the atmosphere {Box 3.1, Box 13.1, Figure 1b}.

The magnitude of the residual in the energy budget in 2010 {TFE.4, Figure 1b, red line} is about 10% of the total energy accumulated for the central value of climate sensitivity of 3°C. A positive residual would mean that the cumulative forcing is apparently greater than the heat lost and stored by the system. Over the period from 1970 to 2012, this residual is small, less than 0.2 W m^{-2}, and is consistent with a climate sensitivity well within the range of climate sensitivities of 2.0°C to 4.5°C {10.9, Box 12.1}. Most of this residual occurs in the last 15 years and would imply a small unaccounted negative forcing of the climate system or a climate sensitivity slightly less than 3.0°C but within the range of accepted values. Nevertheless, with any of these choices, the residual is smaller than the uncertainties and confirms our understanding of climate change and provides evidence that no major forcings of climate are omitted in current climate assessments[7].

In addition to these forced variations in Earth's energy budget, there is also internal variability on decadal time scales. Observations and models indicate that (because of the very small heat capacity of the atmosphere) a decade of steady or even decreasing surface temperature can occur in a warming world. Climate model simulations indicate these periods are associated with a transfer of heat from the upper to the deeper ocean, of the order 0.1 W m^{-2}, with a near steady or an increased radiation to space, again of the order 0.1 W m^{-2}. While these natural fluctuations represent a large amount of heat, they are significantly smaller than the anthropogenic forcing of the Earth's energy budget.

These independent estimates of radiative forcing, observed energy storage, and surface warming combine to give an energy budget for the Earth that is *very likely* closed, and is consistent with our best estimate of climate sensitivity. Changes in the Earth's energy storage are thus a powerful observation for the detection and attribution of climate change.

TS.4.5 Cryosphere

Reductions in Arctic sea ice {4.2.2, 10.5.1, Table 10.1} and northern hemisphere snow cover extent {4.5, 10.5.3}, permafrost degradation {4.6, 10.5.3} and glacier retreat and increased surface melt of Greenland {4.4, 10.5.1} (see TS.2) are evidence of systematic changes in the cryosphere linked to anthropogenic climate change. It is *likely* that anthropogenic forcings have contributed to the reduction in Arctic sea ice and the increased surface melt of Greenland. It is *likely* that there has been an anthropogenic component to

[7] The geothermal heat flux is small (less than 2×10^{21} J from 1970 to 2010 and changes little over the period considered. Although increasing rapidly, the energy released by the burning of fossil fuels is also small, less than 1×10^{21}.

observed reductions in snow cover and permafrost. It is *likely* that glaciers have diminished significantly due to human influence since the 1960s {10.5, Table 10.1}.

Attribution studies, comparing the seasonal evolution of Arctic sea ice extent from observations with those simulated by an ensemble of simulations for 1953–2006, demonstrate that human influence on the sea ice extent changes can be robustly detected since the early 1990s {10.5.1}. The detection result is also robust even if the effect of the internal variability such as Northern Annular Mode on observed sea ice change is removed. The anthropogenic signal is also detectable for individual months from May to December, suggesting that human influence, strongest in late summer, now also extends into colder seasons. On all recent timescales assessed (up to 50+ years), it is *very likely* that the most extreme negative summer sea ice trends observed cannot be explained by modelled internal variability alone (Figure TS.9) {10.4.1}.

Sea ice extent in the Antarctic has increased slightly since the 1970s, though the increase may not be significant compared to internal variability or inconsistent with simulated changes in ice extent. Untangling the processes involved with trends and variability in Antarctica and surrounding waters remains complex and several studies are contradictory. We therefore have *low confidence* in the scientific understanding of the observed increase in Antarctic sea ice extent. However the trends are small in both observations and CMIP5 simulations and within the bounds of internal variability. (Figure TS.9) {10.4.1}

Greenland ice sheets show recent major melting episodes in response to record temperatures relative to the entire 20th century associated with persistent shifts in early summer atmospheric circulation, and these have become more pronounced since 2007. While many Greenland records are relatively short (two decades), regional modelling and observations tell a consistent story of the response of Greenland temperatures and ice sheet runoff to shifts in regional atmospheric circulation associated with larger scale flow patterns and global temperature increases. Mass loss and melt is also occurring in Greenland through the intrusion of warm water into the major fjords containing glaciers such as Jacobshaven Glacier. It is *likely* that anthropogenic forcing and internal variability are both contributors to recent observed changes on the Greenland ice sheet. {10.5.2}

Estimates of ice mass in Antarctica since 2000 show that the greatest losses are at the edges, with a tendency for mass gains in the interior. An analysis of observations underneath a floating ice shelf off West Antarctica leads to the conclusion that ocean warming and more transport of heat by ocean circulation are largely responsible for accelerating melt rates. The underlying cause for the increased melt from the warming oceans depends on whether or not anthropogenic forcing is a contributor of ocean warming in the Southern Ocean {3.2}, and to the changing wind patterns. The observational record of Antarctic mass loss is short and the internal variability of the ice sheet is poorly understood. These factors combined with incomplete models of Antarctic ice sheet mass loss result in *low confidence* in scientific understanding, and attribution of changes in mass balance of Antarctica to human influence is premature {3.2, 4.2, 4.4.3, 10.5.2}.

The robustness of the estimates of observed mass loss {4.3}, the certainty we have for estimates of natural variations and internal variability from long term glacier records, and our understanding of glacier response to climatic drivers provides *high confidence* and it is *likely* that the substantial mass loss of glaciers is due to human influence {10.5.2, Table 10.1}.

TFE.5: Irreversibility and Abrupt Change

Several components or phenomena in the climate system may exhibit abrupt or nonlinear changes, and some have done so in the past. Examples include the Atlantic Meridional Overturning Circulation (AMOC), sea-ice cover {5.7, 5.5.2}, the position of the intertropical convergence zone (ITCZ) and monsoonal circulations {5.7, 14.2.2} and the Amazon forest {12.5.5}. Here, *abrupt climate change* is defined as a large-scale change in the climate system that takes place over a few decades or less, persists (or is anticipated to persist) for at least a few decades, and causes substantial disruptions in human and natural systems. For some events, there is information on potential consequences, but in general there is *low confidence* and little consensus on the likelihood of such events over the 21st century {12.5.5}.

A number of components or phenomena within the Earth system have been proposed as potentially possessing critical thresholds, or tipping points, beyond which an abrupt or irreversible transition to a different state ensues. A change is said to be *irreversible* on a given time scale if the removal of the perturbation that caused the system to pass a tipping point does not lead to a recovery of the component or phenomenon within the Earth system due to natural processes within this time scale. In the context of interest here, the pertinent time scale is centennial. {5.7, 5.8}

Abrupt Climate Change Linked with AMOC

Since AR4, the documentation of abrupt climate changes in the past using multiple sources of proxy evidence has provided important benchmarks to test instability mechanisms in climate models as well as their capacity to simulate teleconnection patterns and inter-hemispheric linkages which are relevant for projections of future climate changes {5.7}.

Since AR4, progress has been made to quantify the magnitude of abrupt temperature changes at different latitudes, and the bipolar sequence of events {5.7}. The abrupt event that occurred under near-modern boundary conditions about 8,200 years ago was due to catastrophic freshwater inflows into the North Atlantic Ocean (10^{14} m^3 possibly within <0.5 year), producing a weakening of the AMOC with worldwide impacts, and a recovery within about 200 years (*high confidence*). New transient climate model simulations have confirmed with *high confidence* that changes of the AMOC induced by freshwater perturbation produce abrupt climate changes with magnitude and pattern resembling reconstructed past abrupt events (with the exception of the rate of abrupt warming in Greenland) {5.8.2}.

Confidence in the link between changes in North Atlantic climate and low-latitude precipitation has increased since AR4. Based on evidence from reconstructions supported by modelling experiments, it is *very likely* that North Atlantic cooling during glacial stadials in combination with a weakening of the AMOC caused southward shifts of the Atlantic ITCZ and affected global monsoon systems, causing droughts in some regions and wet phases in others. {5.7}

While many more model simulations have been conducted since the AR4 under a wide range of future forcing scenarios, projections of the AMOC behaviour have not changed. It remains *very likely* that the AMOC will weaken over the 21st century relative to preindustrial values with a best estimate decrease in 2100 of about 0–5% for the RCP2.6 scenario and 36–44% for the RCP8.5 scenario. It also remains *very unlikely* that the AMOC will undergo an abrupt transition or collapse in the 21st century for the scenarios considered (TFE.5, Figure 1). For an abrupt transition of the AMOC to occur, the sensitivity of the AMOC to forcing would have to be far greater that seen in current models, or would require meltwater flux from the Greenland ice sheet greatly exceeding even the highest of current projections. While neither possibility can be excluded entirely, it is *unlikely* that the AMOC will collapse beyond the end of the 21st century for the scenarios considered. {12.5.5}

[INSERT TFE.5, FIGURE 1 HERE]

TFE.5, Figure 1: Atlantic Meridional Overturning Circulation strength (Sv) as a function of year, from 1850 CE to 2100 CE as simulated by different OAGCMs in response to scenario RCP2.6 (left) and RCP8.5 (right). {Figure 12.35}

Termination Effect of Geoengineering

Since the AR4, it has been recognized that, if solar radiation management (SRM) were put in place to mitigate the effects of CO_2 forcing, there would be a risk of future rapid climate change arising if SRM ceased before CO_2 concentrations returned to present or preindustrial levels. High CO_2 concentrations from anthropogenic emissions will persist in the atmosphere for a long time (for more than a thousand years in the absence of CO_2 reduction). If SRM were used to counter positive forcing, it would be needed as long as the CO_2 concentrations were high. If greenhouse gas concentrations increase, then the scale of SRM to offset the resulting warming would need to increase, with amplifying residual effects from increasingly imperfect compensation (*high confidence*). Simulations have been conducted to assess the impacts of a termination of

SRM, robustly showing rapid rebound to temperature levels consistent with CO_2 forcing within one to two decades {7.7.3}

Irreversibility

Permafrost. The conjunction of a long carbon accumulation time scale and potential decomposition under climatic conditions leading to permafrost thaw suggests potential irreversibility of permafrost carbon decomposition (leading to an increase of atmospheric CO_2 and/or CH_4 concentrations) on timescales of hundreds to thousands of years in a warming climate. The existing modelling studies of permafrost carbon balance under future warming that take into account at least some of the essential permafrost-related processes do not yield consistent results beyond the fact that present-day permafrost will become a net emitter of carbon during the 21st century under plausible future warming scenarios. This also reflects an insufficient understanding of the relevant soil processes during and after permafrost thaw, including processes leading to stabilization of unfrozen soil carbon, and precludes any quantitative assessment of the amplitude of irreversible changes in the climate system potentially related to permafrost degassing and associated global feedbacks at this stage. {6.4.7; 12.5.5}

Clathrates. Deposits of methane clathrates below the sea floor are susceptible to destabilization via ocean warming. However, sea level rise due to changes in ocean mass enhances clathrate stability in the ocean. Anthropogenic warming will *very likely* lead to enhanced methane emissions from both terrestrial and oceanic clathrates. While difficult to formally assess, initial estimates of the 21st century feedback from methane clathrate destabilization are small but not insignificant. On multi-millennial timescales, such methane emissions provide a positive feedback to anthropogenic warming and are irreversible, due to the difference between release and accumulation timescales. {6.4.7; 12.5.5}

Forests. Uncertainty concerning the existence tipping points in the Amazonian and other tropical rainforests purely driven by climate change remains high, and so the possibility of a tipping point being crossed in precipitation volume and duration of dry seasons cannot be ruled out. Potential tipping points in the boreal forest are also highly uncertain, but their existence cannot at present be ruled out. {12.5.5}

Sea ice. The reversibility of sea ice loss has been directly assessed in sensitivity studies to CO_2 increase and decrease with AOGCMs or ESMs. None of them show evidence of a critical irreversible change in Arctic sea ice at any point. By contrast, as a result of the strong coupling between the Southern Ocean's surface and the deep ocean, the Antarctic sea ice in models integrated with ramp-up and ramp-down atmospheric CO_2 concentration exhibits some asymmetric behavior, so that its changes may be considered as irreversible on centennial time scales. {12.5.5}

Ice sheet surface mass balance. Irreversibility of ice sheet volume and extent changes can arise because of the feedback that operates when a decrease of the surface elevation of the ice sheet induces a decreased surface mass balance. This arises generally through increased surface melting, and therefore applies in the 21st century to Greenland, but not to Antarctica, where surface melting is currently very small. Surface melting in Antarctica is projected to become important after several centuries under high-GHG scenarios. With its present topography, surface melting of the Greenland ice sheet is projected to exceed accumulation for global mean surface air temperature over 3.1 [1.9–4.6] °C above preindustrial, leading to ongoing decay of the ice sheet. The reduction in surface elevation as ice is lost increases the vulnerability of the ice sheet; taking this into account, one study estimated a lower threshold of 1.6 [0.8–3.2] °C. The loss of the ice sheet is not irreversible because it has long time scales, and it might re-grow to its original volume or some fraction thereof if global temperatures decline. However, a significant decay of the ice sheet may be irreversible. {13.4.3, 13.4.4}

Ice sheet outflow. Abrupt change in ice-sheet outflow to the sea may be caused by unstable retreat of the grounding line in regions where the bedrock is below sea level and slopes downwards towards the interior of the ice sheet. This mainly applies to West Antarctica, but also to parts of East Antarctica and Greenland. Such abrupt ice discharge is documented from deep sea sediment records to have occurred several times during warm periods of the last 5 million years. Grounding line retreat could be triggered by ice-shelf decay, due to warmer ocean water under ice shelves enhancing submarine ice-shelf melt, or melt water ponds on the

surface of the ice shelf promoting ice-shelf fracture. Because ice sheet growth is a slow process, such changes would be irreversible in the definition adopted here. {13.4.4, Box 13.2}

TS.4.6 Water Cycle

Since the AR4, new evidence has emerged of a detectable human influence on several aspects of the water cycle. There is *medium confidence* that observed changes in near-surface specific humidity contain a detectable anthropogenic component. The anthropogenic water vapour fingerprint simulated by an ensemble of climate models has been detected in lower tropospheric moisture content estimates derived from SSM/I data covering the period 1988–2006, although anthropogenic and natural influence were not separated. An anthropogenic contribution to increases in tropospheric specific humidity is found with *medium confidence*. Remaining observational uncertainties preclude a more confident assessment {2.4, 10.3}.

Attribution studies of global zonal mean terrestrial precipitation and Arctic precipitation both find a detectable anthropogenic influence. Overall we conclude that there is *medium confidence* in a significant human influence on global scale changes in precipitation patterns, including increases in northern hemisphere mid to high latitudes. Remaining observational and modeling uncertainties and the large effect of internal variability on observed precipitation preclude a more confident assessment. {2.5, 10.3}

The collected evidence for changes in (with varying levels of confidence and likelihood) specific humidity, terrestrial precipitation, ocean surface and subsurface salinity, and from physical understanding of precipitation, we conclude that change in the water cycle is *very likely* (*high confidence*) to be in part attributable to rising greenhouse gases. {2.4, 2.5, 3.3, FAQ 3.3, 9.4.1, 10.3, 10.4.2}

TS.4.7 Climate Extremes

Several new attribution studies have found a detectable anthropogenic influence in the observed increased frequency of warm days and nights and decreased frequency of cold days and nights. Since the AR4, there is new evidence for detection of human influence on extremely warm daytime temperature and there is new evidence that the influence of anthropogenic forcing may be detected separately from the influence of natural forcing at global scales and in some continental and sub-continental regions. This strengthens the AR4 conclusion that surface temperature extremes have *likely* been affected by anthropogenic forcing, and we now conclude that it is *very likely* that anthropogenic forcing has contributed to the observed changes in temperature extremes since the mid-20th century. Several new studies have found that the probability of occurrence of some observed extreme warm temperature events has increased substantially due to the large-scale warming since the mid-20th century. Since most of this warming is *very likely* due to the increase in atmospheric greenhouse gas concentrations, it is possible to attribute, via a multi-step process, some of the increase in probability of these events to human influence on climate. Based on such results, we now conclude that it is *likely* that human influence has significantly increased the probability of some observed heat waves. {10.6}

Since the AR4, a number of studies have provided evidence for an anthropogenic influence on extreme precipitation, including formal detection and attribution studies. There is now *medium confidence* that anthropogenic forcing has contributed to a trend towards increases in the frequency of heavy precipitation events over the second half of the 20th century over land regions with sufficient observations. {10.6}

New research demonstrates the sensitivity of cyclone intensity to SST gradients rather than mean SST, suggesting that cyclone intensity is not necessarily expected to increase with SSTs in the corresponding formation region. Globally, there is *low confidence* in any long term increases in tropical cyclone activity and *low confidence* in attribution of global changes to any particular cause. In the North Atlantic region there is *medium confidence* that a reduction in aerosol forcing over the North Atlantic has contributed at least in part to the observed increase in tropical cyclone activity there since the 1970s. There remains substantial disagreement on the relative importance of internal variability, greenhouse gas forcing, and aerosols for this observed trend. {2.6, 10.6}

While the AR4 concluded that it is *more likely than not* that anthropogenic influence has contributed to an increase in the droughts observed in the second half of the 20th century, an updated assessment of the observational evidence indicates that the AR4 conclusions regarding global increasing trends in hydrological droughts since the 1970s are no longer supported. Owing to the *low confidence* in observed large-scale trends in dryness combined with difficulties in distinguishing decadal-scale variability in drought from long-term climate change we now conclude there is *low confidence* in the attribution of changes in drought over global land since the mid-20th century to human influence. {2.6, 10.6}

TS.4.8 From Global to Regional

Taking a longer term perspective shows the substantial role played by external forcings in driving climate variability on hemispheric scales, even in pre-industrial times (Box TS.3). While internal variability of the climate system, with its ability to move heat around the climate system, is important at hemispheric scales, it is *very unlikely* that reconstructed temperatures since 1400 can be explained by natural internal variability alone. Climate model simulations that include only natural forcings can explain a substantial part of the pre-industrial inter-decadal temperature variability since 1400 on hemispheric scales. However such simulations fail to explain more recent warming since 1950 without the inclusion of anthropogenic increases in greenhouse gas concentrations (see Box TS.3). {10.7, Table 10.1}

The evidence is stronger that observed changes in the climate system can now be attributed to human activities on global and regional scales in many components (Figure TS.9). Observational uncertainty has been explored much more thoroughly than previously and fingerprints of human influence deduced from a new generation of climate models. Better understanding of pre-instrumental data shows that warming since the mid-20th century is far outside the range of internal climate variability estimated from such records. There is improved understanding of ocean changes, including salinity changes, that are consistent with large scale intensification of the hydrological cycle predicted by climate models. The changes in near surface temperatures, free atmosphere temperatures, ocean temperatures, and the Northern Hemisphere snow cover and sea ice extent, when taken together, show not just global mean changes, but distinctive regional patterns consistent with the expected fingerprints of change from anthropogenic forcings and the expected responses from volcanic eruptions (Figure TS.9). {10.3–10.6, 10.9}

[INSERT FIGURE TS.9 HERE]

Figure TS.9: Detection and attribution signals in some elements of the climate system. Brown panels are land surface temperature time series, green panels are precipitation time series, blue panels are ocean heat content time series, and white panels are sea-ice time series. On each panel is observations (shown in black or black and shades of grey as in ocean heat content). Blue shading is the model time series for natural forcing simulations and red shading is the natural and anthropogenic forcings. The dark blue and dark red lines are the ensemble means from simulations. For surface temperature the 5 to 95% interval is plotted (and Figure 10.1). The observed surface temperature is from HadCRUT4. For precipitation data the mean and one standard deviation shading of the simulations is plotted. Observed precipitation is from the Global Historical Climatology Network (GHCN). For Ocean Heat Content the mean and one standard deviation shading is plotted for an ensemble of CMIP5 models. Three observed records of OHC are shown. The sea ice extents simulations and observations are the same as in Figure 10.15. More details are in the supplementary materials (Appendix 10.A: Notes and technical details on figures displayed in Chapter 10). {Figure 10.20}

Further evidence has accumulated on the detection and attribution of anthropogenic influence on climate change in different parts of the world. Over every continent except Antarctica, anthropogenic influence has *likely* made a substantial contribution to surface temperature increases since the mid-20th century (Figure TS.9). It is *likely* that there has been significant anthropogenic warming in Arctic land surface temperatures over the past 50 years. Detection and attribution at regional scales due to greenhouse gases is complicated by the greater role played by dynamical factors (circulation changes), a greater range of forcings that may be regionally important, and the greater difficulties of modelling relevant processes at regional scales. Nevertheless, human influence has *likely* contributed to temperature in many sub-continental regions. {10.3}

Changes in atmospheric circulation are important for local climate change since they could lead to greater or smaller changes in climate in a particular region than elsewhere. It is *likely* that human influence has altered sea level pressure patterns globally. There is *medium confidence* that stratospheric ozone depletion has

contributed to the observed poleward shift of the southern Hadley Cell border during Austral summer. It is *likely* that stratospheric ozone depletion has contributed to the positive trend in the Southern Annular Mode seen in Austral summer since 1951 which corresponds to sea level pressure reductions over the high latitudes, an increase in the subtropics, and a southward shift of the storm tracks (Figure TS.10). {10.3}

[INSERT FIGURE TS.10 HERE]

Figure TS.10: Simulated and observed 1951–2011 trends in the Southern Annular Mode (SAM) index (b) by season. The SAM index is a difference between mean SLP at stations located at close to 40°S and stations located close to 65°S. The SAM index is defined without normalization, so that the magnitudes of simulated and observed trends can be compared. Black lines show observed trends from the HadSLP2r dataset (solid), the 20th century Reanalysis (dotted) and the SAM index (dashed). While the synthetic indices have data present from 1951, the SAM index itself begins in 1957. Grey bars show approximate 5th-95th percentile ranges of control trends, and coloured bars show 5–95% significance ranges for ensemble mean trends in response to greenhouse gas (red), aerosols (green), ozone (light blue) and natural (dark blue) forcings, based on CMIP5 individual forcing simulations. {Figure 10.12}

The coherence of observed changes with simulations of anthropogenic and natural forcing in the physical system is remarkable (Figure TS.9), particularly for temperature related variables. Surface temperature and ocean heat content show emerging anthropogenic and natural signals in both records, and a clear separation from the alternative hypothesis of just natural variations (Figure TS.9, Global panels). These signals do not just appear in the global means, but also appear at regional scales on continents and in ocean basins in each of these variables (Figure TS.9). Sea-ice extent emerges clearly from the range of internal variability for the Arctic but this signal remains within the range of internal variability for Antarctica. At sub-continental scales, it is *likely* that human influences have been detected in extremes in temperature {Table 10.1} and human influence is likely to have substantially increased the probability of some observed heat waves {Table 10.1}.

[START BOX TS.2 HERE]

Box TS.2: Model Evaluation

Climate models constitute the primary tools available for investigating the response of the climate system to various forcings, for making climate predictions on seasonal to decadal time scales, and for making projections of future climate over the coming century and beyond. A particular powerful approach to model evaluation relies on the results collected as part of the Coupled Model Intercomparison Projects (e.g., CMIP3 and CMIP5; see also Box TS.4), because these constitute a set of well-controlled and increasingly well-documented climate model experiments. The direct approach to model evaluation is to compare observations with model output and analyze the resulting difference; this requires knowledge of the errors and uncertainties in the observations. Performance metrics, which quantify the level of agreement between models and observations, succinctly summarize model performance and quantify changes in model performance over time (Box TS.2, Figure 1). In cases where observations are lacking, an intercomparison of model results provides some quantification of model 'uncertainty'. {9.8.1}

Since AR4 climate models have improved notably with regards to many important quantities and aspects of the climate system, in particular the simulation of large scale precipitation, Arctic sea ice, ocean heat content, extreme events, and the climate effects of stratospheric ozone. {9.4.1, 9.4.2, 9.4.3, 9.5.4, Figure 9.6, Figure 9.17}

There is *very high confidence* that coupled climate models generally respond correctly to external forcing like changing greenhouse gases. Confidence is based on the realistic simulations of the surface temperature on continental and larger scales, and the global-scale surface temperature increase over the historical period, especially the last fifty years. {9.4.1, Box 9.1, Figure 9.2, Figure 9.8}

The simulation of large-scale patterns of precipitation has improved since the AR4, but there is only *medium confidence* that models correctly simulate precipitation increases in wet areas and precipitation decreases in

dry areas on large spatial scales in a warming climate, based on high agreement among models but only limited evidence that this has been detected in observed trends. {9.4.1, 10.3.2, 11.4.2, 12.4.5}

There is *very high confidence* that CMIP5 models realistically simulate the annual cycle of Arctic sea-ice extent, and there is *high confidence* that they realistically simulate the trend in Arctic sea ice extent over the past decades. Most models simulate a decreasing trend in Antarctic sea ice extent, albeit with larger intermodel spread, as compared to a small increasing trend in observations. {9.4.3}

There is *high confidence* that many models simulate realistically the observed trend in ocean heat content, although some models show substantial deviations from the observations. This gives confidence in using climate models to assess the global energy budget. {9.4.2, Figure 9.17, Box 13.2}

Understanding of past sea level changes requires the combination of information from ocean warming and changes in glacier and ice sheet volume and land water storage. The closure of the observational budget for recent periods within uncertainties represents a significant advance since the AR4 and strengthens the confidence in the physical understanding and modelling of the causes of past global mean sea level change. {4.3.1, 4.4.2, 13.3.6, Table 13.1, Figure 13.4, Figure 13.5, FAQ 3.1}

There has been progress since AR4 in the assessment of model simulations of extreme weather and climate events. There is *high confidence* that the global distribution of temperature extremes is represented well by models. The observed warming trend of temperature extremes in the second half of the 20th century is well captured, but there is *medium confidence* that models tend to overestimate the warming of warm temperature extremes and underestimate the warming of cold temperature extremes. There is *medium confidence* that CMIP5 models tend to simulate more intense and thus more realistic precipitation extremes than CMIP3. Some high-resolution atmospheric models have realistically simulated tracks and counts of tropical cyclones. {9.5}

Since AR4 many climate models have been extended with biogeochemical cycles into 'Earth System' Models (ESMs). There is *high confidence* that most CMIP5 ESMs produce global land and ocean carbon sinks over the latter part of the 20th century that fall within the range of observational estimates. This lends credibility to applying the ESMs to the diagnosis of anthropogenic greenhouse gas emissions compatible with concentration scenarios. {9.4.5}

[INSERT BOX TS.2, FIGURE 1 HERE]

Box TS.2, Figure1: Summary of how well the CMIP5 models simulate important features of the climate of the 20th century. Confidence in the assessment increases towards the right as suggested by the increasing strength of shading. Model quality increases from bottom to top. The color coding indicates improvements from CMIP3 (or models of that generation) to CMIP5 (see Box TS.4). The assessment is mostly based on the multi-model mean, not excluding that deviations for individual models could exist. Note that assessed model quality is simplified for representation in the figure and it is referred to the text for details of each assessment. The figure highlights the following key features, with the sections that back up the assessment added in brackets {Figure 9.45}:

PANEL a (Trends)

AntSIE:	Trend in Antarctic sea ice extent {9.4.3}
ArctSIE:	Trend in Arctic sea ice extent {9.4.3}
GMSL:	Trend in global mean sea level {13.3}
LST:	Lower stratospheric temperature trends {9.4.1.}
OHC:	Global ocean heat content trends {9.4.2}
StratO3:	Total column ozone trends {9.4.1}
TAS:	Surface air temperature trends {9.4.1}
UTT:	Upper-tropospheric temperature trends {9.4.1}

PANEL b (Extremes):

Droughts	Droughts {9.5.4}
Hurric-hr	Year-to-year counts of Atlantic hurricanes in high-resolution AGCMs {9.5.4}
PR_ext	Global distributions of precipitation extremes {9.5.4}
PR_ext-hr	Global distribution of precipitation extremes in high-resolution AGCMs {9.5.4}
PR_ext-t	Global trends in precipitation extremes {9.5.4}
TAS_ext	Global distributions of surface air temperature extremes {9.5.4}
TAS_ext-t	Global trends in surface air temperature extremes {9.5.4}

TC-hr	Tropical cyclone tracks and intensity in high-resolution AGCMs {9.5.4}

[END BOX TS.2 HERE]

[START BOX TS.3 HERE]

Box TS.3: Paleoclimate

Paleoclimate Data Inform the Understanding of Future Climate

Reconstructions from paleoclimate archives {Chapter 5} allow to place current changes in atmospheric composition, sea level, climate including extreme events such as megadroughts and floods {5.5.5} and projections in a broader perspective of past climate variability (see Section TS.2) {10.5.5}. They also document the behavior of slow components of the climate system including the carbon cycle {5.2.2, 6.2} ice sheets {5.6, 13.2.1} or the deep ocean {5.7} for which instrumental records are short compared to characteristic time scales, informing on mechanisms of abrupt {5.7} and irreversible changes {5.8, 13.2.1}. Together with the knowledge of past natural climate forcings {5.2.1, 8.4.2}, syntheses of paleoclimate data have allowed quantification of polar amplification {Box 5.2}, slow and fast feedbacks and equilibrium climate sensitivity {5.3.3, 9.7.2, 10.8.2}. The combination of paleoclimate simulations and reconstructions enables to quantify the response of the climate system to radiative perturbations {5.3.1, 5.3.2, 5.3.4, 10.7.2}, as well as the past patterns of internal climate variability {5.4, 10.7.2, 14.2.2} on inter-annual to multi-centennial scales. Since AR4, the incorporation of paleoclimate simulations in the CMIP5 framework has allowed incorporation of information from paleoclimate data to inform projections. Within uncertainties associated with reconstructions of past climate variables from proxy record and forcings, paleoclimate information from the Mid Holocene, Last Glacial Maximum, and Last Millennium have been used to test the ability of models to simulate realistically the magnitude and large scale patterns of past changes {9.4.1, 9.4.2, 9.5.3}.

Present-day concentrations of atmospheric greenhouse gases (CO_2, CH_4, and N_2O) exceed the range of variability recorded in ice core records during past 800,000 years. Past changes in atmospheric greenhouse-gas concentrations can be determined with *high confidence* from polar ice cores. New data extend the AR4 statement that present-day concentrations *likely* exceed the natural range of variability back to 800,000 years ago {5.2.2}. While orbital forcing is the primary driver of glacial cycles, climate-ice sheet models of different complexities as well as reconstructions show that the internal feedback of CO_2 accounts for a significant fraction of glacial-interglacial climate variability. Since AR4, leads and lags between temperature and CO_2 have been revised. New Antarctic data and dating methods depict simultaneous increases in Antarctic temperature and CO_2 during the last glacial termination, preceding Northern Hemisphere warming due to the bipolar seesaw (*high confidence*) {5.3.2}.

During the pre-industrial period, from 7,000 years ago to year 1750, atmospheric CO_2 concentration increased continuously by 20 ppm. Although the *confidence* in underlying processes is *medium*, emissions from early anthropogenic land use are *unlikely* sufficient to explain this increase. Atmospheric CH_4 concentrations rose between 4,000 years ago until year 1750 by about 100 ppb. It is *as likely as not* that anthropogenic land use significantly contributed to this increase. Causes for CO_2 variations during the last millennium (including a 5–8 ppm decrease around year 1600) remain equivocal. Climatic and anthropogenic forcings have, with *low confidence*, been proposed to explain the atmospheric CH_4 variability during the last millennium, including a 40 ppb decrease in the late 16th century {6.2}.

For average annual Northern Hemisphere temperatures, there is *medium confidence* that 1981–2010 CE was the warmest 30-year period of the last 1300 years and it is *very likely* that it was the warmest of the last 800 years (Box TS.3, Figure 1). This is supported by multiple reconstructions using a variety of proxy data and statistical methods. Before 1200 CE there is only medium evidence and medium agreement because there are fewer independent reconstructions, they rely on fewer proxy records, and the published uncertainty ranges may underestimate the true uncertainty. Simulations forced by natural and anthropogenic radiative changes during the last millennium are consistent with reconstructions of Northern Hemisphere temperature, within

the broad uncertainty ranges (*high confidence*) {5.3.5}. In contrast to the late 20th century, there is *high confidence* that the Medieval Climate Anomaly was not characterized by a pattern of higher temperatures that were consistent across seasons and regions. Detection and attribution analyses suggest that external forcing contributed to warm conditions in the 11th and 12th century, while changes in atmospheric circulation are implied for the onset of the Medieval Climate Anomaly {10.7.2}.

[INSERT FIGURE BOX TS.3, FIGURE 1 HERE]

Box TS.3, Figure 1: Comparisons of simulated and reconstructed Northern Hemisphere temperature changes. (a) Changes over the last millennium. (b) Response to individual volcanic events. (c) Response to multi-decadal periods of volcanic activity. (d) Response to multi-decadal variations in solar activity. (e) Mean change from Medieval Climate Anomaly to Little Ice Age. (f) Mean change from 20th century to Little Ice Age. Note that some reconstructions represent a smaller spatial domain than the full Northern Hemisphere or a specific season, while annual temperatures for the full NH mean are shown for the simulations. (a) Simulations shown by coloured lines (thick lines: multi-model-mean; thin lines: multi-model 90% range; red/blue lines: models forced by stronger/weaker solar variability, though other forcings and model sensitivities also differ between the red and blue groups); overlap of reconstructed temperatures shown by grey shading; all data are expressed as anomalies from their 1500–1850 CE mean. {Figure 5.8}

[**END BOX TS.3 HERE]**

TS.5 Projections of Global and Regional Climate Change

TS.5.1 Introduction

This section summarizes the assessment of climate change projections. First, future forcing and scenarios are reviewed. Then there are four sections addressing various aspects of projections of global and regional climate change. The first covers near-term and long-term projections in the atmosphere, ocean and cryosphere; the second summarizes projections of carbon and other biogeochemical cycles; the third is devoted entirely to projections in sea level change; and the fourth concentrates on changes to climate phenomena and other aspects of regional climate. {11.3, 12.3–12.5, 13.5–13.7, 14.1–14.6}

TS.5.2 Future Forcing and Scenarios

The new RCP scenarios in the AR5 are all mitigation scenarios with implied policy actions that occur throughout the 21st century. This is in contrast to the SRES scenarios in the AR4, which were non-mitigation scenarios with no policy actions to mitigate climate change. The climate model simulations run with the RCPs produce a range of responses from ongoing warming, to stabilized climate, to an aggressive mitigation scenario (RCP2.6) that stabilizes and then slowly reduces warming after mid-21st century. In contrast to the AR4, the climate change from the RCP scenarios in the AR5 is framed as a combination of adaptation and mitigation. Mitigation actions starting now in the various RCP scenarios do not produce discernibly different climate change outcomes for the next 30 years or so, thus implying similar adaptation strategies to near-term climate change, while long-term climate change after mid-century is appreciably different across the RCPs, thus suggesting a variety of adaptation strategies to the different magnitudes of climate change from the various mitigation actions inherent in the RCPs. {Box 1.2}

[START BOX TS.4 HERE]

Box TS.4: The New RCP Scenarios and CMIP5 Models

Most of the results in this report are based on the new Representative Concentration Pathways (RCPs), a set of mitigation scenarios developed to replace the SRES scenarios (Box TS.4, Figure 1). The four RCPs are designed to be representative of a much larger set of mitigation scenarios, and all imply some kind of policy intervention to achieve a certain climate change target, as opposed to the SRES scenarios that were not mitigation scenarios and thus did not take into account policy actions. The comparison between the projections in this report with those in AR4 needs to take into account the changes in scenarios, a new set of

model simulations with these new scenarios in a new generation of climate models (CMIP5) and the change in the reference and future periods. The main points of this comparison are summarized here. {Box 1.2}

[INSERT BOX TS.4, FIGURE 1 HERE]

Box TS.4, Figure 1: Uncertainty estimates for global mean temperature change in 2081–2100 with respect to 1986–2005. Red crosses mark projections from individual CMIP5 models. Red bars indicate mean and 5–95% ranges based on CMIP5 (1.64 standard deviations), which are considered as a *likely range*. Blue bars indicate 5–95% ranges from the pulse response emulation of 18 models . Grey bars mark the range from the mean of CMIP5 minus 40% mean to the mean +60%, assessed as *likely* in AR4 for the SRES scenarios. The yellow bars show the median, 33–66% range and 10–90% range. {Figure 12.8}

It is *unlikely* that the assessment of the mean values and ranges of global mean temperature changes in AR4 would have been substantially different if the CMIP5 models had been used in that report. The differences in global temperature projections can largely be attributed to the different scenarios. {12.4.9} The global mean temperature response simulated by CMIP3 and CMIP5 is very similar, both in the mean and the model range, transiently and in equilibrium. The range of temperature change across all scenarios is wider because the RCPs include a strong mitigation scenario that was absent in SRES. In AR4 the uncertainties in global temperature projections were found to be approximately constant when expressed as a fraction of the model mean warming. For the high RCPs, the uncertainty is now estimated to be smaller than with the AR4 method for long-term climate change, because in contrast to AR4, the carbon cycle climate feedbacks are not considered in the concentration driven RCP projections. When forced with RCP8.5, CO_2 emissions, as opposed to the RCP8.5 CO_2 concentrations, CMIP5 Earth System Models (ESMs) with interactive carbon cycle simulate, on average, a 60 ppm larger atmospheric CO_2 concentration and 0.2°C larger global surface temperature increase by 2100. For the low RCPs the fractional uncertainty is larger because internal variability and non-CO_2 forcings make a larger relative contribution to the total uncertainty. {12.4.1}

The 5–95% range of the CMIP5 projections is considered "*likely*" for projections of global temperature change. The range in anthropogenic aerosol emissions across all scenarios has a larger impact on near-term climate projections than the corresponding range in long-lived greenhouse gases, particularly on regional scales and for hydrological cycle variables {11.3.1, 11.3.6}. The RCP scenarios do not span the range of future aerosol emissions found in the SRES and alternative scenarios. The RCPs all assume future rapid reductions in aerosol emissions and there is robust evidence that collectively these represent the low end of future emissions scenarios for aerosols and other short-lived reactive gases, with the high end represented by the SRES A2 or A1FI scenarios. {1.3.2, 9.4.6, 11.5.3, 11.3.6, Annex II, Tables AII.2.20–AII.2.22 and Tables AII.5.3–AII.5.6}. Probabilistic projections with simpler models and using the IPCC assessment of equilibrium climate sensitivity provide uncertainty ranges that are consistent with those from CMIP5. {11.2.3, 12.4.9}

There is remarkable consistency between the projections based on CMIP3 and CMIP5, for both large-scale patterns and magnitudes of change (Box TS.4, Figure 2), providing increased confidence in projections overall {12.4.9}. Model agreement and confidence in projections depends on the variable and spatial and temporal averaging, with better agreement for larger scales. Confidence is higher for temperature than for those quantities related to the water cycle or circulation {12.4.1, 12.4.5, 12.4.4}. Improved methods to quantify and display model robustness have been developed to indicate where lack of agreement across models on local trends is a result of internal variability, rather than models actually disagreeing on their forced response {Box 12.1}. Understanding of the sources and means of characterizing uncertainties in long-term large scale projections of climate change has not changed significantly since AR4, but new experiments and studies have continued to work towards a more complete and rigorous characterization. {9.7.3, 12.4.9, 12.2}.

The well-established stability of geographical patterns of change during a transient experiment remains valid in the CMIP models (see Box TS.4, Figure 2). Patterns are similar over time and across scenarios and to first order can be scaled by the global mean temperature change. There remain limitations to the validity of this technique when it is applied to strong mitigation scenarios, to scenarios where localized forcing (e.g., aerosols) are significant and vary in time and for variables other than average temperature and precipitation {12.4.2}.

[INSERT BOX TS.4, FIGURE 2 HERE]

Box TS.4, Figure 2: Patterns of temperature (left column) and percent precipitation change (right column) by the end of the 21st century (2081–2100 vs 1986–2005), for the CMIP3 models average (first row) and CMIP5 models average (second row), scaled by the corresponding global average temperature changes. {Figure 12.41}

[END BOX TS.4 HERE]

The CMIP5 presents an unprecedented level of information on which to base projections including new Earth Systems Models, new model experiments and more diagnostics output. A larger number of forcing agents is considered in the CMIP5 models, with respect to aerosols and land use particularly. Black carbon aerosol is now a commonly included forcing agent. Considering CO_2, both 'concentrations-driven' projections and 'emissions-driven' projections are assessed from CMIP5. These allow quantification of the physical response uncertainties as well as climate-carbon cycle interactions. {1.5.2, Box 1.2}

The range in anthropogenic aerosol emissions across all scenarios has a larger impact on near-term climate projections than the corresponding range in long-lived greenhouse gases, particularly on regional scales and for hydrological cycle variables {11.3.1, 11.3.6}. The RCP scenarios do not span the range of future aerosol emissions found in the SRES and alternative scenarios (see Box TS.4).

If rapid reductions in sulphate aerosol are undertaken for improving air quality or as part of decreasing fossil-fuel CO_2 emissions, then there is *medium confidence* that this could lead to rapid near-term warming. There is robust evidence that accompanying controls on methane (CH_4) emissions would offset some of this sulphate-induced warming. While removal of black carbon aerosol could also counter warming associated with sulphate removal, uncertainties are too large to constrain the net sign of the global temperature response to black carbon emission reductions, which depends on co-emitted (reflective) aerosols and aerosol indirect effects {11.3.6}.

Including uncertainties in projecting the chemically reactive greenhouse gases methane (CH_4) and nitrous oxide (N_2O) from RCP emissions gives a range in abundance pathways that is *likely* 30% larger than the range in RCP concentrations used to force the CMIP5 climate models. Including uncertainties in emission estimates from agricultural, forest, and land-use sources, in atmospheric lifetimes, and in chemical feedbacks, results in a much wider range of abundances for N_2O, CH_4, and HFCs and their radiative forcing. In the case of CH_4 it *likely* extends the range up to 500 ppb above RCP8.5 and 250 ppb below RCP2.6 through to 2100, with smaller ranges in the near term. {11.3.5}

There is *low confidence* in projections of natural forcing. Major volcanic eruptions cause a negative radiative forcing up to several W m^{-2}, with a typical lifetime of one year, but the possible occurrence and timing of future eruptions is unknown. Except for the 11-year solar cycle, changes in the total solar irradiance are uncertain. {8} Except where explicitly indicated, future volcanic eruptions and changes in total solar irradiance additional to a repeating 11 year solar cycle are not included in the projections of near- and long-term climate assessed. {11.3.1}

TS.5.3 Projections of Climate Change

The assessed literature supports the conclusion from AR4 that equilibrium climate sensitivity (ECS) is *likely* in the range 2°C–4.5°C, *very likely* above 1.5°C, and *very unlikely* greater than about 6°C–7°C. The most likely value remains near 3°C. Earth system sensitivity (ESS) over millennia timescales including long-term feedbacks not typically included in models could be significantly higher than ECS (see TFE.6 for further details). {Box 12.2}

The transient climate response (TCR) is *very likely* in the range 1°C–3°C, *likely* in the range 1.2°C– 2.6°C estimated from CMIP5 (5–95%), with a most likely value near 1.8°C (see TFE.6 for further details). {Box 12.2}

The ratio of global temperature change to total cumulative anthropogenic carbon emissions is relatively constant and independent of the scenario, but is model dependent, as it is a function of the model airborne fraction and climate sensitivity. For any given temperature target, higher emissions in earlier decades therefore imply lower emissions by about the same amount later on. The transient climate response to cumulative carbon emission (TCRE) is *very likely* between 0.8°C–3°C PgC^{-1} (10^{12} metric tons of carbon), with a best estimate in the range of 1.5°C–2.0°C PgC^{-1}, for cumulative emissions less than 2000PgC until the time at which temperatures peak (see TFE.8 for further details). {Box 12.2}

TS.5.3.1 Near-Term Climate Change

Near-term decadal climate prediction provides information not available from existing seasonal to interannual (months to a year or two) predictions or from long-term (late 21st century and beyond) climate change projections {12, 14}. Prediction efforts on seasonal to interannual timescales require accurate estimates of the initial climate state with less concern extended to changes in external forcing[8], while long-term climate projections rely more heavily on estimations of external forcing with little reliance on the initial state of internal variability. Estimates of near-term climate depend on the committed warming (caused by the inertia of the oceans as they respond to historical external forcing) the time evolution of internally-generated climate variability, and the future path of external forcing. Near-term predictions out to about a decade (Figure TS.11), unlike near-term projections beyond a decade to about mid-century that are affected mostly by the external forcing (Figure TS.12), depend more heavily on an accurate depiction of the internally generated climate variability. {11.1}

[INSERT FIGURE TS.11 HERE]

Figure TS.11: Examples of ensemble-mean correlation with the observations (left column) and time series of 2–5 (middle column) and 6–9 (right column) year average predictions of the global-mean temperature (top row), and AMV (bottom row) from the ENSEMBLES (black), CMIP5 Assim (dark green) and NoAssim (light green) and DePreSys Assim (dark purple) and NoAssim (light purple) forecast systems. The AMV index was computed as the SST anomalies averaged over the region Equator-60ºN and 80ºW–0ºW minus the SST anomalies averaged over 60ºS–60ºN. Predictions initialized once every five years over the period 1960–2005 have been used. The CMIP5 multi-model includes experiments from the HadCM3, MIROC5, MIROC4h and MRI-CGCM3 systems. The one-side 95% confidence level is represented in grey, where the number of degrees of freedom has been computed taking into account the autocorrelation of the observational time series. The observational time series, GISS global-mean temperature and ERSST for the AMV and IPO, are represented with red (positive anomalies) and blue (negative anomalies) vertical bars, where a four-year running mean has been applied for consistency with the time averaging of the predictions. {adapted from Figure 11.6}

[INSERT FIGURE TS.12 HERE]

Figure TS.12: a) Projections of global mean, annual mean surface air temperature 1986–2050 (anomalies relative to 1986–2005) under RCP4.5 from CMIP5 models (grey lines, one ensemble member per model), with five observational estimates for the period 1986–2010 (black lines); b) as a) but showing the range (grey shades, with the multi-model mean in white) of decadal mean CMIP5 projections using (where relevant) the ensemble mean from each model, and decadal mean observational estimates (black lines). An estimate of the projected 5–95% range for decadal mean global mean surface air temperature for the period 2016–2040 derived using the ASK methodology applied to simulations with the HadGEM2ES climate model is also shown (dashed black lines). The red line shows a statistical prediction. {Figure 11.33}

Further near-term warming from past emissions is unavoidable due to thermal inertia of the oceans. This warming will be increased by ongoing emissions of GHGs over the near term, and the climate observed in the near term will also be strongly influenced by the internally generated variability of the climate system. Previous IPCC Assessments only described climate-change projections wherein the externally forced component of future climate was included but no attempt was made to initialize the internally generated climate variability. Decadal climate predictions, on the other hand, are intended to predict both the externally forced component of future climate change, and the internally generated component. Near-term predictions do not provide detailed information of the evolution of weather. Instead they can provide estimated changes in the time evolution of the statistics of near-term climate. {FAQ 11.1, Box 11.1, 11.1, 11.2.2, 11.4.1}

[8] Seasonal-to-interannual predictions typically include the impact of external forcing.

Retrospective prediction experiments have been used to assess forecast quality. There is *high confidence* that the retrospective prediction experiments for forecast periods of 1 to 10 years have statistically significant regional temperature correlations with the observations (exceeding 0.6 over much of the globe). {11.2.2} The initialization improves the temperature correlation over the North Atlantic, regions of the South Pacific and small continental areas of the Northern Hemisphere {11.2.2, Figure 11.8}. While there is high agreement that the initialization consistently improves several aspects of climate (like North Atlantic SSTs with more than 75% of the models agreeing on the improvement signal), there is also high agreement that it can consistently degrade others (like the equatorial Pacific temperatures). Probabilistic temperature predictions are reliable (see Section 11.2.3 for definition of reliability) with *medium confidence*. {11.2.3, Figure 11.9} On multi-annual and decadal time scales the retrospective predictions of continental precipitation have positive correlation with observations over several regions, with maximum values of 0.6. These correlations are significant at the 95% confidence level, and are due mainly to the specified forcing because there is agreement that the initialization does not have an impact {11.2.3}.

TS.5.3.1.1 Projected near-term changes in climate

While differences exist, projections of near-term climate change show modest sensitivity to contrasts in greenhouse gas and aerosol emissions within the range of the RCP scenarios. These scenarios presume that there are no major volcanic eruptions and that anthropogenic aerosol emissions are rapidly reduced during the near term. {11.3.1, 11.3.2} Projected changes given below are expressed as differences (i.e., anomalies) between the period 2016–2035 and the reference period of 1986–2005. {11.3.1, 11.3.2}

TS.5.3.1.2 Projected near-term changes in temperature

The global mean surface air temperature anomaly for the period 2016–2035 relative to the reference period of 1986–2005, will *likely* be in the range 0.4°C–1.0°C (*medium confidence*). It is *more likely than not* that that actual warming will be closer to the lower bound of 0.4°C than the upper bound of 1.0°C (*medium confidence)* (see Table TS.1 and Figure TS.13). {11.3.6.3; Figure 11.33}

There is *high confidence* that higher concentrations of greenhouse gases and lower amounts of sulphate aerosol lead to greater warming, but in the near term the differences between projections for different RCP scenarios are typically smaller than the differences between projections from different climate models. In 2030, the CMIP5 multi-model ensemble mean values for global mean temperature differ by less than 0.3ºC between the RCP scenarios, whereas the model spread (defined as the 5–95% range of the decadal means of the models) is around 0.8ºC. The inter-scenario spread increases in time and by 2050 is comparable to the model spread. In the near term, model uncertainty and natural variability therefore dominate the uncertainty in projections of global mean temperature. Regionally, the largest differences in surface air temperature between RCP scenarios are found in the Arctic. {11.3.2. 11.3.6, Figure 11.32}

The projected warming of global mean temperatures implies *high confidence* that new levels of warming relative to pre-industrial climate will be crossed, particularly under higher greenhouse gas emissions scenarios. Assuming that the global mean warming prior to the reference period of 1986–2005 was 0.6°C, an assessment based on CMIP5 results suggests the following conclusions. By 2050: under RCP2.6 it is *about as likely as not* that the 1.5°C level will be crossed and *very unlikely* that the 2°C level will be crossed; under RCP4.5 and RCP6.0 it is *likely* that the 1.5°C level will be crossed, and *unlikely* that the 2°C level will be crossed; and under RCP8.5 it is *very likely* that the 1.5°C level will be crossed, and *likely* that the 2°C level will be crossed. {11.3.1}

A future volcanic eruption similar in size to the 1991 eruption of Mount Pinatubo would cause a rapid drop in global mean surface air temperature of several tenths of 1°C in the following year, with recovery over the next few years. Larger eruptions, or several eruptions occurring close together in time, would lead to larger and more persistent effects. {11.3.6}

Possible future reductions in solar irradiance would act to cool global mean surface air temperature but such cooling is *unlikely* to exceed 0.1°C by 2050 (*medium confidence*). A return to conditions similar to the Maunder Minimum is considered *very unlikely* in the near term, but were it to occur, would produce a decrease in global temperatures much smaller than the warming expected from increases in anthropogenic

greenhouse gases. However, current understanding of the impacts of solar activity on regional climate remains low. {11.3.6}

The spatial patterns of near-term warming projected by the CMIP5 models following the RCP scenarios (see Figure TS.13) are broadly consistent with the AR4. It is *virtually certain* that anthropogenic warming of surface air temperature over the next few decades will proceed more rapidly over land areas than over oceans, and it is *very likely* that the anthropogenic warming over the Arctic in winter will be greater than the global mean warming. Relative to background levels of internally generated variability there is *high confidence* that the anthropogenic warming relative to the reference period will become apparent soonest in the summer season in low latitude countries. Greatest atmospheric warming is projected to occur in the upper tropical troposphere and in the lower troposphere in the northern high latitudes (*medium confidence*). While cooling is projected in the middle-to-upper stratosphere (*high confidence*), there is *less confidence* in lower stratospheric temperature changes due to opposing influences which include stratospheric O_3 recovery and circulation changes driven by tropospheric warming. {11.3.2, Figures 11.12–11.14}

It is *very likely* that in the next decades the frequency of warm days and warm nights will increase, while the frequency of cold days and cold nights will decrease at the global scale. This trend will *likely* be visible in an increasing number of regions in the near term. Models also project increases in the duration, intensity and spatial extent of heat-waves and warm spells for the near term. These changes may proceed at a different rate than the mean warming. For example, in regional climate modelling efforts for Europe, high-percentile daytime summer temperatures are projected to warm at a faster rate than mean temperatures, while daytime winter temperatures warm at a slower rate (see also TFE.9). {11.3.2; Figures 11.22–11.23}

TS.5.3.1.3 Projected near-term changes in the water cycle

It is *more likely than not* that over the next few decades there will be increases in mean precipitation in regions and seasons where the mean precipitation is relatively high, and decreases in regions and seasons where mean precipitation is relatively low. However, it is *likely* that these changes from 1986–2005 will only be significant, relative to internally generated variability, on the largest spatial scales (e.g., zonal means), and changes in specific smaller regions may show departures from the large-scale pattern. Anthropogenic aerosols and/or changes in atmospheric circulation could have important complicating or dominant effects in some regions. {11.3.2, Figure 11.16}

Over the next few decades increases in near-surface specific humidity are *very likely*. Models project increases in evaporation in most regions. There is little robustness in projected changes in soil moisture and surface run off. Internally generated variability will continue to have a major influence on all aspects of the water cycle. {11.3.2, Figure 11.18}

In the near term, it is *likely* that the frequency and intensity of heavy precipitation events will increase at the global scale. These changes are primarily driven by increases in atmospheric water vapor content, but also affected by changes in atmospheric circulation. While increases in heavy precipitation are *likely* at the global scale and at high latitudes, the impact of anthropogenic forcing at regional scales is less obvious regionally, as regional-scale changes are strongly affected by natural variability and also depend upon the course of future aerosol emissions, volcanic forcing and land use changes (see also TFE 9). {11.3.2, Figures 11.22–11.23}

TS.5.3.1.4 Projected near-term changes in atmospheric circulation

Internally generated climate variability and multiple radiative forcing agents (e.g., volcanoes, greenhouse gases, ozone and anthropogenic aerosols) will all contribute to near-term changes in the atmospheric circulation. For example, it is *likely* that the projected recovery of stratospheric ozone and increases in greenhouse gas concentrations will have counteracting impacts on the width of the Hadley Circulation and the meridional position of the Southern Hemisphere storm track. Therefore it is *unlikely* that they will continue to expand poleward as rapidly as in recent decades. {11.3.2}

There is *low confidence* in near-term projections for a poleward shift of the position and strength of Northern Hemisphere storm tracks. The estimated impact of internally generated climate variability on the position and strength of Northern Hemisphere storm tracks is larger than the projected impact of greenhouse gases by 2016–2035 relative to 1986–2005. {11.3.2}

There is *low confidence* in near-term projections for a weakening of the Walker circulation, relative to 1986–2005. It is *more likely than not* that the Walker circulation will weaken by 2016–2035 relative to 1986–2005, but the projected weakening of the Walker circulation is small relative to simulated internally- generated interdecadal variability. {11.3.2}

There is overall *low confidence* that over the next few decades there will be global and regional increases in the intensity of the strongest tropical cyclones and a decrease in global frequency. This *low confidence* reflects the small number of studies exploring near-term tropical cyclone activity, and the larger relative influence of internal variability and non-greenhouse forcing up to the mid-21st century than at the end of the 21st century. Increased tropical cyclone intensity is projected by studies focusing on the North Atlantic and South Pacific, although there is only *medium confidence* in these projections. It is *very likely* that tropical cyclone frequency, intensity and spatial distribution globally and in individual basins will vary from year-to-year and decade-to-decade in association with natural modes of variability including e.g., ENSO, Atlantic Multidecadal Oscillation (AMO) and the Inter-decadal Pacific Oscillation (IPO). {11.3.2}

TS.5.3.1.5 Projected near-term changes in the ocean

It is *virtually certain* that globally-averaged surface and upper ocean (top 700 m) temperatures averaged over 2016–2035 will be warmer than those averaged over 1986–2005. {11.4.4; Figure 11.28} It is *likely* that internally generated climate variability will be a dominant contributor to changes in the depth and tilt of the equatorial thermocline, and the strength of the east-west gradient of SST across the Pacific through the mid-21st century, thus it is *likely* there will be multi-year periods with increases or decreases, but no clear longer term trend. {11.3.3}

There is *medium confidence* that there will be increases in salinity in the tropical and (especially) subtropical Atlantic, and decreases in the western tropical Pacific over the next few decades. {11.4.4} Overall, it is *likely* that there will be some decline in the Atlantic Meridional Overturning Circulation by 2050. However, the rate and magnitude of weakening is very uncertain and decades when this Circulation increases are also to be expected. {11.3.3}

TS.5.3.1.6 Projected near-term changes in the cryosphere

It is *very likely* that there will be continued near-term loss of sea ice in the Arctic, decreases of snow cover, and reductions of permafrost at high latitudes of the Northern Hemisphere. Though there is the possibility of sudden abrupt changes in the cryosphere, there is *low confidence* that these changes could be predicted with any certainty over the next several decades. Based on an assessment of a subset of models that more closely reproduce recent observed trends, a nearly ice-free Arctic in late summer before 2050 is a very distinct possibility, even though later dates cannot be excluded. For the earlier near-term period of 2016–2035 averaged over all the CMIP5 models compared to the 1986–2005 reference period, the projected decreases of sea ice area for the RCP4.5 scenario are –28% for September, and –6% for February for the Arctic. Projected changes for the Antarctic are decreases of –5% for September, and –13% for February. Reductions in Northern Hemisphere sea ice volume for that same set of models, scenario and time period are projected to be –23% for February, and –4% for September, while for the Southern Hemisphere those values are –12% for February, and –7% for September. Multi-model averages from 21 models in the CMIP5 archive project decreases of Northern Hemisphere snow cover area of –4% ± 1.9% (one standard deviation) for the 2016–2035 time period for a March-April average. The projected reduction in annual mean near- surface permafrost (frozen ground) for the 2016–2035 time period compared to the 1986–2005 reference period for the RCP4.5 scenario for 15 CMIP5 models is -2.9×10^6 km^2, or a decrease of about 18%. {11.3.4}

TS.5.3.1.7 The possibility of near-term abrupt changes in climate

There are various mechanisms that could lead to changes in global or regional climate that are abrupt by comparison with rates experienced in recent decades. The likelihood of such changes is generally lower for the near term than for the long term. {11.3.6} For this reason the relevant mechanisms are primarily assessed in the TS.5 sections on long-term changes and in TFE.5.

TS.5.3.1.8 Projected near-term changes in air quality

There is *high confidence* that baseline surface ozone (O_3) will change over the 21st century, although projections across the RCP, SRES, and alternative scenarios for different regions range from –4 to +5 ppb by

2030 and –14 to +15 ppb by 2100. Baseline values (i.e., those not influenced by local anthropogenic emissions) are controlled by global emissions of ozone precursors, as well as climate change, and these represent the abundances of surface ozone at remote sites and over large areas, upon which local and regional pollution episodes build. A warming climate will change baseline levels: as water vapor rises with temperature, there is *high confidence* that O_3 chemical destruction will increase in much of the unpolluted lower troposphere; but there is medium evidence that other feedbacks may compensate in some regions of the atmosphere, for example, where abundances of ozone precursors are high. {11.35, Annex II, Tables AII.7.1–AII.7.3}

There is *high confidence* that near-term air quality (surface O_3 and fine particulate matter, PM2.5) will improve over North America and Europe under all RCPs except for O_3 in RCP8.5 but will be degraded over Asia at least until mid-century under some scenarios. There is *high confidence* that the range in projected air quality changes in the RCPs is much narrower than under the SRES scenarios, due to the assumption of aggressive air quality controls globally in all RCPs. By 2100, annual mean surface O_3 over Europe, North America, and Asia declines by 3–14 ppb under all RCPs as projected with CMIP5 and ACCMIP models, except for RCP8.5 which has increases of 1–5 ppb. Global, annual mean surface O_3 rises steadily by 12 ppb in 2100 for SRES A2, but by only 3 ppb in RCP8.5. There is *medium confidence* that the projected range in O_3 associated with chemical changes driven by short-lived pollutants and CH_4 in the emission scenarios is much larger than that due to the physical climate changes driven by the greenhouse gases. Aside from episodic dust and wildfire transport events, there is *high confidence* that changes in PM2.5 are largely controlled by regional emissions except where large precipitation changes alter the rainout of aerosols. Future changes at the local or urban level cannot be projected accurately with the models and scenarios evaluated here. {11.35, Figures 11.31, 11.32ab, Annex II, Tables AII.7.1–AII.7.4}

If the frequency of heat-waves and slow-moving high-pressure systems changes in the near-term, then there is *medium confidence* that the frequency of extreme O_3 and PM2.5 pollution events would also change. Based on observations and models, there is *medium confidence* that these extreme weather events can also trigger temperature-driven feedbacks on the sources and sinks of air pollutants, altogether exacerbating O_3 and PM2.5 pollution events by enhancing smog-forming chemistry. The frequency and severity of extreme future pollution events will depend also on changing baselines and local emissions of pollutants not assessed here. {11.3.5}

TS.5.3.2 Long-Term Climate Change

TS.5.3.2.1 Projected long-term global changes

Global-mean surface temperatures are projected to rise over the century under all of the GHG concentration pathways represented by the RCPs. Around the mid-21st century, the rate of global warming begins to be more strongly dependent on the scenario. By 2100, the best estimate global- mean temperature change relative to 1986–2005 in the non-mitigation RCP8.5 is about a factor of 3 higher than in the lowest RCP2.6 (*high confidence*), where warming stabilizes in the second half of this century. {12.4.1}

It is *very likely* that global-mean surface temperatures at the end of the 21st century will be greater than present-day under the specified RCPs. Global-mean surface temperatures for 2081–2100 (relative to 1986–2005) for the CO_2 concentration driven RCPs will *likely* be in the 5–95% range of the CMIP5 models, i.e., 0.2°C–1.8°C (RCP2.6), 1.0°C–2.6°C (RCP4.5), 1.3°C–3.2°C (RCP4.5), 2.6°C–4.8°C (RCP8.5) (see Table TS.1). For RCP4.5, 6.0 and 8.5, global temperatures are projected to *likely* exceed 2ºC warming with respect to preindustrial by 2100, and about *as likely as not* to be above 2°C warming for RCP2.6 (Figure TS.13). {12.4.1}

[INSERT FIGURE TS.13 HERE]

Figure TS.13: Top left: Total global mean radiative forcing for the 4RCP scenarios based on the MAGICC energy balance model (light grey: base period 1986–2005, grey: 2016–2035 and 2081–2100 periods used in maps to the right). Note that the actual forcing simulated by the CMIP5 models differs slightly between models. Global mean near surface temperature change. Bottom left: Time series of global and annual mean surface air temperature anomalies (relative to 1986–2005) from CMIP5 concentration-driven experiments. Projections are shown for each RCP for the multimodel mean (solid lines) and ±1 standard deviation across the distribution of individual models (shading). Discontinuities at 2100 are due to different numbers of models performing the extension runs beyond the 21st century and have no

physical meaning. Numbers in the figure indicate the number of different models contributing to the different time periods. Maps: Multimodel ensemble average of annual mean surface air temperature change (compared to 1986–2005 base period) for 2016–2035 and 2081–2100, for RCP2.6, 4.5, 6.0 and 8.5. Hatching indicates regions where the multi model mean is less than one standard deviation of internal variability. Stippling indicates regions where the multi model mean is greater than two standard deviations of internal variability and where 90% of the models agree on the sign of change. {Box 12.1} The number of CMIP5 models used is indicated in the upper right corner of each panel. {adapted from Figure 12.4, Figure 12.5, Annex I}

[INSERT TABLE TS.1 HERE]

Table TS.1: Projected change in global average surface air temperature (SAT) and sea level rise (SLR) for three time horizons during the 21st century. {Table 12.2, Table 13.5, 12.4.1, 11.3.2}

It is *virtually certain* that global mean precipitation will increase with global mean surface air temperature in the next century, with an increase per °C smaller than that of atmospheric water vapour. It is *likely* that the rate of increase of precipitation with temperature will be in the range 1–3% $°C^{-1}$, for scenarios other than RCP2.6. For RCP2.6 the range of sensitivities in the CMIP5 models is 0.5–4% $°C^{-1}$ at the end of the 21st century. {12.4.1}

TS.5.3.2.2 Long-term projections in temperature and energy budget

Future changes in global land surface air temperature exceed changes in global average ocean-area surface air temperature by a factor of ~1.5 ± 0.2 (one standard deviation), as was found in AR4 (*very high confidence*). The Arctic region is projected to warm most rapidly (*very high confidence*) (Figure TS.13). As global mean surface temperature rises, the pattern of atmospheric zonal-mean temperatures show warming throughout the troposphere and cooling in the stratosphere, consistent with previous assessments. The consistency is especially clear in the tropical upper troposphere and the northern high latitudes, indicating that the greatest atmospheric warming is *very likely* to occur in these regions {12.4.3}.

It is *virtually certain* that, in most places, there will be more hot and fewer cold temperature extremes as global temperature increases. These changes are expected for events defined as extremes on both daily and seasonal time scales. Since AR4, the understanding of mechanisms and feedbacks leading to projected changes in extremes has improved. Increases in the frequency, duration and magnitude of hot extremes along with heat stress are expected, however occasional cold winter extremes will continue to occur. Projected changes in 20-year return values of high and low temperature events experience greater increases than mean temperatures in many regions, with the largest changes in the return values of low temperatures at high latitudes. Under RCP8.5 it is *likely* that, in most regions, a 20 year maximum temperature event will occur more frequently (at least doubling its frequency, but in many regions becoming an annual or two-year event) and that a 20 year minimum temperature event will become exceedingly rare by the end of the 21st century under RCP8.5. {12.4.3.3}

Models simulate a decrease in cloud amount in the future over most of the tropics and mid-latitudes, due mostly to reductions in low cloud. Changes in marine boundary layer clouds are most uncertain. Increases in cloud fraction and cloud optical depth and therefore cloud reflection are simulated in high latitudes, poleward of 50° (*medium confidence*). {12.4.3}

TS.5.3.2.3 Projected long-term changes in atmospheric circulation

A robust feature of the pattern of mean sea level pressure change is a decrease in high latitudes and increases in the mid-latitudes as global temperatures rise. Poleward shifts in the mid-latitude jets of 1–2 degrees are *likely* at the end of the 21st century under RCP8.5. In austral summer, the additional influence of stratospheric ozone recovery in the Southern Hemisphere opposes changes due to greenhouse gases there, though the net response varies strongly across models and scenarios. {12.4.4}

A poleward shift of several degrees in Southern Hemisphere storm tracks is *likely* by the end of the 21st century under the RCP8.5 scenario. There is some uncertainty in the degree of shift but the consistency of behaviour with observation-based trends, consistency between CMIP5 and CMIP3 projections and the physical consistency of the storm response with other climatic changes provides *high confidence* in this

response. Substantial uncertainty and thus *low confidence* remains in projecting changes in Northern Hemisphere storm tracks, especially for the North Atlantic basin. {12.4.4}

As the climate warms, the Hadley cell in the Northern Hemisphere and Walker circulation are *likely* to slow down. The weakening is linked to changes in moisture transport from the boundary layer to the free atmosphere associated with changes in precipitation. The Hadley cell is *likely* to widen, which translates to broader tropical regions and a poleward encroachment of subtropical dry zones. In the stratosphere, the Brewer-Dobson circulation is *likely* to strengthen as global temperatures increase. {12.4.4}

TS.5.3.2.4 Projected long-term changes in the water cycle (see also TFE.1)

On the planetary scale, relative humidity is projected to remain roughly constant, but specific humidity to increase in warmer climates. The projected differential warming of land and ocean promotes changes in atmospheric circulation and resulting moisture transport that lead to decreases in near-surface relative humidity over most land areas with the notable exceptions of tropical Africa and Polar Regions (*medium confidence*) (see TFE.1, Figure 1). {12.4.5}

It is *virtually certain* that changes in average precipitation in a much warmer world will not be uniform, with regions experiencing increases, or decreases or no significant change at all. The high latitudes are *very likely* to experience greater amounts of precipitation (TFE.1, Figure 1). This is due to the additional water carrying capacity of the warmer troposphere as well as increased transport of water vapour from the tropics. Many mid-latitude arid and semi-arid regions will *likely* experience less precipitation and many moist mid-latitude regions will *likely* experience more precipitation. The largest precipitation changes over northern Eurasia and North America are projected to occur during the winter. {12.4.5}

Regional to global-scale projections of soil moisture and drought remain relatively uncertain compared to other aspects of the hydrological cycle. Drying in the Mediterranean, southwestern U.S. and southern African regions is consistent with projected changes in Hadley circulation and increased surface temperatures, so surface drying in these regions as global temperatures increase is *likely*. Despite *high confidence* of projected precipitation increases in certain regions, there are no regions of confident projected increases in surface soil moisture (TFE.1, Figure 1). {12.4.5}

Decreases in runoff are *likely* in southern Europe, the Middle East, and southwestern U.S. The CMIP5 models project consistent increases in high latitude runoff, consistent with AR4, but confidence in this projection is tempered by large biases in their simulation of present-day snow cover (TFE.1, Figure 1). {12.4.5}

Annual surface evaporation is projected to increase as global temperatures rise over most of the ocean and is projected to change over land following a similar pattern to precipitation. Prominent areas of projected decreases in evaporation include the southwestern U.S./northwestern Mexico, southern Africa and land bordering the Mediterranean. Evaporation increases over land in the northern high latitudes, consistent with the increase in precipitation and an overall warming, increasing potential evaporation. There is *high confidence* in patterns of this change but there is *low confidence* in the magnitude (TFE.1, Figure 1). {12.4.5}

The frequency distribution of precipitation events is projected to *very likely* undergo changes. For short-duration events, a shift to more intense individual storms and fewer weak storms is *likely*. In moist and some arid and semi-arid regions, extreme precipitation events will *very likely* be more intense and more frequent. Over land areas where increased evapotranspiration is projected, the evidence indicates that soil moisture will decrease over many land areas over the 21st century with *medium confidence* of decrease in dry regions despite an increase in the likelihood of more intense individual storms. {12.4.5}

TS.5.3.2.5 Projected long-term changes in the cryosphere

It is *very likely* that the Arctic sea ice cover will continue shrinking and thinning in the course of the 21st century as global temperature rises (Figure TS.14). The CMIP5 multi-model projections give average reductions in sea ice extent ranging from 39% for RCP2.6 to 94% for RCP8.5 in September and from 9% to 35% in February by the end of the century. It is *very likely* that the September Arctic sea ice will nearly vanish (ice extent less than 1×10^6 km^2) before the end of the century under RCP8.5 forcing. There is also a

high confidence that an increase in annual mean global surface temperature greater than 2°C above present will eventually lead to a nearly ice-free Arctic Ocean in late summer. The CMIP5 multi-model mean projects, for the end of the 21st century, a decrease in Southern Hemisphere sea ice extent from 14% for RCP2.6 to 57% for RCP8.5 in February and from 9% to 29% in September, with a large inter-model scatter. {12.4.6}

[INSERT FIGURE TS.14 HERE]

Figure TS.14: Anomalies in sea ice extent (5-year running mean) as simulated by CMIP5 models over the late 20th century and the whole 21st century under RCP2.6, RCP4.5, RCP6.0 and RCP8.5 for Northern Hemisphere September. Northern Hemisphere spring (March to April average) relative snow covered area (RSCA) in the CMIP5 MMD, obtained through dividing the simulated 5-year box smoothed spring snow covered area (SCA) by the simulated average spring SCA of 1986–2005 reference period. Blue: RCP2.6; Light blue: RCP4.5; Orange: RCP6.0; Red: RCP8.5. Thick lines: MMD average. Shading and thin dotted lines indicate the inter-model spread (one standard deviation). Northern hemisphere diagnosed near-surface permafrost area in the CMIP5 MMD and using 20-year average monthly surface air temperatures and snow depths. Blue: RCP2.6; Light blue: RCP4.5; Orange: RCP6.0; Red: RCP8.5. Thick lines: MMD average. Shading and thin lines indicate the inter-model spread (one standard deviation). {Figures 12.28, 12.32, 12.33}

Some climate change projections exhibit 5–10 year periods of very rapid summer Arctic sea ice decline—greater than has occurred in the period 2008–2012. Nonetheless, there is little evidence in global climate models of a critical threshold in the transition from a perennial ice-covered to a seasonally ice-free Arctic Ocean beyond which further sea ice loss is unstoppable and irreversible. While instances of rapid summer Arctic sea ice loss are *likely* to occur in the future, it appears *unlikely* that these result from a tipping point in the system. {12.4.6}

Snow cover changes result from precipitation and ablation changes, which are sometimes opposite. It is *very likely* that Northern Hemisphere snow cover will reduce as global temperatures rise over the coming century. Projections of the Northern Hemisphere spring snow covered area by the end of the 21st century vary between 7% (RCP2.6) and 25% (RCP8.5) and are fairly coherent among models (Figure TS.14). {12.4.6}

A retreat of permafrost extent with rising global temperatures is *virtually certain*. The projected changes in permafrost are a response not only to warming, but also to changes in snow cover, which exerts a control on the underlying soil. By the end of the 21st century, diagnosed near-surface permafrost area is projected to decrease by between 37% (RCP2.6) to 81% (RCP8.5) (Figure TS.14). {12.4.6}

TS.5.3.2.6 Projected long-term changes in the ocean

It is *very likely* that the AMOC will weaken over the 21st century. It also is *very unlikely* that the AMOC will undergo an abrupt transition or collapse in the 21st century and it is *unlikely* that the AMOC will collapse beyond the end of the 21st century. There is a best estimate decrease in 2100 of about 20–30% for the RCP4.5 scenario and 36–44% for the RCP 8.5 scenario (see also TFE.5). {12.5.5}

On multidecadal timescales, the rate of ocean heat uptake is projected to increase while the radiative forcing increases. Because the ocean integrates the surface heat flux, projections of ocean heat content change following different scenarios do not significantly diverge for several decades. For the period 2081 to 2100, compared to 1986 to 2005, global mean sea level rise due to thermal expansion, which is approximately proportional to the increase in ocean heat content, is *likely* to be in the range 0.14 [0.10 to 0.18] m for RCP2.6, 0.19 [0.14 to 0.23] m for RCP4.5, 0.19 [0.15 to 0.24] m for RCP6.0 and 0.27 [0.21 to 0.33] m for RCP8.5. {13.4.1, 13.5.1}

TS.5.3.2.7 Projected long-term climate change beyond 2100 (see also TFE.8)

Continuing greenhouse gas emissions beyond 2100 as in the RCP8.5 extension induces a total radiative forcing above 12 W m^{-2} by 2300 that would lead to a warming of 8.7°C (range 5.0–11.6) by 2300 (relative to 1986–2005). Continuously reducing emissions beyond 2100, inducing a total radiative forcing below 2 W m^{-2} by 2300 as in the RCP2.6 extension would reduce the warming to 0.6°C (range 0.3–1.0) by 2300 {12.5.1}. If radiative forcing were stabilized, the fraction of realized warming at that point would be between 40 and 90% of the total equilibrium warming. It is strongly dependent on the history of the forcing.

Equilibrium would be reached only after centuries to millennia. {12.5.2} The persistence of warming is substantially longer than the lifetime of anthropogenic greenhouse gases themselves, as a result of non-linear absorption effects as well as the slow heat transfer into and out of the ocean. In much the same way as the warming to a rapid increase of forcing is delayed, the cooling after a decrease of radiative forcing is also delayed. {12.5.2}

TFE.6: Climate Sensitivity and Feedbacks

The description of climate change as a response to a forcing that is amplified by feedbacks goes back many decades. The concepts of radiative forcing and climate feedbacks continue to be refined, and limitations are now better understood; for instance, feedbacks may be much faster than the surface warming (termed rapid adjustments, in which case they may be counted as part of the adjusted forcing, see Box TS.1), feedbacks depend on the type of forcing agent, or may have intrinsic timescales (associated mainly with vegetation change and ice sheets) of several centuries to millennia. Feedbacks relate to the climate sensitivity and present a simplified view of the climate system. Nevertheless, the analysis of physical feedbacks in models and from observations remains a powerful framework that provides constraints on future warming and, combined with estimates of carbon cycle feedbacks (see TFE.5), determines the greenhouse gas emissions that are compatible with climate stabilization targets (see TFE.8). {9.7.2}

The water-vapour/lapse-rate, albedo and cloud feedbacks are the principal determinants of equilibrium climate sensitivity (ECS, the equilibrium change in global mean surface air temperature following a doubling of the atmospheric equivalent CO_2 concentration). All of these feedbacks are *likely* or *very likely* positive. Therefore, there is *very high confidence* that the net feedbacks are strongly positive and the black body response of the climate to a forcing will therefore be amplified. Cloud feedbacks continue to be the largest uncertainty. The transient climate response (TCR, the change in global mean surface air temperature in a 1% per year CO_2 increase experiment at the time of CO_2 doubling) is smaller than the equilibrium response due to transient heat uptake of the ocean. The net "clear-sky" feedback from water vapour and lapse rate changes together is *very likely* positive and approximately doubles the black body response. The mean value and spread in climate models are essentially unchanged from AR4, but are now supported by stronger observational evidence and better process understanding of what determines relative humidity distributions. {7.2.4}. Clouds respond to climate forcing mechanisms in multiple ways and individual cloud feedbacks can be positive or negative. Key issues include the representation of both deep and shallow cumulus convection, microphysical processes in ice clouds, and partial cloudiness that results from small-scale variations of cloud-producing and cloud-dissipating processes. New approaches to diagnosing cloud feedback in GCMs have clarified robust cloud responses, while continuing to implicate low cloud cover as the most important source of intermodel spread in simulated cloud feedbacks. The net radiative feedback due to all cloud types is *likely* positive, although a negative feedback (damping global climate changes) is still possible. This conclusion is reached by considering a plausible range for unknown contributions by processes yet to be accounted for, in addition to those occurring in current climate models. Observations alone do not currently provide a robust, direct constraint, but multiple lines of evidence now indicate positive feedback contributions from changes in both the height of high clouds and the horizontal distribution of clouds. The additional feedback from low cloud amount is also positive in most climate models, but that result is not well understood, nor effectively constrained by observations, so *confidence* in it is *low*. {7.2.4}

Aerosol-cloud processes give rise to a positive feedback on aerosol forcing. The representation of aerosol-cloud processes in climate models continues to be a challenge. Aerosol and cloud variability at scales significantly smaller than those resolved in climate models, and the subtle responses of clouds to aerosol at those scales, mean that, for the foreseeable future, climate models will continue to rely on parameterizations of aerosol-cloud interactions or other methods that represent subgrid variability. This implies large uncertainties for estimates of the forcings associated with aerosol-cloud interactions. {7.4, 7.5.2}

The equilibrium climate sensitivity (ECS) of the CMIP5 models ranges from 2.1 to 4.7°C, which is very similar to the assessed *likely* range in AR4 and in this assessment {12.5.3, Box 12.2}, and the range covered by CMIP3. High climate sensitivities are found in some perturbed parameter ensembles models (PPE), but recent work shows that these are much less likely than those in the consensus range of 2°C–4.5°C. {9.7.3.3} The range of TCR in CMIP5 is also similar in CMIP5 and CMIP3. No correlation is found between biases in

global-mean surface temperature and ECS. {9.7.2} A negative but not significant correlation across the multi-model ensemble between the ECSs and the adjusted 20th century forcings applied to each individual model exists. The evidence for a mechanism compensating for the large range in ECS to produce a narrow range in 20th century temperature change is therefore weaker in CMIP5 than in CMIP3. {9.7.2.3} Relationships between climatological quantities and climate sensitivity are often found within a specific PPE but in many cases the relationship is not robust across PPEs from different models or in CMIP3/5. The assessed literature suggests that the range of climate sensitivities and transient responses covered by CMIP3/5 cannot be narrowed significantly by constraining the models with observations of the mean climate and variability. {9.2.2, 9.7.3} Studies based on PPEs and CMIP3 support the conclusion that a credible representation of the mean climate and variability is very difficult to achieve with ECSs below 2°C. {9.7.3}

Improved and longer records of surface warming and ocean heat uptake, and stronger evidence from a wider range of models have strengthened the observational constraint on TCR, but have not significantly changed the assessment of ECS. The present top of the atmosphere radiation budgets appear consistent with estimates of climate sensitivity based on other methods but uncertainties are too large to provide further constraint. {10.8.2} Thus, credible estimates of ECS from the response to volcanic eruptions and internal variability do not disagree with other estimates, but at present cannot provide more reliable estimates of ECS. {10.8.2}

New estimates of ECS using climate reconstructions and simulations for the Last Glacial Maximum (LGM) indicate that values below 1.4°C or above 6°C are *very unlikely*. This range is also supported by evidence for the last 65 million years. However, asymmetries associated for example with cloud feedbacks, suggest that sensitivity estimates for colder climate conditions are not directly applicable to warmer climate conditions (*low confidence*). Estimates of an Earth System sensitivity including slow feedbacks (e.g., ice sheets or vegetation) are even more difficult to relate to climate sensitivity of the current climate state. {5.3.3} The main limitations of ECS estimates from paleoclimate states are uncertainties in proxy data, spatial coverage of the data, uncertainties in some forcings, and structural limitations in models used in model-data comparisons. {5.3}

Bayesian methods to constrain ECS or TCR in general are sensitive to the assumed prior distributions combining constraints from the observed warming trend, volcanic eruptions, model climatology, and paleoclimate in principle yields narrower estimate, but there is no consensus on how this should be done statistically. This approach is sensitive to the assumptions regarding the independence of the various lines of evidence, the possibility of shared biases in models or feedback estimates, and the assumption that each individual line of evidence is unbiased. {Box 12.2} The combination of different estimates in this assessment is based on expert judgment.

With considerable advances in climate models and in understanding and quantifying climate feedbacks, an ECS greater than about 6°C–7°C is now assessed to be *very unlikely*. The assessed literature supports but does not further constrain the AR4 *likely* range of ECS. ECS is assessed to be *likely* in the range 2°C–4.5°C, and *very likely* above 1.5°C. The most likely value remains near 3°C. The improved high ECS constraint is an expert judgment informed by several lines of evidence. First, the comprehensive climate models used in CMIP3/5 continue to produce an ECS range of 2.1°C–4.7°C. {9.7.2} Second, those perturbed-parameter model versions that show a very high ECS are generally less compelling in their representation of the present climate system. {9.7.3} Third, there is increasing evidence that the adjusted aerosol forcing of the twentieth century is not strongly negative {7.5}, which makes it *unlikely* that the observed warming was caused by a very small net forcing together with very large ECS. And fourth, multiple and at least partly independent observational constraints from the satellite period, instrumental period and palaeoclimate studies continue to yield very low probabilities for ECS above 7°C. {Box 12.2}

On timescales of many centuries and longer, additional feedbacks with their own intrinsic timescales (e.g., vegetation, ice sheets) may become important but are not usually modelled in AOGCMs. The resulting equilibrium temperature response to a doubling of CO_2 on millennial timescales or Earth System Sensitivity is less well constrained but *likely* to be larger than ECS, implying that lower atmospheric CO_2 concentrations are needed to meet a given temperature. These slow feedbacks are less likely to be proportional to global mean temperature change, implying that climate sensitivity changes over time. {12.5.3, 10.8.2} Estimates of Earth System Sensitivity are also difficult to relate to climate sensitivity of the current climate state. {5.3.3}

For the warming over the 21st century, TCR is a more accurate and hence useful indicator of future climate than ECS. The transient climate response (TCR) is *very likely* in the range 1°C–3°C, *likely* in the range 1.2°C–2.6°C (corresponding to the 5–95% of the CMIP5 ensemble), with a most likely value near 1.8°C. These estimates are based in part on the TCR of the CMIP3 and CMIP5 models themselves {9.7.2}, and in part on studies which constrain TCR using observed surface temperature changes, and in some cases also ocean heat uptake and radiative forcing estimates. {10.8.1}

There is *high confidence* in the assessments of ECS and TCR. Both are supported by several different and partly independent lines of evidence, each based on multiple studies, models and datasets. The different lines of evidence are from energy balance studies, CMIP3 and CMIP5 climate model results, perturbed physics model studies, and analysis of the paleoclimate data. All are largely consistent, and the overall assessment of the feedbacks, ECS and TCR is consistent with the observed warming, the estimated forcing, and the projected future warming. {Box 12.2}

TS.5.4 Long-Term Projections of Carbon and Other Biogeochemical Cycles

Projections of the global carbon cycle to 2100 using the CMIP5 Earth System Models (ESMs) that represent a wider range of complex interactions between the carbon cycle and the physical climate system, consistently estimate a positive feedback between climate and the carbon cycle, i.e., reduced natural sinks or increased natural CO_2 sources in response to future climate change (see TFE.7). These results are consistent with the previous AR4 coupled carbon climate simulation results. According to CMIP5 model results it is *very likely* that the global ocean will continue as a net carbon sink for all four RCP concentration scenarios. For scenarios with decreasing areas of anthropogenic land-use (RCP4.5, RCP6.0), it is *very likely* global land will continue as a net carbon sink. For scenarios with increasing areas of land-use (RCP2.6, RCP8.5), a net land sink remains *likely* but some models project a source by 2100. CMIP5 models predict that carbon sinks in tropical land ecosystems are *very likely* to decrease because of climate change. CMIP5 model projections of ocean carbon uptake show less spread in response to CO_2 and climate than the previous C^4MIP generation of models, but there is still significant model spread (4–5 times greater than ocean carbon) in future land carbon storage. Future land use change, and the response of terrestrial ecosystems to it, is an important driver of future terrestrial carbon cycle and contributes significant additional spread to model estimates (see TFE.7). {6.4, Figure 6.19, Figure 6.20, Figure 6.21, Figure 6.22, Figure 6.24}

When forced with RCP8.5 CO_2 emissions, as opposed to the RCP8.5 CO_2 concentrations, CMIP5 ESMs with interactive carbon cycle simulate, on average, a 60 ppm larger atmospheric CO_2 concentration and 0.2°C larger global surface temperature increase by 2100. The value of 60 ppm is uncertain with a range of ±70 ppm in the small number of models available. {12.4.8}

The availability of nitrogen for plant growth will *likely* limit 21st century land carbon uptake resulting in higher atmospheric CO_2 concentration. A key update since AR4 is the introduction of nutrient dynamics in some land carbon models, in particular the limitations imposed by nitrogen availability. Models including the nitrogen cycle predict that the future uptake of anthropogenic CO_2 by land ecosystems is *very likely* to be less than when no nitrogen limitation is modeled. These models also predict that this limitation effect is partly offset by nitrogen supplied by atmospheric deposition, and increased soil nitrogen availability due to warming. In all cases, the net effect is a smaller predicted land sink for a given trajectory of anthropogenic CO_2 emissions. CMIP5 models that neglect nitrogen cycle interactions project excessive land carbon uptake by 2100 by up to 400PgC (see TFE.7). {6.4.6, Figure 6.36}

The combined effect of all processes on future ocean and land carbon uptake allows us to quantify the trajectory of fossil fuel emissions compatible with the RCP future CO_2 concentration pathway scenarios. For RCP2.6 all CMIP5 models project large reductions in emissions relative to present day levels. It is about *as likely as not* that sustained globally negative emissions will be required to achieve the reductions in atmospheric CO_2 in this scenario. CMIP5 models are generally consistent with RCP scenario emissions except for RCP8.5 where the CMIP5 ESMs project lower natural carbon uptake and lower compatible emissions than in this RCP scenario. This difference would be greater if nitrogen limitation on land carbon uptake was included in more of the CMIP5 models. {6.4, Figure 6.25, Figure 6.26} Further details on climate stabilization are given in TFE.8.

With *very high confidence*, the increased storage of carbon by the ocean will increase acidification in the future, continuing the observed trends of the past decades. Ocean carbon cycle models consistently project continued ocean acidification worldwide to 2100 for all RCP pathways. The largest decrease in pH and surface carbonate ion (CO_3^{2-}) is projected to occur in the warmer low and mid-latitudes. However, it is the colder high-latitude oceans that are projected to first become undersaturated with respect to aragonite. Aragonite undersaturation in surface waters is *likely* to be reached by 2100 in the Southern Ocean as highlighted in AR4, but new studies project that undersaturation will even *likely* occur before 2100 in the Arctic (see TFE.7). {6.4, Box 6.5, Figure 6.28}

Ocean carbon and oxygen models suggest that it is *likely* that large decreases in oceanic dissolved oxygen will occur during the 21st century, predominantly in the sub-surface mid-latitude oceans, due to enhanced stratification and warming (see TFE.7). {6.4.5, Box 6.5}

With *very high confidence*, ocean and land ecosystems will continue to respond to climate change and atmospheric CO_2 increases created during the 21st century, even for centuries after any stabilization of CO_2 and climate (see TFE.7).

Carbon Dioxide Removal (CDR) has been proposed to accelerate and/or augment the removal of CO_2 from the atmosphere to reduce climate change. Solar Radiation Management (SRM) is *likely* to impact the carbon cycle through their climate effects (see TFE.8). {6.5}

TFE.7: Carbon Cycle

The AR4 noted that the global increase in temperature since the 1950's is *very likely* caused by increasing greenhouse gases. The three most influential greenhouse gases are carbon dioxide (CO_2), methane (CH_4) and nitrous oxide (N_2O), since they altogether amount to 80% of the total radiative forcing from long-lived greenhouse gases. With a *very high* level of *confidence*, the concentration increase of these greenhouse gases is caused by anthropogenic emissions, and modulated by natural biogeochemical processes. {6.1}

Past changes in these atmospheric greenhouse gas concentrations have been documented back to 800 ka (thousand years ago) from ice cores. The new data expand the AR4 statement that present-day concentrations *very likely* exceed by far the natural range of variability back to 800,000 years ago. On the basis of geological data, which provide indirect and less precise information than ice core records of past CO_2 concentrations, it is *likely* that the present CO_2 concentrations were not exceeded for the past 2.7 million years. There is a *high* level of *confidence* that atmospheric CO_2 concentration exceeded the pre-industrial level for extended periods (on a million-year timescale) during the past 65 million years, though the reconstructed values obtained from geological archives are very uncertain. {5.2}

The natural carbon cycle has been perturbed since the beginning of the Industrial Revolution (~1750) by the anthropogenic release of CO_2 to the atmosphere from fossil fuel burning and changes in land use. Fossil fuel burning is a process related to energy production. Fossil fuel carbon comes from geological deposits of coal, oil and gas that were buried in the Earth crust for millions of years. Land use change is a process related to food and wood production. Land use emitted carbon comes from the decomposition of plants and organic carbon in soils. For instance when a forest is cleared, the decaying dead biomass and soil carbon will release CO_2 to the atmosphere for many years. {6.3}

The human caused release of CO_2 to the atmosphere is partly removed from the atmosphere by natural carbon sinks in land ecosystems and in the ocean. Natural carbon sinks are due to physical, biological and chemical processes acting on different time scales. An excess of atmospheric CO_2 absorbed by land ecosystems gets stored as organic matter in diverse carbon pools, from short lived (leaves, fine roots) to long-lived (stems, soil carbon). An excess of atmospheric CO_2 absorbed by the surface ocean {3.8.1}, then gets mixed and stored into the deep waters on time scales of decades to centuries, and further reacts with ocean carbonate sediments on time scales of centuries to millennia. Finally, on geological time scales of 10,000 years or longer, CO_2 is removed very slowly from the atmosphere by rock weathering. {Box 6.2}

Ocean and land ecosystems will continue to respond to climate change and atmospheric CO_2 increases created during the 21st century, even for centuries after any stabilization. Ocean acidification {3.8.2, FAQ 3.2} will continue in the future as long as atmospheric CO_2 remains above preindustrial levels, with surface waters becoming more corrosive to aragonite shells before the end of the 21st century. Committed land ecosystem carbon cycle changes, i.e., induced changes in CO_2 sources and sinks, will manifest themselves further beyond the end of the 21st century. In addition, there is *medium confidence* that large areas of permafrost will experience thawing, but uncertainty over the magnitude of frozen carbon losses through CO_2 or CH_4 emissions to the atmosphere are large. The thawing of carbon in frozen soils constitutes a positive radiative forcing feedback that is missing in current coupled carbon-climate models projections. {6.4}

Future projections of the coupled carbon-climate system during the 21st century based on CMIP5 coupled models calculate ocean sinks and natural terrestrial ecosystem sinks affected by future climate change by prescribing a set of future atmospheric radiative forcing trajectories, from the Representative Concentration Pathway (RCP) used consistently throughout this report. Stabilization of global temperature requires limiting cumulative carbon emissions to a finite budget (TFE.7, Figure 1, TFE.8). The new CMIP5 models used in this report consistently estimate a positive feedback, i.e., reduced natural sinks or increased natural CO_2 sources in response to future climate change. According CMIP5 model results, carbon sinks in tropical land ecosystems are *very likely* to decrease because of climate change. The simulated carbon cycle - climate feedbacks are about *as likely as not* to differ significantly between the CMIP5 and the C^4MIP models ensembles, but it should be noted that both ensembles were run with differing forcing scenarios and cannot be compared easily. {6.4, Figures 6.19–6.26}

[INSERT TFE.7, FIGURE 1 HERE]

TFE.7, Figure 1: Compatible fossil fuel emissions simulated by the CMIP5 models for the 4 RCP scenarios. Top: timeseries of instantaneous emission rate. Thick lines represent the historical estimates and emissions calculated by the integrated assessment models (IAM) used to define the RCP scenarios, thin lines show results from CMIP5 ESMs. Bottom: cumulative emissions for the historical period (1860–2005) and 21st century (defined in CMIP5 as 2005–2100) for historical estimates and RCP scenarios (bars) and ESMs (symbols). In the CMIP5 model results, total carbon in the land-atmosphere-ocean system can be tracked and changes in this total must equal fossil fuel emissions to the system (see also Table 6.13). Other sources and sinks of CO_2 such as from volcanism, sedimentation or rock weathering, which are very small on centennial timescales, are not considered here. Hence the compatible emissions are given by cumulative-Emissions = $\Delta C_A + \Delta C_L + \Delta C_O$ remission rate = d/dt $[C_A + C_L + C_O]$, where C_A, C_L, C_O are carbon stored in atmosphere, land and ocean respectively. {adapted from Figure 6.25}

Biogeochemical cycles and feedbacks other than the carbon cycle play an important role in the future of the climate system, although the carbon cycle represents the strongest of these. Natural CH_4 emissions from wetland and fires are sensitive to climate change. {6.4.7} Changes in the nitrogen cycle, in addition to interactions with CO_2 sources and sinks, affect emissions of N_2O both on land and from the ocean. {6.4.6} A key update since AR4 is the introduction of nutrient dynamics in some land carbon models, in particular the limitations on plant growth imposed by nitrogen availability. Models including the nitrogen cycle predict a significantly lower uptake of anthropogenic CO_2 in land ecosystems than the C^4MIP model mean. These nutrient-enabled models also predict that this effect is partly offset by direct stimulation of growth due to airborne nitrogen deposition, and increased nutrient availability due to warming. In all cases, the net effect is a smaller predicted land sink for a given trajectory of anthropogenic CO_2 emissions. {6.4.8}

Multi-model projections show large 21st century decreases in oceanic dissolved oxygen caused by enhanced stratification and warming, and mainly located in the sub-surface mid-latitude oceans. There is however no consensus on the future evolution of the volume of hypoxic and suboxic waters, due to the large uncertainties in potential biogeochemical effects and in the evolution of tropical ocean dynamics. A similar degree of complexity exists in the biogeochemical interactions between land, atmosphere and ocean cycles. Many processes, however, are not yet represented in coupled climate-biogeochemistry models and so their magnitudes have to be estimated in offline or simpler models which make their quantitative assessment difficult. It is *likely* there will be non-linear interactions between many of these processes, but these are not yet quantified. Therefore any assessment of the future feedbacks between climate and biogeochemical cycles still contains large uncertainty. {6.4.5}

TFE.8: Climate Targets and Stabilization

Climate Targets

Future anthropogenic emissions of greenhouse gases, aerosol particles and other forcing agents such as land use change are dependent on socio-economic factors including global geopolitical agreements to control those emissions. AR4 made extensive use of the SRES scenarios developed using a sequential approach, i.e., socio-economic factors feed into emissions scenarios, which are then used either to directly force the climate models or to determine concentrations of greenhouse gases, and other agents required to drive these models. In this report, outcomes of simulations that use the new scenarios referred to as "Representative Concentration Pathways" (RCP) are assessed. These RCPs were developed using a parallel process whereby different targets in terms of radiative forcing at 2100 were selected (2.6, 4.5, 6.0 and 8.5 W m^{-2}) and greenhouse gas and aerosol emissions consistent with those targets and their corresponding socio-economic drivers were developed simultaneously (Box TS.4). {Box 1.2, 12.3.1}

Global-mean surface temperatures are projected to rise over the century under all of the GHG concentration pathways represented by the RCPs. Around the mid-21st century, the rate of global warming begins to be more strongly dependent on the scenario. By 2100, the best estimate global mean temperature change relative to 1986–2005 in the non-mitigation RCP8.5 is about a factor of three higher than in the lowest RCP2.6 (*high confidence*), where warming stabilizes in the second half of this century. It is *very likely* that global-mean surface temperatures at the end of the 21st century will be greater than present-day under the specified RCPs. Global-mean surface temperatures for 2081–2100 (relative to 1986–2005) for the CO_2 concentration driven RCPs will *likely* be in the 5–95% range of the CMIP5 models, i.e., 0.2°C–1.8°C (RCP2.6), 1.0°C–2.6°C (RCP4.5), 1.3°C–3.2°C (RCP6.0), 2.6°C–4.8°C (RCP8.5). For RCP4.5, 6.0 and 8.5, global temperatures are projected to *likely* exceed 2°C warming with respect to preindustrial by 2100, and about *as likely as not* to be above 2°C warming for RCP2.6. {12.4.1, Table 12.2}

Continuing greenhouse gas emissions beyond 2100 as in the RCP8.5 extension induces a total radiative forcing above 12 W m^{-2} by 2300 that would lead to a warming of 8.7°C (range 5.0–11.6) by 2300 (relative to 1986–2005). Continuously reducing emissions beyond 2100, inducing a total radiative forcing below 2 W m^{-2} by 2300 as in the RCP2.6 extension would reduce the warming to 0.6°C (range 0.3–1.0) by 2300. For RCP2.6 all CMIP5 models project large reductions in emissions relative to present day levels. It is about *as likely as not* that sustained globally negative emissions will be required to achieve the reductions in atmospheric CO_2 in this scenario. {12.5.1, Figure 12.42}

There is significant spread between ESMs, but no systematic inconsistency between the ESMs compatible fossil fuel emissions and the "original" emissions themselves estimated by the Integrated Assessment Models (IAMs) to define each RCP scenario. By the end of RCP8.5 on average, the CMIP5 models project lower compatible emissions than the IAMs. The IAMs predict that global negative emissions are required to achieve the RCP2.6 decline in radiative forcing from 3 W m^{-2} to 2.6 W m^{-2} by 2100 (see TFE.8, Figure 1). There is disagreement between the complex ESMs over the necessity for global emissions to become negative to achieve this, with four ESM models simulating negative compatible emissions and four ESM models simulating positive emissions from 2080 to 2100. It is important to note that the ESMs themselves make no assumptions about how the compatible emissions could or would be achieved, merely the global total that is required to follow the CO_2 concentration pathway. {6.4.3.3, Box 6.4, 12.3.1}

[INSERT TFE.8, FIGURE 1 HERE]

TFE.8, Figure 1: a) CO_2 emissions for the RCP3PD scenario (black) and three illustrative modified emission pathways leading to the same warming, b) global temperature change relative to preindustrial for the pathways shown in panel a. c) Coloured bands show IAM emission pathways over the twenty-first century. The pathways were grouped based on ranges of *likely* avoided temperature increase in the twenty-first century. Pathways in the yellow, orange and red bands *likely* stay below 2°C, 3°C, 4°C by 2100, respectively, while those in the purple band are higher than that. Emission corridors were defined by, at each year, identifying the 20th to 80th percentile range of emissions and drawing the corresponding coloured bands across the range. Individual scenarios that follow the upper edge of the bands early on tend to follow the lower edge of the band later on, d) global temperature relative to preindustrial for the pathways in panel a. {Figure 12.47}

Climate Stabilization

Stabilization of global temperature requires limiting cumulative carbon emissions to a finite budget. In cumulative terms, the 2°C temperature target implies cumulative carbon emissions by 2100 of about 1000–1300 Pg in the set of scenarios considered, of which about 550 Pg were emitted by 2010. From current emissions (10 Pg yr^{-1} by 2010), this implies carbon emission to decrease by on average about 10% per decade. Analysis of a range of multi-gas emission pathways from integrated assessment models shows that pathways that *likely* limit warming below 2°C (above pre-industrial) by 2100 consist of CO_2-equivalent emissions emissions of about 8.5–12.6 PgC yr^{-1} by 2020, and 4.6–6.3 PgC yr^{-1} by 2050, respectively. Median 2010 emissions of all models are 13.1 PgC yr^{-1} (see TFE.8, Figure 1). {12.5.4}

The near-linear relationship between total carbon emissions and global temperature makes it possible to define a new policy relevant quantity. {12.5.4, Figure 12.45}

The ratio of global temperature change to total cumulative anthropogenic carbon emissions is relatively constant and independent of the scenario, but is model dependent, as it is a function of the model airborne fraction and climate sensitivity. For any given temperature target, higher emissions in earlier decades therefore imply lower emissions by about the same amount later on. The transient climate response to cumulative carbon emission (TCRE) is *very likely* between 0.8°C–3°C PgC^{-1} , with a best estimate in the range of 1.5°C–2.0°C PgC^{-1}, for cumulative emissions less than 2000 PgC until the time at which temperatures peak. Under these conditions, and for low to medium estimates of climate sensitivity, the TCRE is near identical to the peak climate response to cumulated carbon emissions. {12.5.4, Figure 12.45}

The climate system has multiple timescales associated with different thermal reservoirs and reservoirs of carbon. If radiative forcing were stabilized, the fraction of realized warming at that point would be between 40 and 90% of the total equilibrium warming. It is strongly dependent on the history of the forcing. Equilibrium would be reached only after centuries to millennia. The persistence of warming is substantially longer than the lifetime of anthropogenic greenhouse gases themselves, as a result of non-linear absorption effects as well as the slow heat transfer into and out of the ocean. In much the same way as the warming to a rapid increase of forcing is delayed, the cooling after a decrease of radiative forcing is also delayed. For high climate sensitivities, and in particular if sulfate aerosol emissions are eliminated at the same time as greenhouse gas emissions, the commitment from past emission can be strongly positive, and is a superposition of a fast response to reduced aerosols emissions and a slow response to reduced CO_2. {12.5.4}

Stabilization of global temperature does not imply stabilization for all aspects of the climate system. Processes related to vegetation change, changes in the ice sheets, deep ocean warming and associated sea level rise and potential feedbacks linking for example ocean and the ice sheets have their own intrinsic long timescales. Those may result in significant changes hundreds to thousands of years after global temperature is stabilized (see TFE.6). {12.5.4}

Geoengineering - Carbon Dioxide Removal Methods

Several methods have been proposed to remove CO_2 from the atmosphere in the future. They are categorized as Carbon Dioxide Removal (CDR) methods under a broad class of proposals to moderate future climate change. Examples are afforestation/reforestation, carbon sequestration in soils, biomass energy and carbon capture and storage, ocean fertilization, accelerated weathering and direct air capture of CO_2. {6.5.1}

Scientific considerations for evaluating CDR methods include their storage capacity, the permanence of the storage and potential adverse side effects, and the rebound effect, i.e., when carbon is stored in a reservoir, the concentration gradient between the atmosphere and carbon reservoirs is reduced and thereby the subsequent rate of removal of CO_2 from the atmosphere. CDR schemes may not present a viable option to rapidly affect climate on decadal and centennial time scales because of the long time required by relevant natural carbon cycle processes to remove atmospheric CO_2. Currently, the maximum physical potential of atmospheric CO_2 removal by any single CDR scheme that rely on natural carbon cycle processes is at most about 1 PgC yr^{-1}. {6.5.2}

CDR based on land use options may not be achievable in the real world because of other constraints, such as competing demands for land. The level of scientific knowledge on the effectiveness of CDR methods, their side effects on climate, and their potential effects on carbon and other biogeochemical cycles, including ocean acidification and de-oxygenation, is low and uncertainties are very large. {6.5.3}

Geoengineering – Solar Radiation Management

Theory, model studies and observations suggest that some Solar Radiation Management (SRM) methods, if realizable, could substantially offset a global temperature rise and some of its effects. {7.7}

There is *medium confidence* (medium evidence, medium agreement) that stratospheric aerosol SRM is scalable to counter the radiative forcing (RF) and some of the climate effects expected from a twofold increase in CO_2 concentration. Models cited in this assessment explored various source injection strategies and treated aerosol microphysics differently; these variations produce significantly different estimates for the injection rate of chemicals needed to generate the required RF. {7.7.2, 7.7.3}

There is no consensus on whether a similarly large RF could be achieved from cloud brightening SRM due to insufficient understanding of aerosol-cloud interactions. It does not appear that land albedo change SRM can produce a large RF. Limited literature on other SRM methods precludes their assessment. {7.7.2}

SRM would produce an inexact compensation for the RF by greenhouse gases. There is *very high confidence* that there would be residual regional differences in climate (e.g., temperature and rainfall) in comparison to an unperturbed climate, however models consistently suggest that SRM would generally reduce climate differences compared to a world with the same elevated greenhouse gas concentrations and no SRM. {7.7.3, Figures 7.22–7.23}

Numerous side effects and risks from SRM have been identified. For example, there is *high confidence* that SRM by stratospheric sulfate aerosols would increase polar stratospheric ozone depletion. Moreover, if SRM were used to counter a large RF by greenhouse gases and then terminated, most of the warming that had been offset would become evident within a few decades, and the rate of climate change would exceed the rate that would have occurred in the absence of SRM. Other side effects have been identified, and there would be other unanticipated or unexplored impacts. SRM will not compensate for ocean acidification from increasing CO_2. {7.7.2–7.7.4, Figure 7.24}

TS.5.5 Long-Term Projections of Sea Level Change

TS.5.5.1 Projections of Global Mean Sea Level Change for the 21st Century

For the period 2081 to 2100, compared to 1986 to 2005, global mean sea level rise is *likely* to be in the range 0.29–0.55 m for RCP2.6, 0.36–0.63 m for RCP4.5, 0.37–0.64 m for RCP6.0, and 0.48–0.82 m (0.56–0.96 m by 2100) for RCP8.5 (see Table TS.1 and Figure TS.15). Unlike in the AR4, these projections include a contribution from changes in ice-sheet outflow, for which the central projection is 0.11 m. The central projections for global mean sea level rise in all scenarios lie within a range of 0.05 m until the middle of the century, when they begin to separate; by the end of the century, they have a spread of about 0.2 m. Although RCP4.5 and RCP6.0 are very similar at the end of the century, RCP4.5 has a greater rate of rise earlier in the century than RCP6.0. {13.5.1, Table 13.6}

[INSERT FIGURE TS.15 HERE]

Figure TS.15: Projections from process-based models with *likely* ranges and median values for global-mean sea-level rise and its contributions in 2081–2100 relative to 1986–2005 for the four RCP scenarios and scenario SRES A1B used in the AR4. Contributions from ice-sheet dynamical change and anthropogenic land water storage are included in the sum; they are independent of scenario, and are treated as having uniform probability distributions. See discussion in Sections 13.5.1.1 and 13.5.1.3 and Appendix 13.A for methods. {Figure 13.8}

Under all the RCP scenarios, the time-mean rate of global mean sea level rise during the 21st century is *very likely* to exceed the rate observed during 1971-2010. In the projections, the rate of rise initially increases. In RCP2.6 it becomes roughly constant (central projection ~5 mm yr^{-1}) before the middle of the century, and in RCP4.5 and RCP6.0 by the end of the century, whereas acceleration continues throughout the century in RCP8.5 (reaching 8–15 mm yr^{-1} during the last decade). {13.5.1, 13.5.1}

In all RCP scenarios, thermal expansion is the largest contribution, accounting for 30–50% of the total in the central projections, and glaciers are the next largest. The increase in surface melting in Greenland is projected to exceed the increase in accumulation. On the Antarctic ice sheet, surface melting is projected to remain small, while we have *medium confidence* that snowfall will increase (Figure TS.15). {13.3.3, 13.4.3, 13.4.4, 13.5.1, Table 13.6}

We have *medium confidence* in the ability to model future changes in ice-sheet dynamics on decadal timescales. At the time of the AR4, scientific understanding was not sufficient to allow an assessment of the possibility of such changes. Since the publication of the AR4, there has been substantial progress in understanding the relevant processes as well as in developing new ice-sheet models that are capable of simulating them. However, the published literature does not yet offer a sufficient basis for a scenario-dependent assessment. In our projections of global mean sea level rise by 2091–2100, the central estimate of the contribution from dynamical changes on decadal timescales is 0.12 m from the two ice sheets combined, and is the main reason why the projections are greater than those given in the AR4, which did not include such a contribution. {13.1.5, 13.5.1}

It is not understood why semi-empirical models project a higher rate of rise than process-based models and there is no consensus about the reliability of their projections. This difference implies either that there is some contribution which is presently unidentified or underestimated by process-based models, or that the projections of semi-empirical models are overestimates. For RCP4.5, semi-empirical models give central projections in the range 0.73–1.15 m, and similarly for SRES A1B, and their upper bounds extend to about 1.5 m. Semi-empirical models are designed to reproduce the observed sea level record over their period of calibration, but do not attribute sea level rise to its individual physical components. Making projections with a semi-empirical model assumes that sea level change in the future will have the same relationship as it has had in the past to radiative forcing or global mean temperature change. This may not hold if potentially non-linear physical processes do not scale in the future in ways which can be calibrated from the past. In our assessment, ice sheet dynamical changes on decadal timescales cannot be reliably extrapolated from the observed data from which semi-empirical models are calibrated. {13.5.1}

We have *medium confidence* in the projected *likely* ranges of global mean sea level rise during the 21st century. This *confidence* comes from the consistency of process-based models with observations and physical understanding. Larger values cannot be excluded, but current scientific understanding is insufficient for evaluating their probability. {13.5.1}

TS.5.5.2 Projections of Global Mean Sea Level Change Beyond 2100

Global mean sea level rise will *very likely* continue beyond 2100. Ocean thermosteric sea level rise will continue for centuries to millennia, unless global temperatures decline. The amount of ocean thermal expansion increases with global warming (0.2–0.6 m $°C^{-1}$). The glacier contribution decreases over time as their volume (currently ~0.6 m sea level equivalent) decreases. {13.5.2, Figures 3.10–3.11}

Currently available information indicates that the dynamical contribution of the ice sheets will continue beyond 2100, but *confidence* in projections is *low*. In Greenland, ice outflow induced from interaction with the ocean is self-limiting as the ice-sheet margin retreats inland from the coast. By contrast, the bedrock topography of Antarctica is such that there may be enhanced rates of mass loss as the ice retreats. {13.5.2}

With its present topography, surface melting of the Greenland ice sheet is projected to exceed accumulation for global mean surface air temperature over 3.1 [1.9–4.6] °C above preindustrial, leading to ongoing decay of the ice sheet. The reduction in surface elevation as ice is lost increases the vulnerability of the ice sheet; taking this into account, one study estimated a lower threshold of 1.6 [0.8–3.2] °C. The loss of the ice sheet is not inevitable because it has long time scales, and it might re-grow to its original volume or some fraction

thereof if global temperatures decline. However, a significant decay of the ice sheet may be irreversible (se TFE.5). In Antarctica, beyond 2100 and with higher greenhouse gas scenarios, the increase in surface melting could exceed the increase in accumulation. {13.4.3, 13.4.4, Figure 13.11}

Longer-term sea level rise depends on future emissions. The few available model results indicate global mean sea level rise by 2300 is *likely* to be less than 1 m for greenhouse gas concentrations below 500 ppm CO_2-equivalent but rise as much as 1-3 m for concentrations above 700 ppm CO_2-equivalents. {13.5.2, Figures 13.10 and 13.11}

TS.5.5.3 Projections of Regional Sea Level Change

There is *high confidence* that, over the next few decades, the largest sea-level changes will continue to be associated with interannual to decadal sea-level variability. It is *very likely* that, towards the end of the 21st century, sea level change will have a strong regional pattern, which will dominate over variability, with many regions experiencing significant deviations from the global mean change (Figure TS.16). By the end of the 21st century, about 72% and 77% of the global coastlines are projected to experience a sea-level change within 20% of the global mean sea level change, for RCP4.5 and 8.5, respectively. It is *very likely* that over about 95% of the ocean will experience regional sea level rise, but less than about 5% will experience a sea level fall (see Figure 13.15). {13.6.5, 13.6.7}

[INSERT FIGURE TS.16 HERE]

Figure TS.16: Ensemble mean regional sea-level change (m) evaluated from CMIP5 models for scenarios RCP2.6 and RCP8.5 between 1986–2005 and 2081–2100. [PLACEHOLDER FOR FINAL DRAFT: this figure is derived by related methods to those used for Figure 13.15a, but is not entirely consistent; this will be resolved in the final draft.]

Variability in regional sea level change will be caused by ocean dynamical change, mass redistribution, and change in atmospheric pressure. Ocean dynamical ocean change results from changes in wind forcing, associated changes in the circulation, and redistribution of heat and freshwater. Ice-sheet mass loss (both contemporary and past), glacier mass loss and changes in terrestrial hydrology cause water mass redistribution among the cryosphere, the land and the oceans, giving rise to distinctive regional changes in the solid Earth, Earth rotation and the gravity field. Over timescales longer than a few days, regional sea level also adjusts nearly isostatically to regional changes in sea level atmospheric pressure relative to its mean over the ocean. {13.6.2, 13.6.3, 13.6.4}

TS.5.5.4 Projections of Change in Sea Level Extremes and Waves During the 21st Century

It is *very likely* that there will be an increase in the occurrence of future extreme sea level and related coastal flooding events. There is *high confidence* that extremes will increase with global mean sea level rise, however, there is *low confidence* in region-specific projections in storminess and storm surges. The impact on the return period for exceeding given threshold levels is *likely* to be high, for example with current 100-year return period events decreasing to 10-year and possibly 1-year events by the end of the 21st century. {13.7.2, Figure 13.19}

For most regions, there is *low confidence* in wave projections. This reflects the challenge of down-scaling future wind states from coarse resolution climate models into regional and global wave model projections, but dynamical and statistical techniques for wave projections are improving, and ensemble assessments of wave-model projections are beginning to quantify uncertainties. The regions with the largest projected changes in surface wave height are the Southern Ocean, for which projections have *medium confidence*, associated with the projected strengthening of the Westerlies, and the tropical South Pacific, associated with a projected strengthening of austral winter easterly trade winds. A consistent mean decrease in surface wave height is projected for all other ocean basins. {13.7.3, Figure 13.20}

TS.5.6 Climate Phenomena and Regional Climate Change

This section assesses projected changes in large-scale climate phenomena that affect regional climate. Some of these phenomena are defined by climatology (e.g., monsoons), and some by interannual variability (e.g., El Nino), the latter affecting climate extremes such as floods, droughts and heat waves. Changes in statistics of extreme weather phenomena such as tropical cyclones and extratropical storms are also summarized here

TS.5.6.1 Monsoon Systems

There is *medium to high confidence* that the global measure of monsoon precipitation is *likely* to increase in the 21st century while the monsoon circulation weakens. The total surface area affected by monsoons is projected to increase too. Monsoon onset dates are *likely* to become earlier or not to change much and the monsoon retreat dates are *very likely* to delay, resulting in a lengthening of the monsoon season. The increase in seasonal-mean precipitation is pronounced in the East and South Asian summer monsoons while the change in other monsoon regions is subject to large uncertainties (Figure TS.17). {14.2}

[INSERT FIGURE TS.17 HERE]

Figure TS.17: (a) Future change in global monsoon statistics between the present-day (1986–2005) and the future (2080–2099) based on 21 CMIP5 models: area (GMA), seasonal average precipitation (Pav), standard deviation of inter-annual variability in seasonal precipitation (Psd), seasonal maximum 5-day precipitation total (R5d), and monsoon season duration (DUR). Units are % for GMA, Pav, Psd and R5d, and days for DUR. (b) Regional land monsoon domain determined by multi-model mean precipitation in the present-day. (c)-(i) Future change in regional land monsoon statistics: (c) East Asia (EAS), (d) North America (NAM), (e) North Africa (NAF), (f) South Asia (SAS), (g) South America (SAM), (h) South Africa (SAF), and (i) Australia (AUS). Box-whisker plots in blue (red) color are for the RCP4.5 (RCP8.5) scenario. The 10th, 25th, 50th, 75th, and 90th percentiles refer to 3th, 6th, 11th, 16th, and 19th values in ascending order among the 21 models, respectively. All the indices are calculated for the summer season (May-September (MJJAS) for the Northern Hemisphere (NH), November-March (NDJFM) for the Southern Hemisphere (SH) over monsoon domains which are determined in each model and each scenario. The monsoon domains are defined where the annual range of precipitation (difference between MJJAS and NDJFM means) exceeds 2.5 mm per day. {adapted from Figure 14.4}

There is *high confidence* that extreme precipitation will *very likely* increase in all monsoon regions (Figure TS.17), a change much more robust than the seasonal mean. There is *medium confidence* that interannual rainfall variability is *likely* to increase in the future and the relationship between monsoon and El Niño is *likely* to remain, subject to slow natural modulations. {14.2.1}

There is *medium to high confidence* that overall precipitation associated with the Asian-Australian monsoon system is *likely* to increase but with a north-south asymmetry: the Indian monsoon rainfall increases while the changes in the Australian summer monsoon rainfall are small. There is *medium confidence* that the Indian summer monsoon circulation will weaken, compensated by increased atmospheric moisture content *likely* leading to more rainfall. For the East Asian summer monsoon region, both monsoon circulation and rainfall will *likely* increase. It is *likely* that rainfall will increase due to enhanced monsoon circulation and increased water vapour, but there is *low confidence* in the spatial distribution of such rainfall change. There is *medium confidence* that over the Maritime continent monsoon the austral summer precipitation is *likely* to increase. There is *high confidence* that the Australian summer monsoon over the Java archipelago and northernmost Australia will *very likely* to be delayed and shortened while there is a *medium confidence* in the delay of monsoon over the interior of Australia. There is *medium confidence* that the Western North Pacific monsoon is *likely* to weaken, but compensating moisture effects will enhance precipitation. {14.2.2}

There is *low confidence* in projections of the American monsoon precipitation changes. It is *likely* that precipitation associated with the NAMS will arrive later in the annual cycle, and persist longer. Future changes in the timing and duration of the SAMS are also *likely*, but details of these changes remain uncertain. {14.2.3}

There is *medium confidence* that a small delay in the development of the West African mean rainy season is *likely*; but with an intensification of late-season rains. The limitations of model simulations in the region suggest a cautious approach towards future projections. {14.2.4}

TS.5.6.2 Tropical Phenomena and Modes of Variability

There is *medium to high confidence* that annual rainfall change over tropical oceans is *likely to* follow a 'warmer-get-wetter' pattern, increasing where the sea surface temperature (SST) warming exceeds the tropical mean and vice versa. The SST pattern delays the Australian monsoon and shifts the SPCZ. One third of inter-model differences in precipitation projection are due to those in SST pattern. The SST pattern effect on precipitation change is a new finding after AR4. {14.3}

There is *low confidence* in the projection of annual precipitation along the ITCZ, which is generally weak. There is *medium confidence* that the frequency of zonally-oriented SPCZ events is *likely* to increase, with the SPCZ lying well to the northeast of its average position. A reduction of precipitation associated with the SACZ, or southward shifting of the precipitation band, in future projections is *likely*, leading to an increase in precipitation over southeastern South America. {14.3.1} There is *low confidence* in assessing the future changes in MJO due to the poor skill in simulating MJO and its sensitivity to SST warming patterns that are subject to large uncertainties in their future projection. {14.3.2}

There is *medium to high confidence* that the tropical Indian Ocean is *likely* to feature a zonal pattern with reduced (enhanced) warming and decreased (increased) rainfall in the east (west), a pattern especially pronounced during August-November. There is *high confidence* that the Indian Ocean dipole mode will *likely* remain active, with interannual variability unchanged in SST but decreasing in thermocline depth. {14.3.3} There is *low confidence* in the projections over the tropical Atlantic - both for the mean and interannual modes, because of large errors in model simulations of current climate. {14.3.4}

TS.5.6.3 El Nino-Southern Oscillation

There is *high confidence* that ENSO *very likely* remains as the dominant mode of interannual variability in the future. There is *high confidence* that both El Niño and La Niña-induced teleconnection patterns over the extra-tropical Northern Hemisphere are *likely* to move eastwards in the future. There are indications that the central Pacific type of El Niño will become more frequent in a warmer climate but the confidence is *low* because of large natural modulations of El Niño patterns (Figure TS.18). {14.4}

[INSERT FIGURE TS.18 HERE]

Figure TS.18: Comparison of Southern Oscillation index (SOI) standard deviation between the pre-industrial (PiControl) run and RCP8.5 projection (2050–2099). (a) Scatter plot (Unit: hPa) in 20 CMIP5 models. The error bars denote the 95th and 5th percentiles in 50-year windows of PiControl. (b) Ensemble mean standard deviation of SOI in PiControl (blue bar) and RCP8.5 (red), normalized by PiControl value in each model. The dot and error bars denote the 50th, 75th and 25th percentiles in 50-year windows for PiControl, and for inter-model variability for RCP8.5.

TS.5.6.4 Annular and Dipolar Modes of Variability

There is *high confidence* that future boreal wintertime NAO is *very likely* to exhibit large natural variations of similar magnitude to those observed in the past. It is also *very likely* to be differ quantitatively in long-term trend from individual climate model projections and is *likely* to become slightly more positive (on average) due to increases in greenhouse gases. There is *high confidence* that the austral summer/autumn positive trend in SAM is *likely* to weaken considerably as ozone depletion recovers through to the mid-21st century. It is *likely* to continue in austral winter with increasing greenhouse gases, resulting in a continued acceleration of the surface Westerlies in the Southern Ocean. There is *medium confidence* from recent studies that projected changes in NAO and SAM are sensitive to processes that are not yet well represented in many climate models currently used for projections, e.g., stratosphere-troposphere interaction, ozone chemistry, and atmospheric response to sea ice loss. {14.5}

TS.5.6.5 Additional Phenomena of Relevance

There is *low to medium confidence* that it is *likely* that the frequency of Northern Hemisphere and Southern Hemisphere blocking will decrease under increasing GHG concentrations, while trends in blocking intensity and persistence are uncertain. Future strengthening of the zonal wind and meridional jet displacements, e.g.,

associated with changes in NAM and SAM, may partially account for the projected decrease in blocking frequency. {14.6.3}

There is *low to medium confidence* that Tropospheric Biennial Oscillation (TBO) strengthens in the future but the internally generated decadal timescale variability complicates the interpretation of such future changes. {14.6.4}

On the basis of the recent literature, it is *as likely as not* that the Quasi-Biennial Oscillation (QBO) may weaken in future, and its period may increase slightly. {14.6.5} Future changes in the Pacific Decadal Oscillation (PDO) /Inter-decadal Pacific Oscillation (IPO) are uncertain and have not been investigated in any depth. It is presently *as likely as not* that the PDO/IPO will change its form or temporal behaviour in future. {14.6.6} It is *unlikely* that the Atlantic Multidecadal Oscillation (AMO) will change its behaviour as the mean climate changes. However, natural fluctuations in interdecadal modes such as the PDO and AMO over the coming few decades are *likely* to influence regional climates at least as strongly as will human-induced changes (see also Section TS.5.3.1.4). {14.6.7}

TS.5.6.6 Tropical Cyclones

Projections for the 21st century indicate that it is *likely* that the global frequency of tropical cyclones will either decrease or remain essentially unchanged, concurrent with a *likely* global increase in both tropical cyclone maximum wind speed and rainfall rates, but there is *lower confidence* in region-specific projections. For individual basins, the SST warming pattern and multi-decadal climate variability will affect tropical cyclone activity through much of the 21st century (Figure TS.19, see also TFE.9). {Box 14.2}

[INSERT FIGURE TS.19 HERE]

Figure TS.19: Tropical cyclone characteristics: General consensus assessment of the numerical experiments described in Box 14.2, Tables 1–4. All values represent expected percent change (year 2100 relative to 2000) under an A1B-like scenario, based on expert judgment after subjective normalization of the model projections. Four metrics were considered: the percent change in 1) the total annual frequency of tropical storms, 2) the annual frequency of Category 4 and 5 storms, 3) the mean Lifetime Maximum Intensity (LMI; the maximum intensity achieved during a storm's lifetime), and 4) the precipitation rate within 200 km of storm center at the time of LMI. For each metric, the first numeric value is the best guess of the expected percent change, and the range in parentheses is the 67% (*likely*) confidence interval for this value. Nine regions were considered: Global, Northern Hemisphere, Southern Hemisphere, Eastern North Pacific, North Atlantic, Northern Indian, Southern Indian, Western North Pacific, and South Pacific. {Box 14.2, Figure 1}

TS.5.6.7 Extra-Tropical Cyclones

There is *high confidence* that the global number of extra-tropical cyclones is *unlikely* to decrease by more than a few percent due to global warming and that future changes in storms are *likely* to be small compared to natural interannual variability and substantial variations between model simulations of storms. There is *high confidence* that a small poleward shift is *likely* in the Southern Hemisphere storm track, but the magnitude is model-dependent. There is *medium confidence* that a poleward shift in the North Pacific storm track is *more likely than not,* and that storm activity over the North Atlantic is *likely* to increase along the storm track and extends farther downstream into Europe, and to decrease on both the north and south flanks, especially over the Mediterranean. There is *low confidence* in the impact of storm track changes on regional climate at the surface especially for extreme events. {Box 14.3}

TFE.9: Climate Extremes

Assessing changes in climate extremes poses unique challenges, not just because of the intrinsically rare nature of these events, but because, they invariably happen in conjunction with disruptive conditions. They are strongly influenced by both small and large-scale weather patterns, modes of variability, thermodynamic processes, land-atmosphere feedbacks and antecedent conditions. Much progress has been made since AR4 particularly by the comprehensive assessment of extremes undertaken by the SREX. {2.6, Box 2.4}

For some climate extremes such as droughts, floods and heat waves, several factors need to be combined to produce an extreme event. Analyses of rarer extremes such as 1-in-20 to 1-in-100 year events using Extreme Value Theory are making their way into a growing body of literature. {Box 2.4, 12.4.3} Other recent advances concern the notion of "fraction of attributable risk" that aims to link a particular extreme event to specific causal relationships. {10}

TFE.9, Table 1 indicates some of the widespread changes that have been observed in a range of extremes indices over the last 50 years, the probability that those changes are related to a human influence and how those extremes are expected to change in the future. {2.6, 11.3.2, 12.4.3}

[INSERT TFE.9, TABLE 1 HERE]

TFE.9, Table 1: Recent trends, assessment of human influence on the trend, and projections for extreme weather and climate events for which there is an observed late-20th century trend. Bold indicates a revised assessment since AR4 (2007), (*) indicates a revised assessment from the SREX (2012) and (#) indicates that an assessment was not provided by either AR4 or SREX. {2.6, 11.3.2, 12.4.3, 12.4.4, 12.4.5}

Temperature Extremes, Heat Waves and Warm Spells

For temperature extremes, particularly those related to minimum temperature, it is *very likely* there have been statistically significant changes associated with warming since the mid-20th century. These changes are well simulated by current climate models and it is *very likely* that anthropogenic forcing has affected the frequency of these extremes. This supports AR4 and SREX conclusions although with greater confidence in the anthropogenic forcing component compared to AR4. {10.6.1}

For land areas with sufficient data there has been an overall increase in the number of warm days and nights (with warming trends between 2.48 ± 0.64 and 5.75 ± 1.33 days per decade dependent on index). Similar decreases are seen in the number of cold days and nights. Warm spells or heat waves containing consecutive extremely hot days or nights are often associated with quasi-stationary anticyclonic circulation anomalies and are also affected by pre-existing soil conditions and the persistence of soil moisture anomalies that can amplify or dampen heat waves particularly in moisture-limited regions. Most global land areas, with a few exceptions, have experienced more heat waves since the middle of the 20th century. Several studies suggest that increases in mean temperature account for most of the changes in heat wave frequency, however, heat wave intensity/amplitude is highly sensitive to changes in temperature variability and shape and heat wave definition also plays a role. {2.6} For regions such as Europe, where historical temperature reconstructions exist going back several hundreds of years, the hot summer temperatures between 2001 and 2010 stand substantially above any other decade since 1500. {Box 2.5}

While the observed features of temperature extremes and heat waves are well simulated by climate models, they tend to overestimate (underestimate) the warming of warm (cold) extremes. {9} Regional downscaling now offers credible information on the spatial scales required for assessing extremes and improvements in the simulation of the El Nino-Southern Oscillation from CMIP3 to CMIP5 and other large-scale phenomenon is crucial. {2.6, 9.5.3, 9.6, 14.4} However simulated changes in frequency and intensity of extreme events is limited by observed data availability and quality issues and by the ability of models to reliably simulate soil moisture feedbacks and mean changes in key features of circulation such as blocking. {2, 9, 10}

Since AR4, the understanding of mechanisms and feedbacks leading to projected changes in extremes has improved. There continues to be strengthening evidence for a human influence on the observed frequency of extreme temperatures and some heat waves. {10} Near-term (decadal) projections suggest *very likely* increases in temperature extremes but with little distinguishable separation between emissions scenarios {11.3.2}, (TFE.9, Figure 1). However future changes associated with the warming of temperature extremes in the long-term are *virtually certain* and scale with the strength of emissions scenario i.e., greater anthropogenic emissions correspond to greater warming of extremes (TFE.9, Figure 1). For high emissions scenarios, it is *likely* that a 20-year maximum temperature event will become a one-in-two to one-in-five

year event by the end of the 21st century. {12} The magnitude of both high and low temperature extremes will increase faster than the mean. {12}

[INSERT TFE.9, FIGURE 1 HERE]

TFE.9, Figure 1: Maps indicate the CMIP5 multi-model ensemble of (a) annual maximum of maximum daily temperature and (c) annual maximum five-day precipitation accumulation as percent change over the 2081–2100 period relative to 1986–2005 in the RCP8.5 experiments. Timeseries plots show global mean projections for the occurrence of (b) annual maximum of maximum daily temperature (c) precipitation intensity, and (d) annual maximum five-day precipitation accumulation from CMIP5 for the RCP2.6, RCP4.5 and RCP8.5 scenarios relative to 1986–2005. Panel (a) shows percentage of cold days (tx10p: Tmax below the 10th percentile), panel (b) shows percentage of warm days (tx90p: Tmax exceeds the 90th percentile), panel (c) shows relative change of simple precipitation intensity (sdii: average daily wet-day precipitation amount) and panel (d) shows relative changes of annual maximum consecutive 5-day precipitation amounts. Map (left hand side) show the CMIP5 multi-model median change in 20-year return values of annual warm temperature extremes as simulated by CMIP5 models in 2081–2100 relative to 1986–2005 in the RCP8.5 experiments; and map (right hand side) indicates CMIP5 multi-model ensemble R5dmax, the annual maximum five-day precipitation accumulation as percent change over the 2081–2100 period relative to 1986–2005 in the RCP8.5 experiments. {Figure 12.26, 12.13}

Precipitation Extremes

It is *likely* that there have been statistically significant increases in the number of heavy precipitation events in more regions than there have been statistically significant decreases, but there are strong regional and sub-regional variations. There is *medium confidence* that anthropogenic forcing has contributed to this trend over land regions with sufficient observational coverage. {2.6.2}

There is *medium confidence* that CMIP5 models tend to simulate more intense and thus more realistic precipitation extremes than CMIP3. Lack of understanding of soil moisture, clouds and precipitation interactions, as well as controls on local circulation, limits confidence in projections of precipitation changes on even the largest catchment scale. {7.6.2, 7.6.3, 7.6.5}

The frequency distribution of precipitation events is projected to *very likely* undergo changes. While regional changes will vary and are hard to predict, a physical basis exists to suggest that wet regions are *likely* to become wetter and dry regions drier as the climate warms. {7} The temperature-dependence (Clausius-Clapeyron relationship) of short-duration precipitation extremes is *likely* to increase more strongly than associated increases in mean precipitation but varies by region. {7.6.2, 7.6.3, 7.6.5} Regionally the intensity of rain events is *likely* to increase while the number of rainy days is expected to decrease e.g., in southern Asia during the monsoon season. The overall most consistent trends towards heavier precipitation events are found in North America (*likely* increase over the continent). {12.4.5}

For the near- and long-term, CMIP5 projections confirm a clear tendency for increases in heavy precipitation events in the global mean seen in the AR4, but there are significant variations across regions (TFE.9, Figure 1). {11.3.2, 12.4.5}

Floods and Droughts

There continues to be a lack of evidence and thus *low confidence* regarding the sign of trend in the magnitude and/or frequency of floods on a global scale. The current assessment does not support the AR4 conclusions regarding global increasing trends in droughts but rather concludes that there is not enough evidence at present to suggest *high confidence* in observed trends in dryness. Regional to global-scale projections of drought remain relatively uncertain although drying in the Mediterranean, southwestern U.S. and southern Africa is *likely*. {2.6.2}

There is *low confidence* in observed large-scale trends in dryness (lack of rainfall), due to lack of direct observations, dependencies of inferred trends on the index choice and geographical inconsistencies in the trends. {2.6.2} On millennial timescales, proxy information provides evidence of megadroughts and paleoflood discharges of greater magnitude than observed during the 20th century. However in some regions

(e.g., near East, India, central North America) modern large floods are comparable or surpass in magnitude and/or frequency historical floods. There is *high confidence* that during the Little Ice Age more megadroughts occurred in Asia with wetter conditions in the South American monsoon region compared to the Medieval Climate Anomaly and 20th century. {5.5.4, 5.5.5}

Over land areas where increased evapotranspiration is projected, more frequent and more intense periods of agricultural drought will follow despite an increase in the likelihood of more intense individual storms. {12.4.5}

Tropical and Extratropical Cyclones

Recent re-assessments of tropical cyclone data do not support the AR4 conclusions of an increase in the most intense tropical cyclones or an upward trend in the potential destructiveness of all storms since the 1970s. There is *low confidence* that any reported long-term changes are robust, after accounting for past changes in observing capabilities. However over the satellite era, increases in the intensity of the strongest storms in the Atlantic appear robust. {2.6.3}

Some high-resolution atmospheric models have realistically simulated tracks and counts of tropical cyclones but there is *low confidence* in attribution of changes in tropical cyclone activity to human influence due to insufficient observational evidence and a low level of scientific understanding. {10.6.1}

While projections indicate that it is *likely* that the global frequency of tropical cyclones will either decrease or remain essentially unchanged, concurrent with a *likely* increase in both global mean tropical cyclone maximum wind speed and rainfall rates, there is lower confidence in region-specific projections of frequency and intensity. It is *more likely than not* that the frequency of the most intense storms will increase substantially in some basins under projected 21st century warming. {Box 14.2}

Research subsequent to the AR4 and SREX continues to support a *likely* poleward shift of extratropical cyclones since the 1950s. However over the last century there is *low confidence* of a clear trend in storminess due to inconsistencies between studies or lack of long-term data in some parts of the world (particularly in the Southern Hemisphere). There is *low confidence* in trends in extreme winds due to quality and consistency issues with analysed data. {2.6.4}

It is *likely* that there has been an anthropogenic contribution to a southward shift of the storm tracks in the Southern Hemisphere. In the Northern Hemisphere winter, there is an overall reduced frequency of storms and less indication of a poleward shift in the tracks, except possibly over East Asia. A poleward shift in Southern Hemisphere storm tracks is *very likely* by the end of the 21st century. A reduction in the occurrence of Northern Hemisphere extratropical storms is *likely*, although, the most intense storms reaching Europe will *likely* increase in the strength. An increase in the North Atlantic Oscillation is *likely* to increase both the number of wintertime storms heading into Northern Europe and also increase the average intensity of precipitation per storm. {Box 14.3}

TS.6 Key Uncertainties

TS.6.1 Observation of Changes in the Climate System

- There is only *medium to low confidence* in the rate of change of tropospheric warming and its vertical structure. Estimates of tropospheric warming rates encompass surface temperature warming rate estimates. There is *low confidence* in the rate and vertical structure of the stratospheric cooling. {2.4.4}

- *Confidence* in global precipitation change over land is *low* prior to 1950 and *medium* afterwards because of incomplete data coverage. {2.5.1}

- Substantial ambiguity and therefore *low confidence* remains in the observations of global-scale cloud variability and trends. {2.5.7}

- There continues to be insufficient evidence and thus *low confidence* for consistent trends in the magnitude or frequency of floods on a global scale. {2.6.2}

- Not enough evidence exists at present to suggest anything else than *low confidence* in observed large-scale trends in dryness (lack of rainfall), due to lack of direct observations, dependencies of inferred trends on the index choice and geographical inconsistencies in the trends. {2.6.2}

- There is *low confidence* that any reported long-term changes in tropical cyclone characteristics are robust, after accounting for past changes in observing capabilities. However over the satellite era, increases in the intensity of the strongest storms in the Atlantic appear robust. {2.6.3}

- Large variability on interannual to decadal time scales and remaining differences between data sets hamper robust conclusions on long-term changes in large-scale atmospheric circulation. {2.7}

- Even after removing the substantial biases in the ocean temperature instrumental records, different global estimates have variations at different times and for different periods, suggesting that sub-decadal variability in the temperature and upper ocean heat content (0–700 m) is still poorly characterized in the historical record. {3.1}

- Below an ocean depth of 700 m the sparse sampling in space and time prevents reliable estimates of temperature and ocean heat content change, since the vertical gradients (especially between 700 m and 2000 m depth) are still sufficiently large for transient variations (ocean eddies, internal waves, and internal tides) to alias estimates from sparse data sets. Towards the bottom, vertical gradients are weaker, and estimates are more reliable. {3.2.4}

- Changes in the temperature and salinity of the upper ocean have resulted in changes in the properties of major water masses in each of the ocean basins. However, the presence of energetic interannual to multi-decadal variability makes it difficult to detect significant trends from the short and incomplete observational record. {3.5}

- In Antarctica, available data are inadequate to assess the status of change of many characteristics of sea ice (e.g., thickness and volume). There are also contrasting regions around the Antarctic where, over the period of satellite observations, the ice-free season has lengthened, and others where it has shortened. {4.2.3}

- Time series of global glacier mass change seem to overestimate recent loss. On a global scale the mass loss from melting at calving fronts and iceberg calving are not yet comprehensively assessed. The largest uncertainty in estimated mass change from glaciers comes from the Antarctic periphery where most recent estimates show lower losses than previously estimated. {4.3.3}

- Although there is high confidence in recent observations that suggest that observed changes in ice flow are *likely* due to oceanic changes in glacial fjords (Greenland) and beneath ice shelves (West Antarctica), the observational record of ice-ocean interactions around both ice sheets remains poor. {4.4}

- In the Southern Hemisphere, very few long snow cover records exist; satellite records of snow water equivalent date from 1979, but show no trends. {4.5.2}

TS.6.2 Drivers of Climate Change

- The anthropogenic forcing under any of the RCPs is projected to dwarf natural forcing over the 21st century. This does not exclude the possibility of a large volcanic eruption that would induce a negative RF similar in magnitude to the anthropogenic forcing, but only for a few years. {8.5}

- Although the availability of satellite observations and a better understanding of the processes lead to a narrower range of RF estimates, the large uncertainty in aerosol forcing is the dominant contributor to overall net anthropogenic forcing uncertainty. {7.4}

- There is now a better understanding of carbon cycle, water vapour and cloud feedbacks on climate. Carbon cycle feedback is *very likely* positive; water vapour feedback is *virtually certain* positive, while the cloud feedback is *likely* positive but remains a key uncertainty for assessing climate change. {6.4, 7.2}

TS.6.3 Understanding the Climate System and its Recent Changes

- Robustness of detection is subject to climate models correctly simulating internal variability. While comparison with observations indicates that climate models have an adequate simulation of multi-decadal scale variability it is difficult to estimate multi-decadal variability directly from the observational record. {10.1, 10.2}
- Observational uncertainties for climate variables, uncertainties in forcings such as aerosols, and limits in process understanding continue to hamper attribution of changes in many aspects of the climate system, making it more difficult to discriminate between natural internal variability and externally forced changes. {10.9.1}
- Components of the water cycle generally remain less reliably modelled than temperature related quantities, limiting confidence in attribution assessments. Observational uncertainties and the large effect of natural variability on observed precipitation also preclude a more confident assessment of precipitation changes and their attribution. {10.3.2}
- In some aspects of the climate system, including drought, tropical cyclone activity, Antarctic warming, and Antarctic mass balance, *confidence* in attribution remains *low* due to observational and modelling uncertainties. {10.5.2, 10.6.1}
- At regional scales considerable challenges remain in attributing observed changes to external forcing. Modelling uncertainties related to model resolution and incorporation of relevant processes become more important at regional scales, and the effects of internal variability become more significant in masking or enhancing externally forced changes. {10.3.1}
- Increased understanding of the uncertainties associated with radiosonde and satellite records makes assessment of causes of observed trends in the upper troposphere less confident than an assessment of overall atmospheric temperature changes. {10.3.1}
- The ability to simulate changes in frequency and intensity of some extreme events is limited by the available observational information on these rare events and the ability of models to reliably simulate mean changes in key features. {10.6.1}
- There is *low confidence* in the attribution of warming in Antarctica, due to the large observational uncertainties in estimating Antarctic temperatures. Any attribution of changes in Antarctic ice sheet mass balance to human influence is premature, and there is limited scientific understanding regarding changes in Antarctic sea ice distribution {10.5.2}

TS.6.4 Projections of Global and Regional Climate Change

- Based on model results there is *medium confidence* in the predictability of yearly to decadal averages of temperature both for the global average and for some geographical regions. Multi-model results for precipitation indicate generally low predictability. Short-term climate projection is also limited by the *low confidence* in projections of natural forcing. {11.1, 11.2.2, 11.3.1, Box 11.1}
- There is *low confidence* in near-term projections for a poleward shift of the position and strength of Northern Hemisphere storm tracks. {11.3.2}
- There is generally *low confidence* in basin-scale projections of significant trends in tropical cyclone frequency and intensity in the 21st century. {11.3.2, Box 14.2}
- There is little robustness in projected changes in near-term soil moisture and surface run off. {11.3.2, Figure 11.18}

- Except for the Atlantic Meridional Overturning Circulation there is generally *low confidence* and little consensus on the possibility and likelihood of abrupt or nonlinear changes in the climate system over the 21st century. Likewise there is no consensus that such events can be excluded to occur. {12.5.5}

- There is *medium confidence* in the magnitude of carbon losses through CO_2 or CH_4 emissions to the atmosphere from thawing permafrost. There is limited confidence in future methane emissions from natural sources due to changes in wetlands and gas hydrate release from the sea floor. {6.4.3}

- There is *medium confidence* in the projected contributions to sea level rise by models of ice sheet dynamics for the 21st century, and *low confidence* in their projections beyond 2100. There is no consensus about the reliability of semi-empirical models, which give higher projections of sea level rise than process-based models. {13.3.3}

- There is *low confidence* in projections in many aspects of climate phenomena, including changes in the amplitude and spatial pattern of modes of climate variability. {9.5.3, 14.2–14.6}

Tables

Table TS.1: Projected change in global average surface air temperature (SAT) and sea level rise (SLR) for three time horizons during the 21st century. {Table 12.2, Table 13.5, 12.4.1, 11.3.2}

Variable	Scenario	2016–2035**	Level of Confidence*	2046–2065	Level of Confidence*	2081–2100	Level of Confidence*
ΔSAT[a] [°C]	RCP2.6	0.7 [n/a]	n/a	1.0 [n/a]	n/a	1.0 [0.2–1.8]	*high*
	RCP4.5	0.7 [n/a]	n/a	1.4 [n/a]	n/a	1.8 [1.0–2.6]	*high*
	RCP6.0	0.7 [n/a]	n/a	1.3 [n/a]	n/a	2.3 [1.3–3.2]	*high*
	RCP8.5	0.8 [n/a]	n/a	2.0 [n/a]	n/a	3.7 [2.6–4.8]	*high*
Total SLR[b] [m]	RCP2.6	0.11 [0.08–0.14]	*medium*	0.25 [0.19–0.33]	*medium*	0.42 [0.29–0.55]	*medium*
	RCP4.5	0.11 [0.08–0.14]	*medium*	0.27 [0.20–0.35]	*medium*	0.49 [0.36–0.63]	*medium*
	RCP6.0	0.11 [0.07–0.14]	*medium*	0.26 [0.19–0.34]	*medium*	0.50 [0.37–0.64]	*medium*
	RCP8.5	0.12 [0.08–0.15]	*medium*	0.31 [0.23–0.39]	*medium*	0.64 [0.48–0.82]	*medium*

Notes:
(a) CMIP5 ensemble; anomalies calculated with respect to 1986–2005; Numbers are in the format: mean [likely range]
(b) 21 CMIP5 models; anomalies calculated with respect to 1986–2005. Where CMIP5 results were not available for a particular AOGCM and scenario, they were estimated as explained in Chapter 13, Table 13.5. The contributions from ice sheet dynamical change and anthropogenic land water storage are treated as independent of scenario, since scenario dependence cannot be evaluated on the basis of existing literature, and as having uniform probability distributions, uncorrelated with the magnitude of global climate change. Numbers are in the format: mean [likely range]
* [PLACEHOLDER FOR FINAL DRAFT: Level of confidence to be updated]
** [PLACEHOLDER FOR FINAL DRAFT: Near-term values and ranges to be updated]

TFE.9, Table 1: Recent trends, assessment of human influence on the trend, and projections for extreme weather and climate events for which there is an observed late-20th century trend. Bold indicates a revised assessment since AR4 (2007), (*) indicates a revised assessment from the SREX (2012) and (#) indicates that an assessment was not provided by either AR4 or SREX. {2.6, 11.3.2, 12.4.3, 12.4.4, 12.4.5}

Phenomenon and direction of trend	**Likelihood that trend occurred in late 20th century (typically post 1950)**	**Likelihood of a human contribution to observed trend**	**Likelihood of future trends based on projections for the next few decades#**	**Likelihood of future trends based on projections for 21st century using RCP scenarios**
Warmer and fewer cold days and nights over most land areas	*Very likely*	***Very likely**** [a]	*Very likely*	*Virtually certain*
Warmer and more frequent hot days and nights over most land areas	*Very likely*	***Very likely**** [a]	*Very likely*	*Virtually certain*
Warm spells/heat waves. Frequency increases over most land areas	***Medium confidence***	***Likely*** [b]	*Likely*	*Very likely*
Heavy precipitation events. Frequency (or proportion of total rainfall from heavy falls) increases over more areas than decreases	*Likely*	***Medium confidence***	*Likely*	*Very likely** [c]
Increases in frequency and/or intensity of drought[d]	*Low confidence** [d]	*Low confidence** [d]	Not assessed	*Likely* in some regions* [d]
Intense tropical cyclone activity increases	***Low confidence*** [e]	***Low confidence*** [e]	*Low confidence*	***Medium confidence***

Notes:
(a) SREX assessed *likely* anthropogenic influence on trends at the global scale.
(b) SREX did not provide an explicit attribution of warm spells/heat waves to human contributions.
(c) SREX assessed a *likely* increase in the frequency of heavy precipitation events or increase in the proportion of total rainfall from heavy falls over many areas of the globe, in particular in high latitudes and tropical regions.
(d) AR4 assessed the overall area affected by drought. SREX assessed with *medium confidence* that some regions of the world had experienced more intense and longer droughts, and *medium confidence* that anthropogenic influence had contributed to some observed changes in drought pattern. There was also *medium confidence* in a projected increase in duration and intensity of droughts in some regions of the world.
(e) Assessments of 50-year global trends limited by data uncertainties. Higher confidence of increased activity in some regions linked to anthropogenic aerosol forcing.

Climate Change 2013: The Physical Science Basis

Technical Summary

Coordinating Lead Authors: Thomas Stocker (Switzerland), Qin Dahe (China), Gian-Kasper Plattner (Switzerland)

Lead Authors: Lisa Alexander (Australia), Simon Allen (Switzerland), Nathaniel Bindoff (Australia), Francois-Marie Breon (France), John Church (Australia), Ulrich Cubasch (Germany), Seita Emori (Japan), Piers Forster (United Kingdom), Pierre Friedlingstein (United Kingdom), Nathan Gillett (Canada), Jonathan Gregory (United Kingdom), Dennis Hartmann (USA), Eystein Jansen (Norway), Ben Kirtman (USA), Reto Knutti (Switzerland), Krishna Kumar Kanikicharla (India), Peter Lemke (Germany), Jochem Marotzke (Germany), Valerie Masson-Delmotte (France), Gerald Meehl (USA), Igor Mokhov (Russia), Shilong Piao (China), Venkatachalam Ramaswamy (USA), David Randall (USA), Monika Rhein (Germany), Maisa Rojas (Chile), Christopher Sabine (USA), Drew Shindell (USA), Lynne Talley (USA), David Vaughan (United Kingdom), Shang-Ping Xie (USA)

Contributing Authors (list to be updated): Olivier Boucher (France), Philippe Ciais (France), Peter Clark (USA), Matthew Collins (United Kingdom), Joey Comiso (USA), Gregory Flato (Canada), Jens Hesselbjerg Christensen (Denmark), Albert Klein Tank (Netherlands), Gunnar Myhre (Norway), Scott Power (Australia), Stephen Rintoul (Germany), Matilde Rusticucci (Argentina), Michael Schulz (Germany), Peter Stott (United Kingdom), Donald Wuebbles (USA)

Review Editors: Sylvie Joussaume (France), Joyce Penner (USA), Fredolin Tangang (Malaysia)

Date of Draft: 5 October 2012

Notes: TSU Compiled Version

Figures

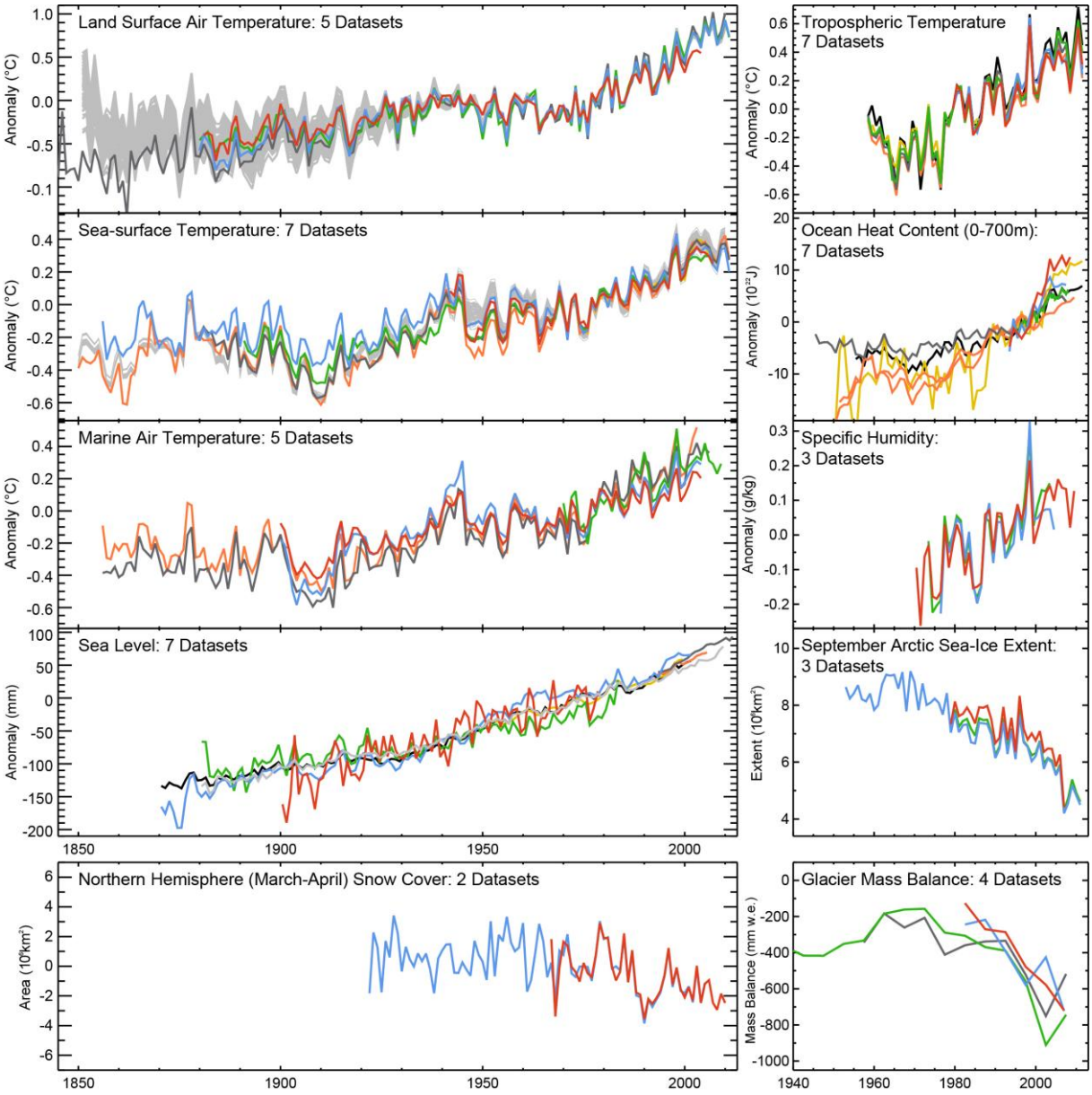

Figure TS.1: Multiple complementary indicators of a changing global climate. Each line represents an independently-derived estimate of change in the climate element. All publicly-available, documented, datasets known to the authors have been used in this latest version. In each panel all datasets have been normalized to a common period of record. A full detailing of which source datasets go into which panel is given in the Appendix to Chapter 2. {FAQ 2.1, Figure 1}

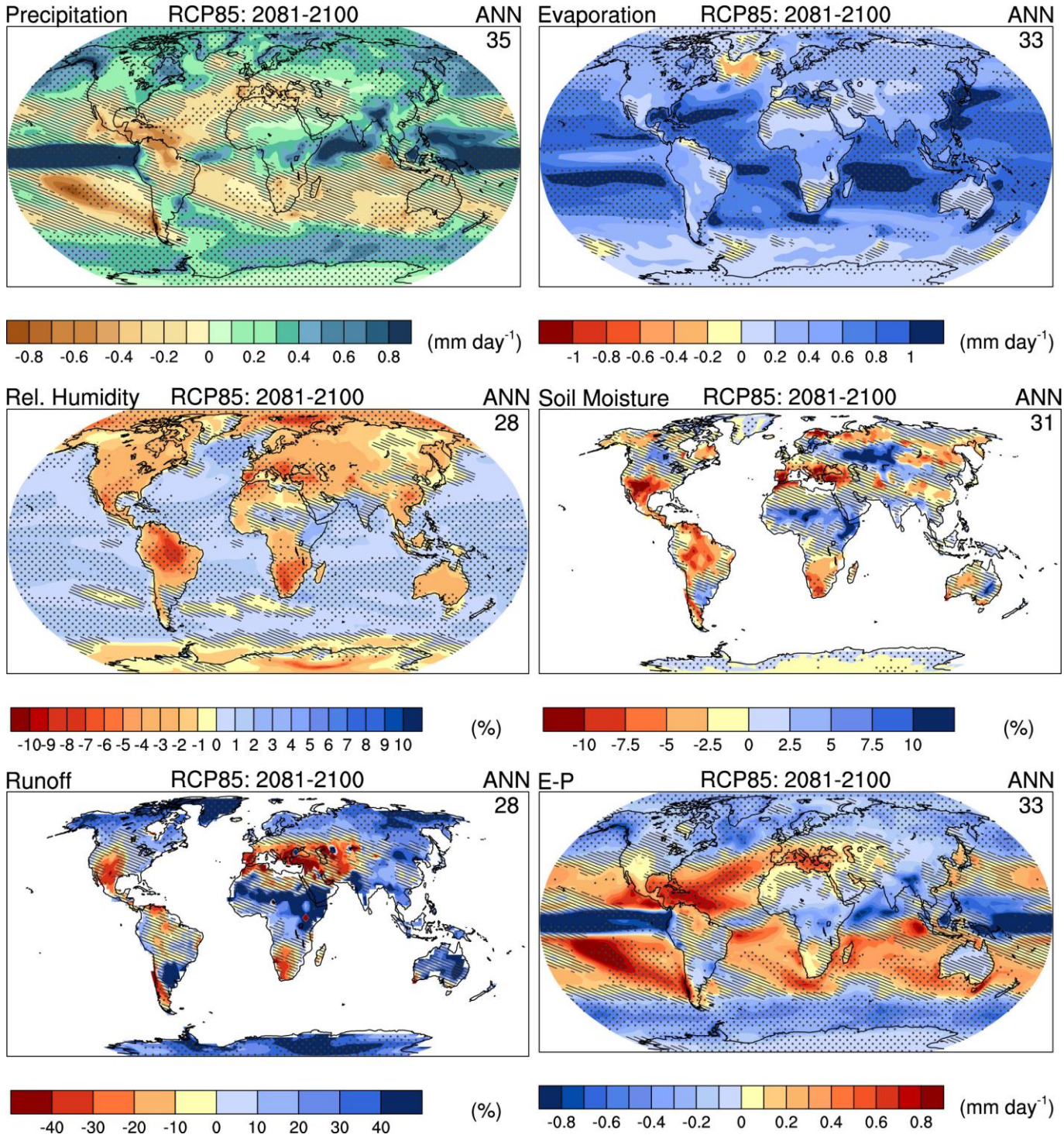

TFE.1, Figure 1: Annual mean changes in precipitation (P), evaporation (E), relative humidity, soil moisture, runoff, and E-P, for 2081–2100 relative to 1986–2005 under the RCP8.5 scenario (see Box TS.4). {Figures 12.25–12.27}

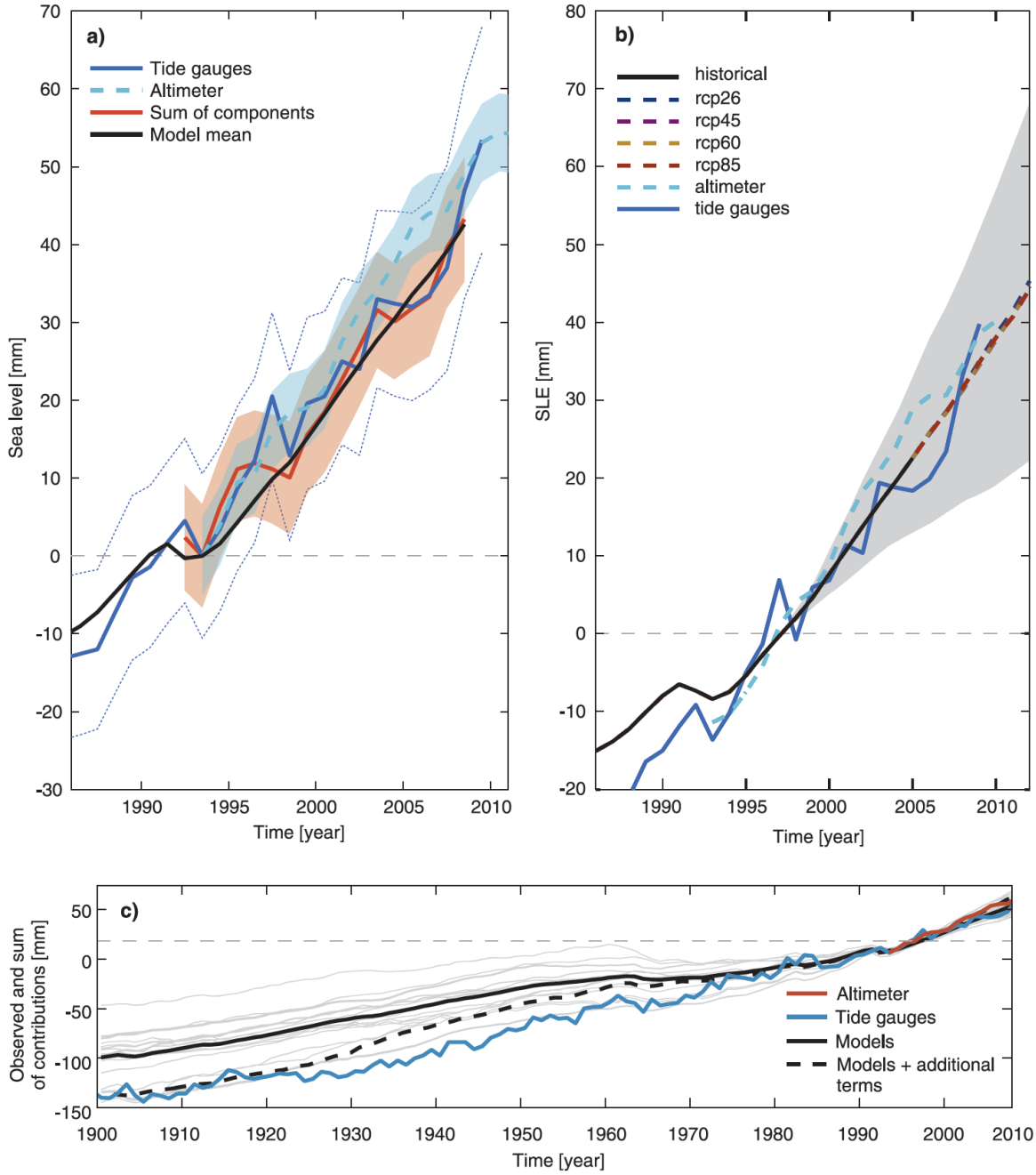

TFE.2, Figure 1: Observed and modelled global-mean sea level. (a) Observed GMSL from satellites (light blue dashed) and estimated from tide gauges (dark blue solid) and the sum of contributions (red). The shading indicates 5-95% confidence limits. The mean sea level from the sum of modeled thermal expansion, glaciers and land water storage is in black. (b) The projected sea level rise relative to the 1986–2005 average (black and coloured lines for the four scenarios, with shading indicating the likely range). Also shown is the observed sea level from (a), set to have the same value as the projections over 1993 to 2001. (c) Observed sea level (blue - tide gauges; red - altimeter) and modeled sea level (black, the sum of ocean thermal expansion, glaciers and land water storage, and black dashed also including a small long-term contributions from ice sheets, the possible underestimate in modelled thermal expansion from not including preindustrial volcanic forcing, and from greater mass loss from glaciers during the 1930's due to unforced climate variability). {Figures 13.4, 13.5}

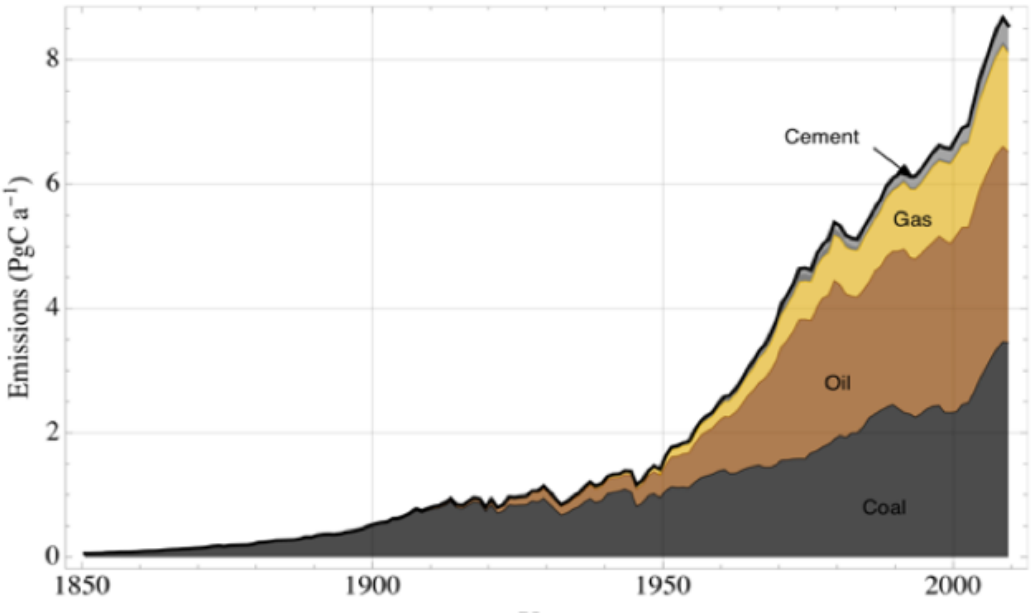

Figure TS.2: Anthropogenic emissions of carbon dioxide from the indicated fuel or activity. {Figure 6.8}

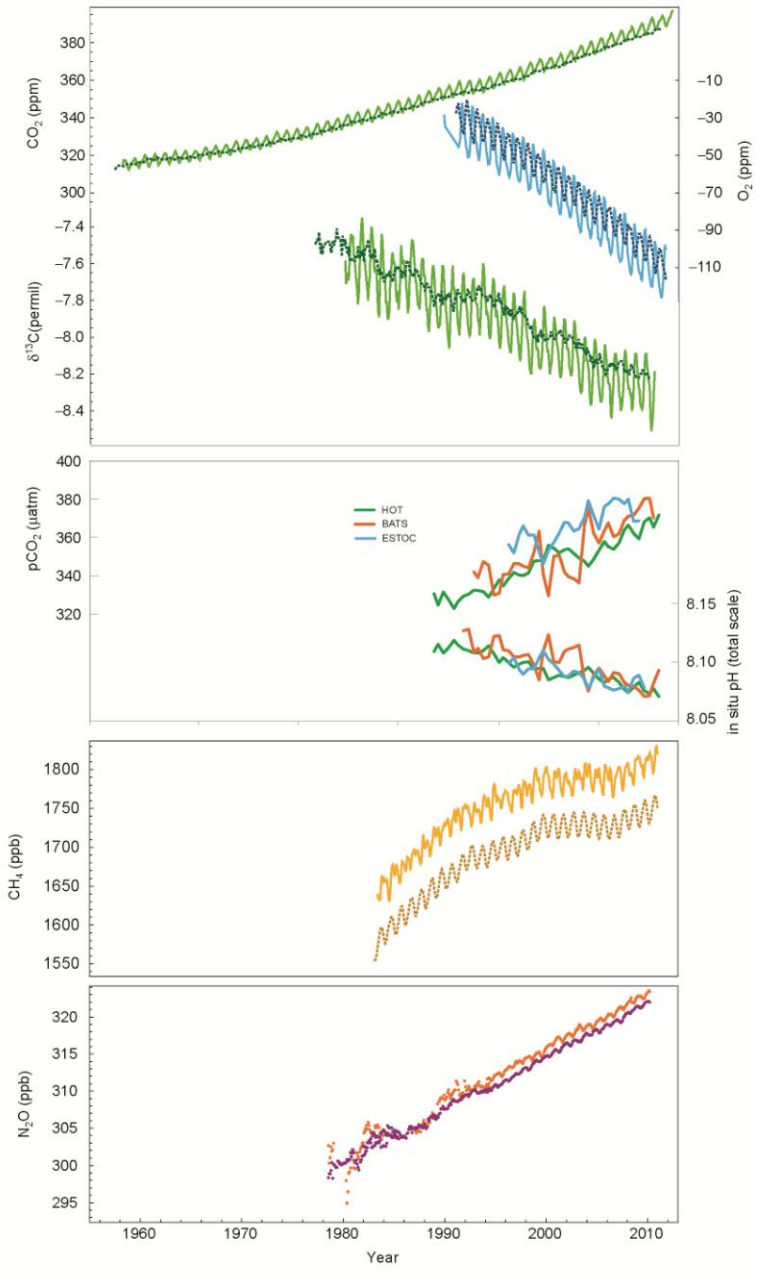

Figure TS.3: Atmospheric concentration of CO_2, oxygen, $^{13}C/^{12}C$ stable isotope ratio in CO_2, CH_4 and N_2O, and oceanic surface observations of pCO_2 and pH, recorded over the last decades at representative stations in the northern and the southern hemisphere from the observatories and time series stations. MLO: Mauna Loa Observatory; SPO: South Pole; HOT: Hawaii ocean Time series station; MHD: Mace Head; CGO: Cape Grim; ALT: Alert. {Figure 6.3 and FAQ 3.2, Figure 1}

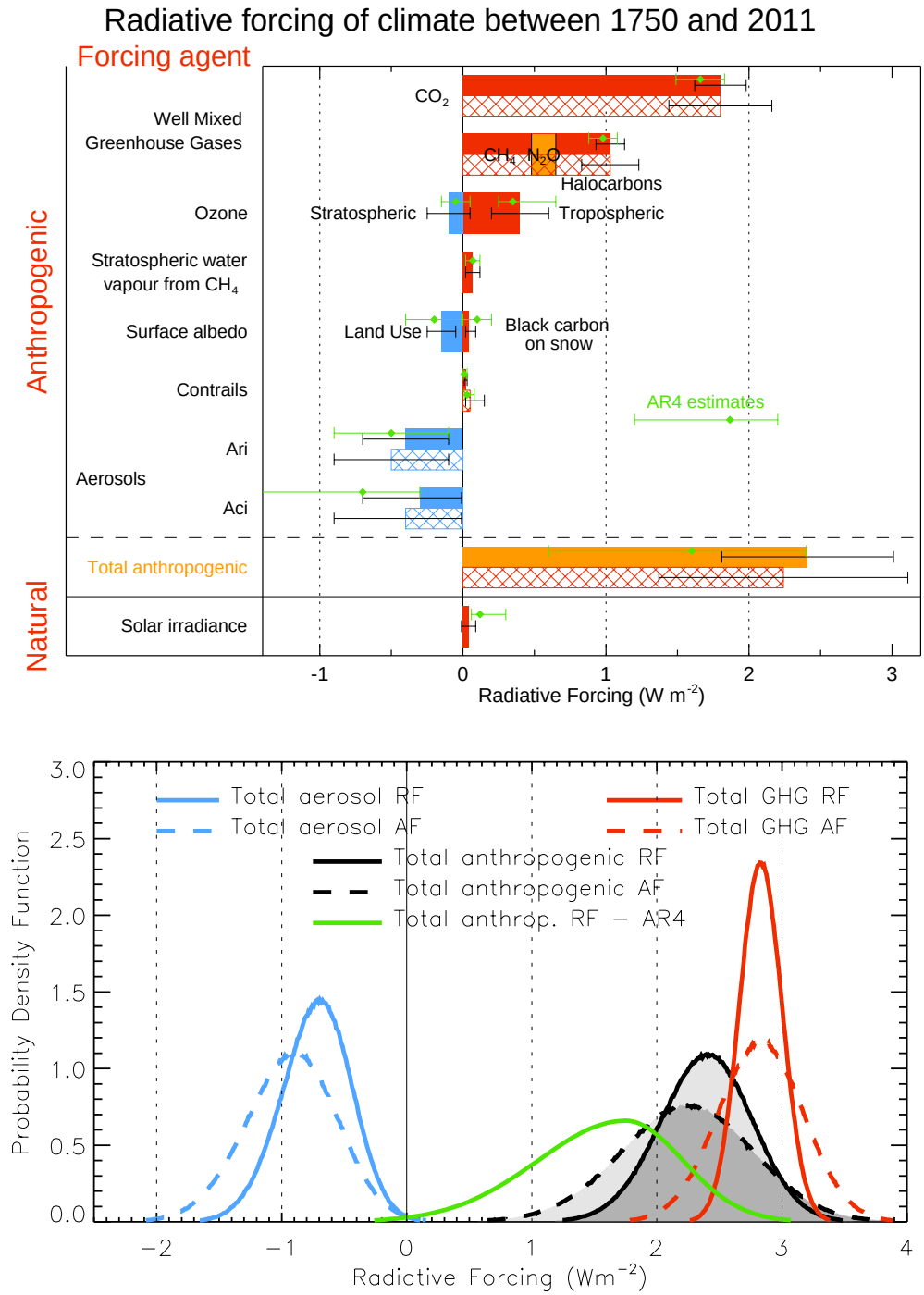

Figure TS.4: Radiative forcing (RF) and Adjusted forcing (AF) of climate change during the industrial era. Top: Forcing by concentration between 1750 and 2010 with associated uncertainty range (solid bars are RF, hatched bars are AF, green diamonds and associated uncertainties are those assessed in AR4). Bottom: Probability Density Functions for both the AR and AF, for the aerosol, WMGHG and total. The green line shows the AR4 estimate for the total anthropogenic RF and shall be compared to the black line which is the same for AR5. ArI=Aerosol Radiative Forcing through interaction with radiation, AcI=Aerosol Radiative Forcing through effects on clouds. {Figure 8.17}

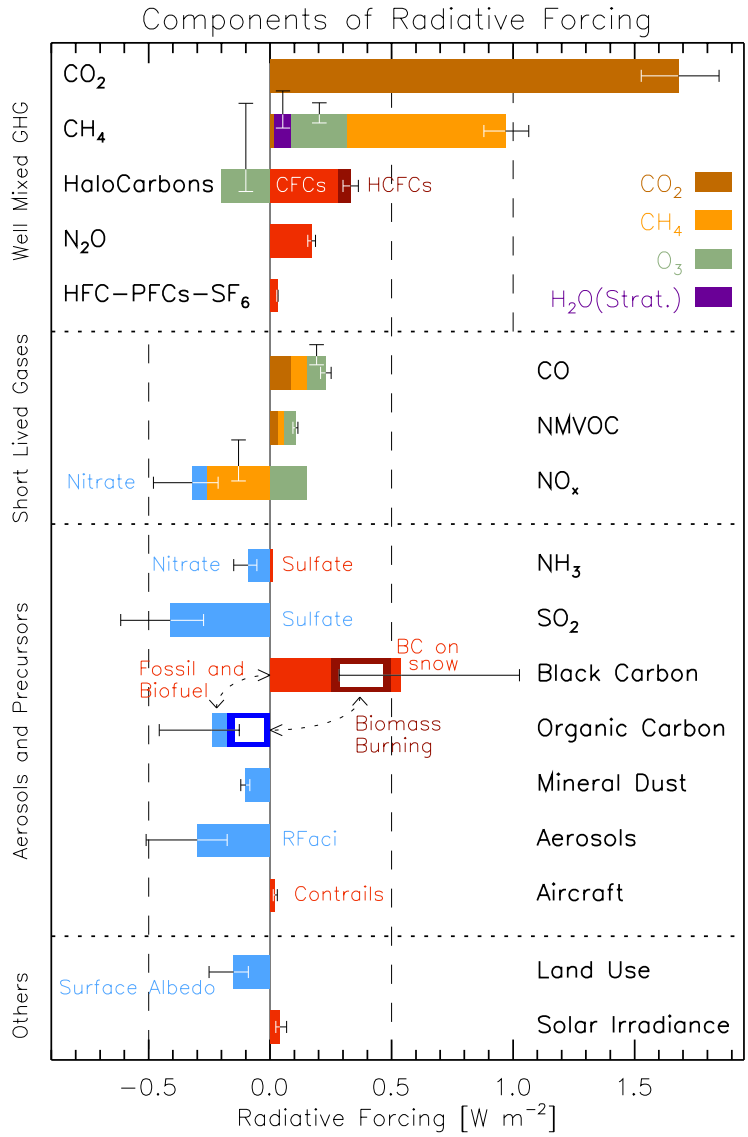

Figure TS.5: Radiative forcing of climate change during the industrial era shown by emitted components from 1750 to 2010. The horizontal bars indicate the overall uncertainty, while the vertical bars are for the individual components. CFCs= Chlorofluorocarbons, HCFCs= Hydrochlorofluorocarbons, HFCs=Hydrofluorocarbons, PFCs= Perfluorocarbons, NMVOC= Non Methane Volatile Organic Compounds, BC= Black Carbon, RFaci= Aerosol Radiative Forcing through effects on clouds. {Figure 8.17}

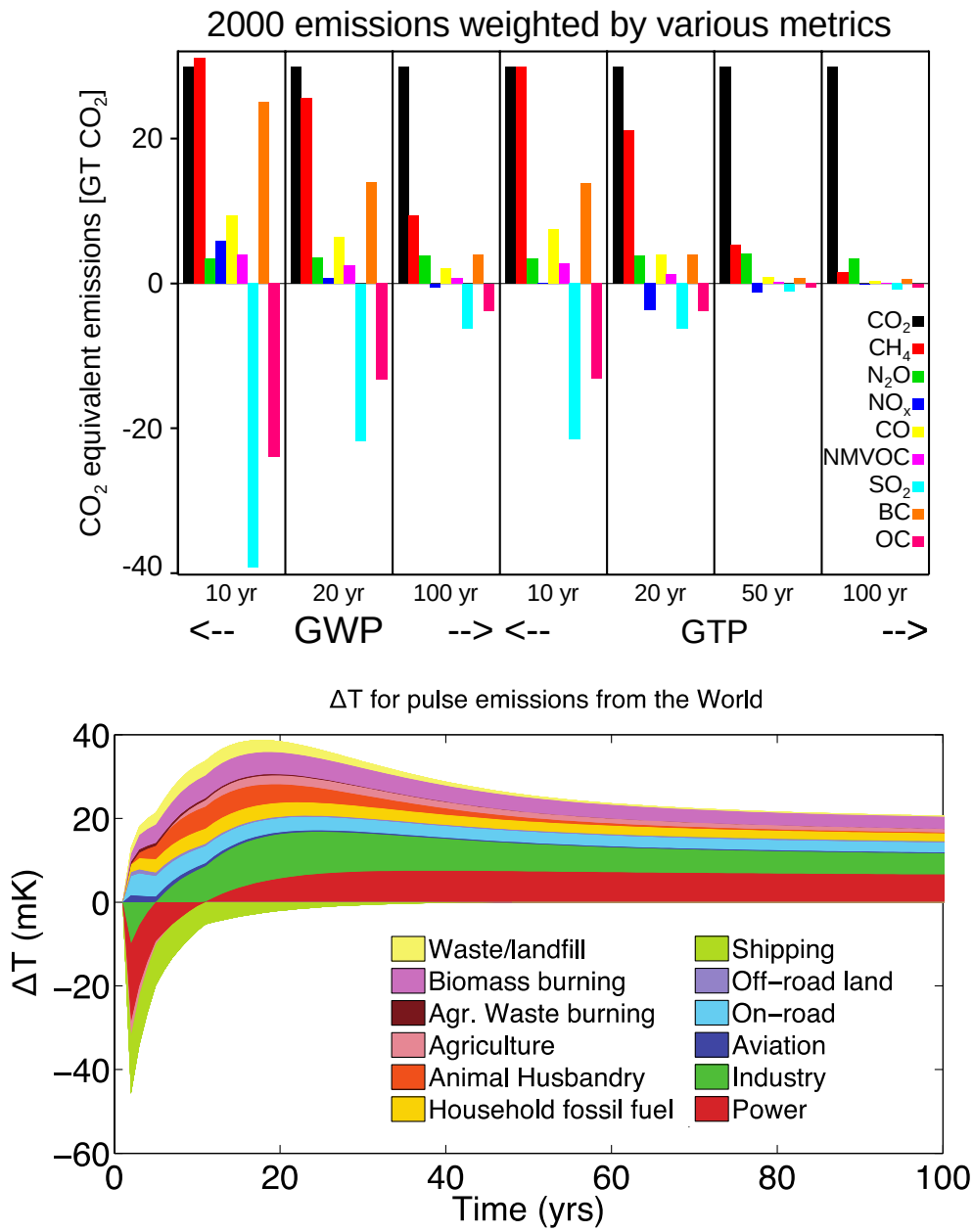

Figure TS.6: Global anthropogenic present-day emissions weighted by GWP and GTP for the chosen time horizons (top). Effective amount of year 2010 (single-year pulse) emissions using the Global Warming Potential (GWP), which is the global mean radiative forcing integrated over the indicated number of years relative to the forcing from CO_2 emissions, and the Global Temperature Potential (GTP) which estimates the impact on global mean temperature based on the temporal evolution of both radiative forcing and climate response relative to the impact of CO_2 emissions. The Absolute GTP (AGTP) as a function of time multiplied by the present-day emissions of all compounds from the indicated sector is used to estimate global mean temperature response (bottom; AGTP is the same as GTP, except is not normalized by the impact of CO_2 emissions). The effects of aerosols on clouds (and in the case of black carbon, on surface albedo) and aviation-induced cirrus are not included. {Figure 8.31, Figure 8.32}

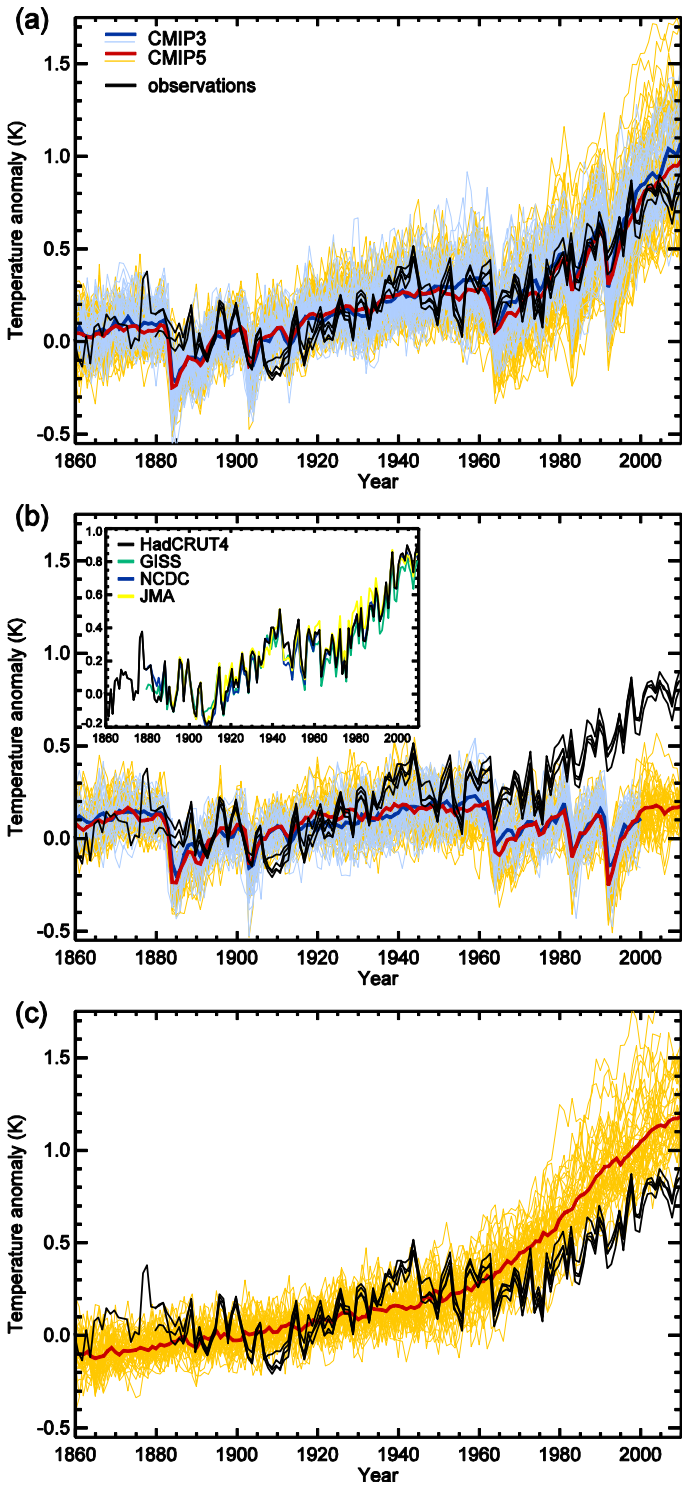

Figure TS.7: Four observational estimates of global mean temperature (black lines) from HadCRUT4, GISTEMP, and NOAA NCDC, JMA, compared to model simulations [both CMIP3 – thin blue lines and CMIP5 models – thin yellow lines] with greenhouse gas forcings only (bottom panel), natural forcings only (middle panel) and anthropogenic and natural forcings (upper panel). Thick red and blue lines are averages across all available CMIP3 and CMIP5 simulations respectively. Ensemble members are shown by thin yellow lines for CMIP5, thin blue lines for CMIP3. All simulated and observed data were masked using the HadCRUT4 coverage, and global average anomalies are shown with respect to 1880–1919, where all data are first calculated as anomalies relative to 1961–1990 in each grid box. Inset to middle panel shows the four observational datasets distinguished by different colours. {Figure 10.1}

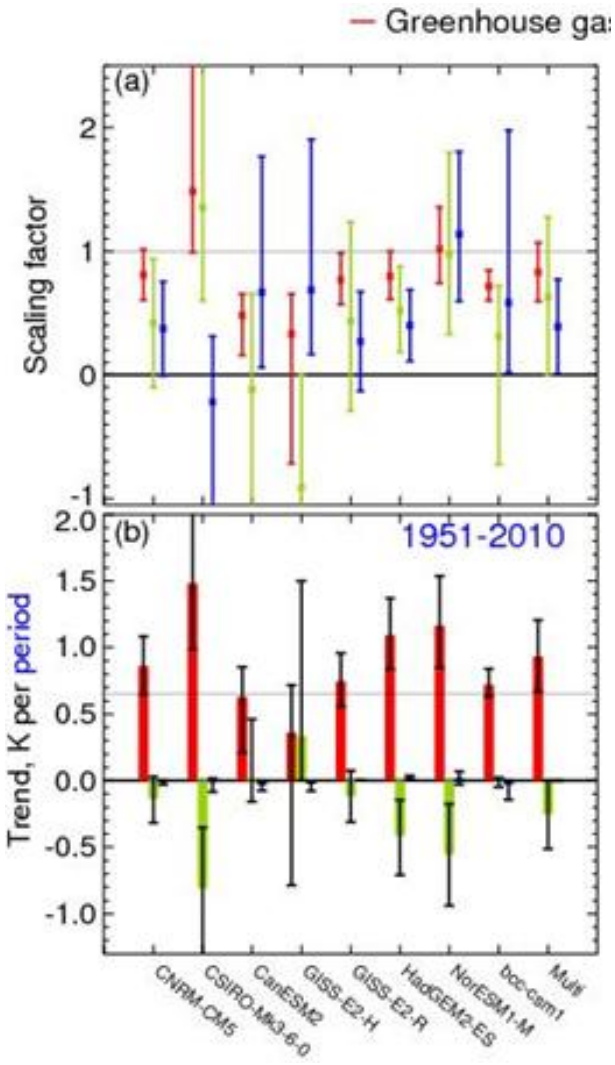

Figure TS.8: Estimated contributions from greenhouse gas (red), other anthropogenic (green) and natural (blue) components to observed global surface temperature changes a) from HadCRUT4 showing 5 to 95% uncertainty limits on scaling factors estimated using 8 climate models and a multi-model average (multi) and based on an analysis over the 1951–2010 period and b) The corresponding estimated contributions of forced changes to temperature trends over the 1951–2010 period. {Figure 10.4}

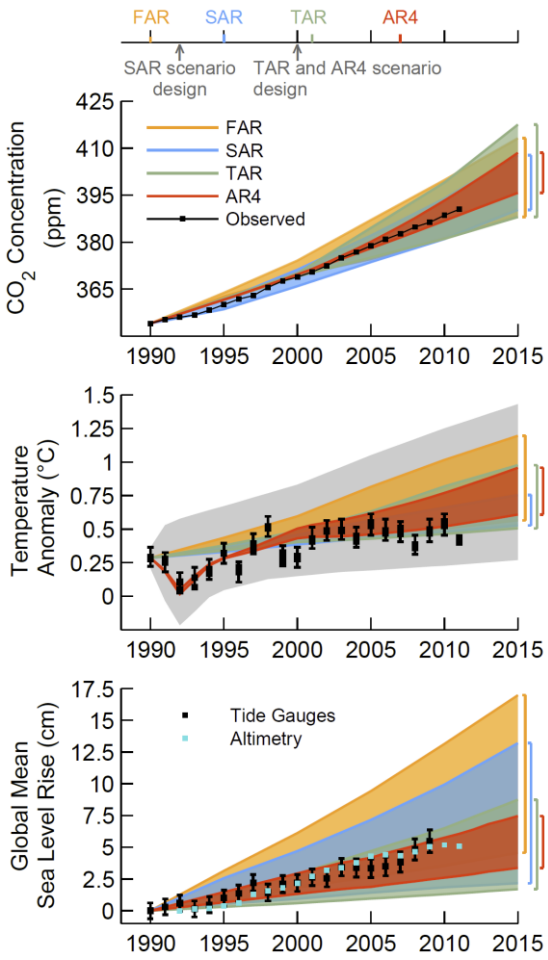

TFE.3, Figure 1: [PLACEHOLDER FOR FINAL DRAFT: Observational datasets will be updated as soon as they become available] (top) Observed globally and annually averaged carbon dioxide concentrations in parts per million (ppm) since 1990 compared with projections from the previous IPCC assessments. Observed global annual CO_2 concentrations are shown in black (based on NOAA Earth System Research Laboratory measurements). The uncertainty of the observed values is 0.1 ppm. The shading shows the largest model projected range of global annual CO_2 concentrations from 1990 to 2015 from FAR (Scenario D and business-as-usual), SAR (IS92c and IS92e), TAR (B2 and A1p), and AR4 (B2 and A1B). (middle) Estimated changes in the observed globally and annually averaged surface temperature (in °C) since 1990 compared with the range of projections from the previous IPCC assessments. Values are aligned to match the average observed value at 1990. Observed global annual temperature change, relative to 1961–1990, is shown as black squares (NASA, NOAA, and UK Hadley Centre reanalyses). Whiskers indicate the 90% uncertainty range from measurement and sampling, bias and coverage (see Supplementary Material for Chapter 1 for methods). The coloured shading shows the projected range of global annual mean near surface temperature change from 1990 to 2015 for models used in FAR (Scenario D and business-as-usual), SAR (IS92c/1.5 and IS92e/4.5), TAR (full range of TAR Figure 9.13(b) based on the GFDL_R15_a and DOE PCM parameter settings), and AR4 (A1B and A1T). The 90% uncertainty estimate due to observational uncertainty and internal variability based on the HadCRUT4 temperature data for 1951–1980 is depicted by the grey shading. Moreover, the publication years of the assessment reports and the scenario design are shown. (bottom) Estimated changes in the observed global annual sea level since 1990. Estimated changes in global annual sea level anomalies from tide gauge data (black error bars showing 1σ uncertainty) and based on annual averages from TOPEX and Jason satellites (blue dots) starting in 1992 (the values have been aligned to fit the 1993 value of the tide gauge data). The shading shows the largest model projected range of global annual sea level rise from 1990 to 2015 for FAR (Scenario D and business-as-usual), SAR (IS92c and IS92e), TAR (A2 and A1FI) and based on the CMIP3 model results available at the time of AR4 using the SRES A1B scenario. Additional details and references for data given in Chapter 1 {1.3.1, 1.3.2}. {Figure 1.4, Figure 1.6, Figure 1.11}

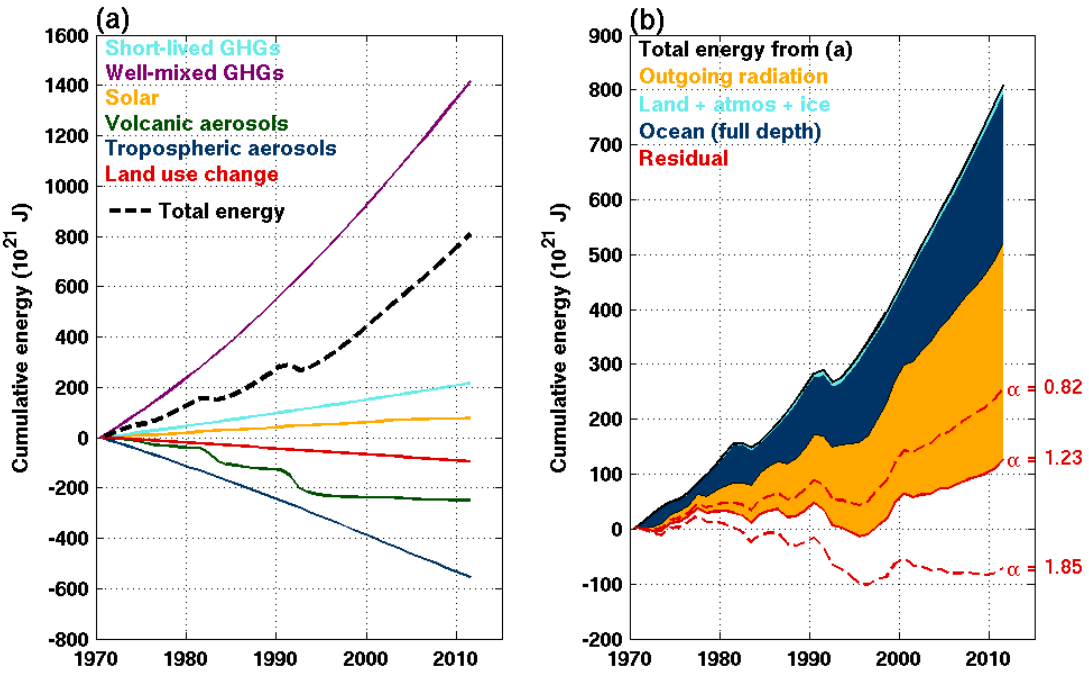

TFE.4, Figure 1: The Earth's energy budget from 1970 through 2010. (a) The cumulative energy flux into the Earth system from changes in well-mixed greenhouse gases, short-lived greenhouse gases, solar forcing, surface albedo caused by land use, volcanic forcing, and tropospheric aerosol forcing are shown by the coloured lines; these contributions are added to give the total energy changes (dashed black line). (b) The cumulative total energy change from (a), with an expanded scale, is balanced by the energy absorbed in the melting of ice; the warming of the atmosphere, the land, and the ocean; and the increase in outgoing radiation inferred from the temperature change of a warming Earth. These terms are represented by the time-varying thicknesses of the coloured regions. The residuals in the cumulative energy budget are indicated by the difference between the red lines and the horizontal zero line. {Box 13.1, Figure 1}

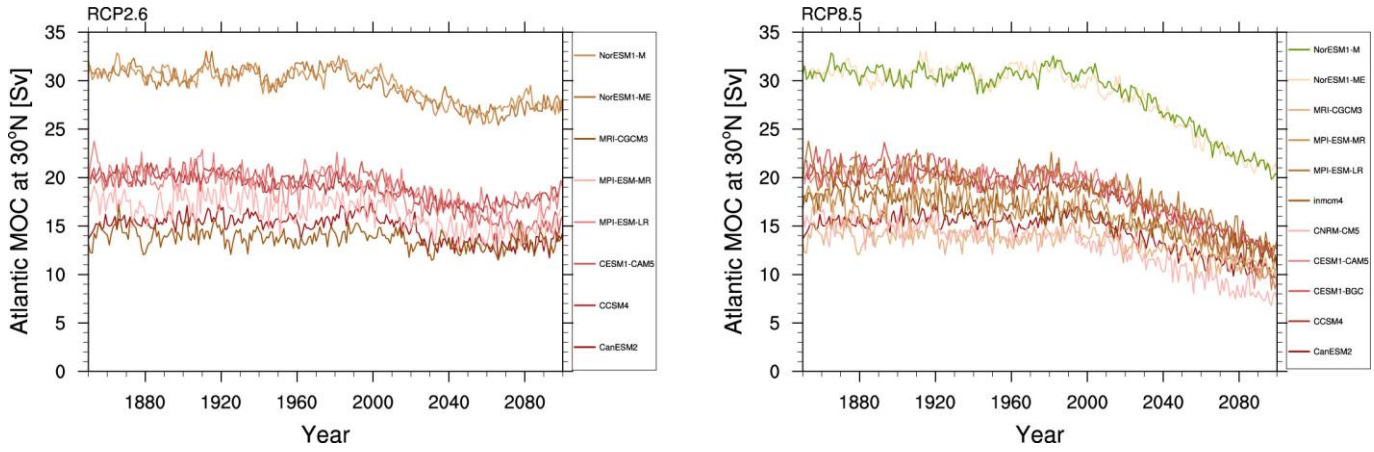

TFE.5, Figure 1: Atlantic Meridional Overturning Circulation strength (Sv) as a function of year, from 1850 CE to 2100 CE as simulated by different OAGCMs in response to scenario RCP2.6 (left) and RCP8.5 (right). {Figure 12.35}

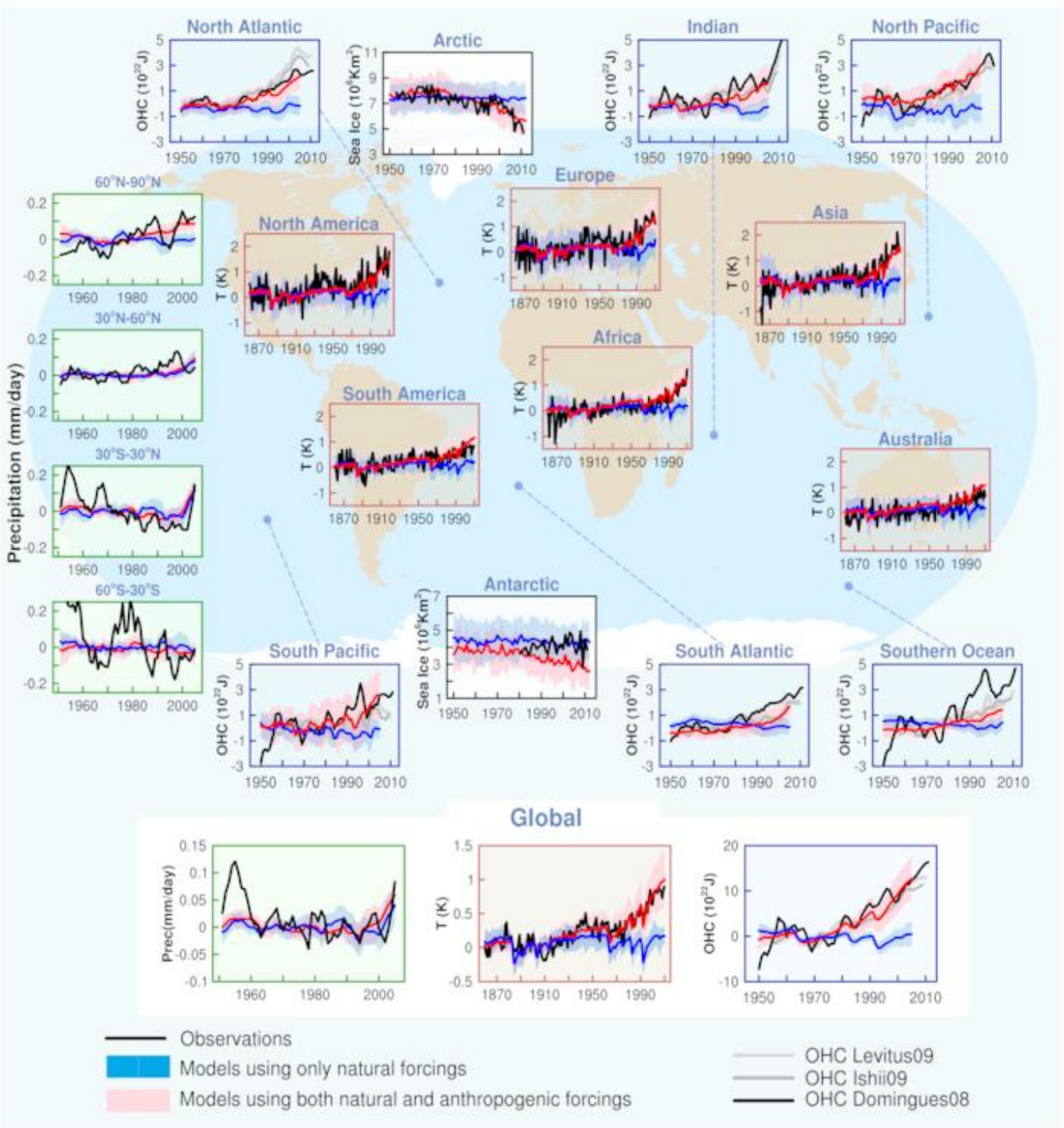

Figure TS.9: Detection and attribution signals in some elements of the climate system. Brown panels are land surface temperature time series, green panels are precipitation time series, blue panels are ocean heat content time series, and white panels are sea-ice time series. On each panel is observations (shown in black or black and shades of grey as in ocean heat content). Blue shading is the model time series for natural forcing simulations and red shading is the natural and anthropogenic forcings. The dark blue and dark red lines are the ensemble means from simulations. For surface temperature the 5 to 95% interval is plotted (and Figure 10.1). The observed surface temperature is from HadCRUT4. For precipitation data the mean and one standard deviation shading of the simulations is plotted. Observed precipitation is from the Global Historical Climatology Network (GHCN). For Ocean Heat Content the mean and one standard deviation shading is plotted for an ensemble of CMIP5 models. Three observed records of OHC are shown. The sea ice extents simulations and observations are the same as in Figure 10.15. More details are in the supplementary materials (Appendix 10.A: Notes and technical details on figures displayed in Chapter 10). {Figure 10.20}

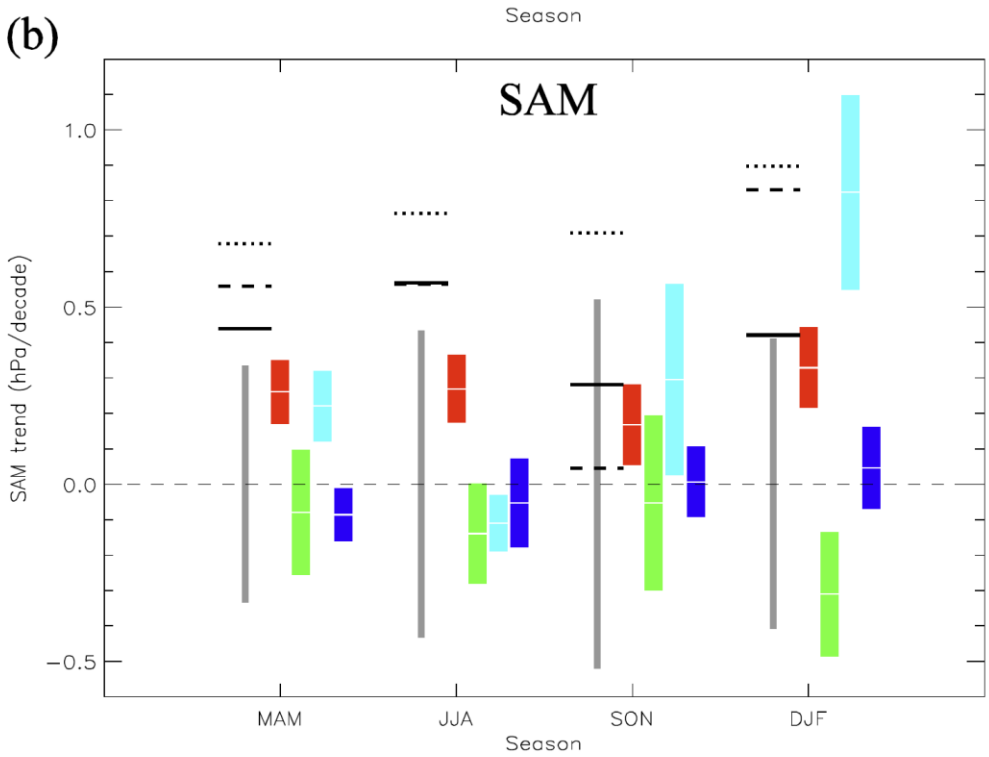

Figure TS.10: Simulated and observed 1951–2011 trends in the Southern Annular Mode (SAM) index (b) by season. The SAM index is a difference between mean SLP at stations located at close to 40°S and stations located close to 65°S. The SAM index is defined without normalization, so that the magnitudes of simulated and observed trends can be compared. Black lines show observed trends from the HadSLP2r dataset (solid), the 20th century Reanalysis (dotted) and the SAM index (dashed). While the synthetic indices have data present from 1951, the SAM index itself begins in 1957. Grey bars show approximate 5th-95th percentile ranges of control trends, and coloured bars show 5–95% significance ranges for ensemble mean trends in response to greenhouse gas (red), aerosols (green), ozone (light blue) and natural (dark blue) forcings, based on CMIP5 individual forcing simulations. {Figure 10.12}

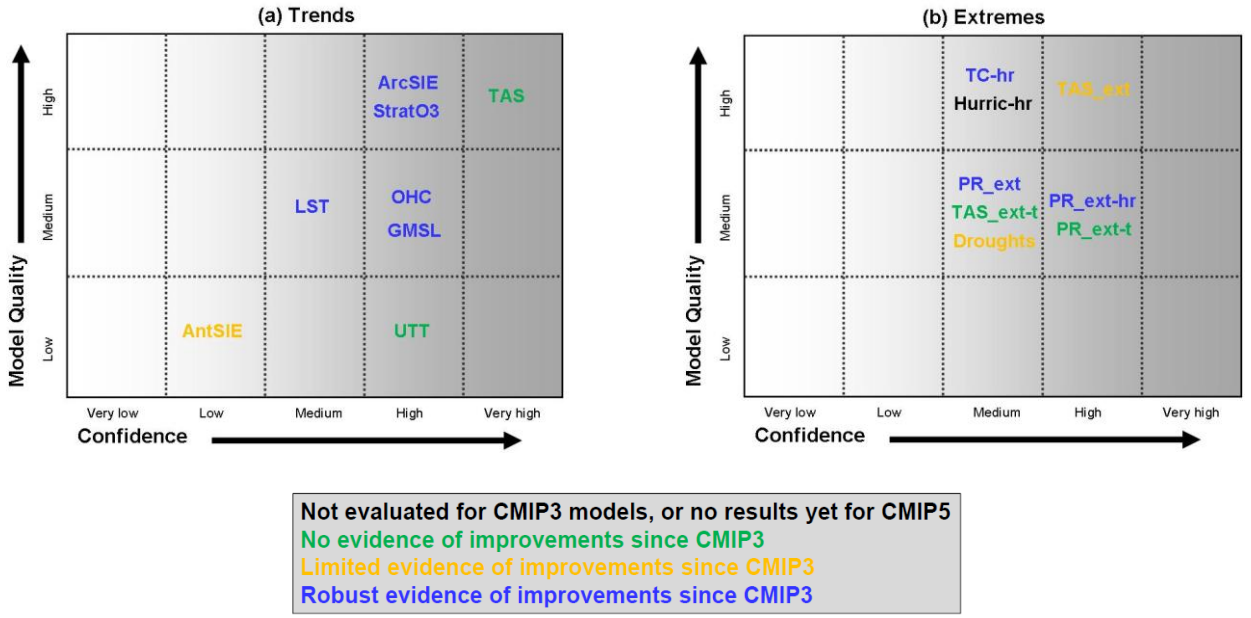

Box TS.2, Figure1: Summary of how well the CMIP5 models simulate important features of the climate of the 20th century. Confidence in the assessment increases towards the right as suggested by the increasing strength of shading. Model quality increases from bottom to top. The color coding indicates improvements from CMIP3 (or models of that generation) to CMIP5 (see Box TS.4). The assessment is mostly based on the multi-model mean, not excluding that deviations for individual models could exist. Note that assessed model quality is simplified for representation in the figure and it is referred to the text for details of each assessment. The figure highlights the following key features, with the sections that back up the assessment added in brackets {Figure 9.45}:

PANEL a (Trends)

AntSIE:	Trend in Antarctic sea ice extent {9.4.3}
ArctSIE:	Trend in Arctic sea ice extent {9.4.3}
GMSL:	Trend in global mean sea level {13.3}
LST:	Lower stratospheric temperature trends {9.4.1.}
OHC:	Global ocean heat content trends {9.4.2}
StratO3:	Total column ozone trends {9.4.1}
TAS:	Surface air temperature trends {9.4.1}
UTT:	Upper-tropospheric temperature trends {9.4.1}

PANEL b (Extremes):

Droughts	Droughts {9.5.4}
Hurric-hr	Year-to-year counts of Atlantic hurricanes in high-resolution AGCMs {9.5.4}
PR_ext	Global distributions of precipitation extremes {9.5.4}
PR_ext-hr	Global distribution of precipitation extremes in high-resolution AGCMs {9.5.4}
PR_ext-t	Global trends in precipitation extremes {9.5.4}
TAS_ext	Global distributions of surface air temperature extremes {9.5.4}
TAS_ext-t	Global trends in surface air temperature extremes {9.5.4}
TC-hr	Tropical cyclone tracks and intensity in high-resolution AGCMs {9.5.4}

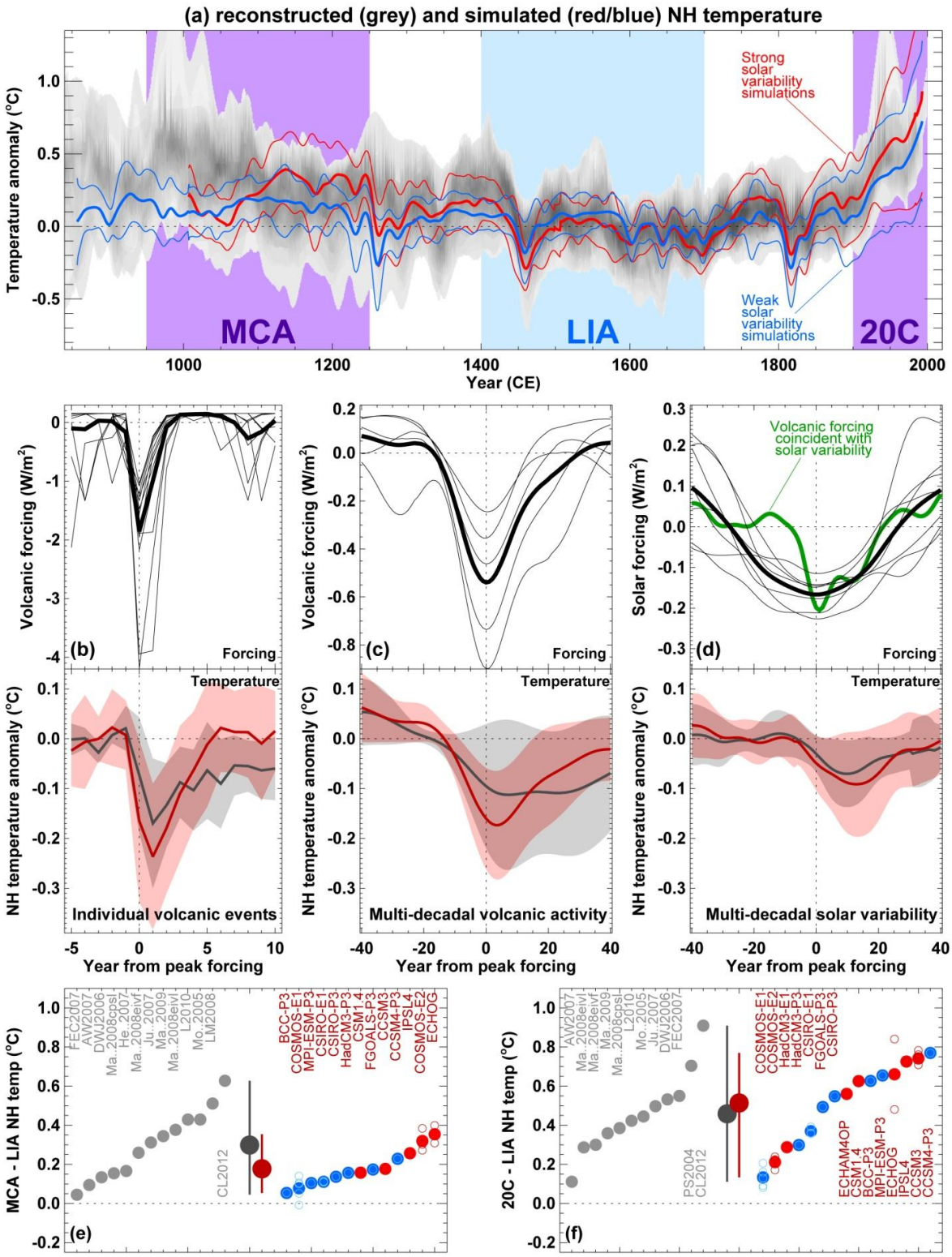

Box TS.3, Figure 1: Comparisons of simulated and reconstructed Northern Hemisphere temperature changes. (a) Changes over the last millennium. (b) Response to individual volcanic events. (c) Response to multi-decadal periods of volcanic activity. (d) Response to multi-decadal variations in solar activity. (e) Mean change from Medieval Climate Anomaly to Little Ice Age. (f) Mean change from 20th century to Little Ice Age. Note that some reconstructions represent a smaller spatial domain than the full Northern Hemisphere or a specific season, while annual temperatures for the full NH mean are shown for the simulations. (a) Simulations shown by coloured lines (thick lines: multi-model-mean; thin lines: multi-model 90% range; red/blue lines: models forced by stronger/weaker solar variability, though other forcings and model sensitivities also differ between the red and blue groups); overlap of reconstructed temperatures shown by grey shading; all data are expressed as anomalies from their 1500–1850 CE mean. {Figure 5.8}

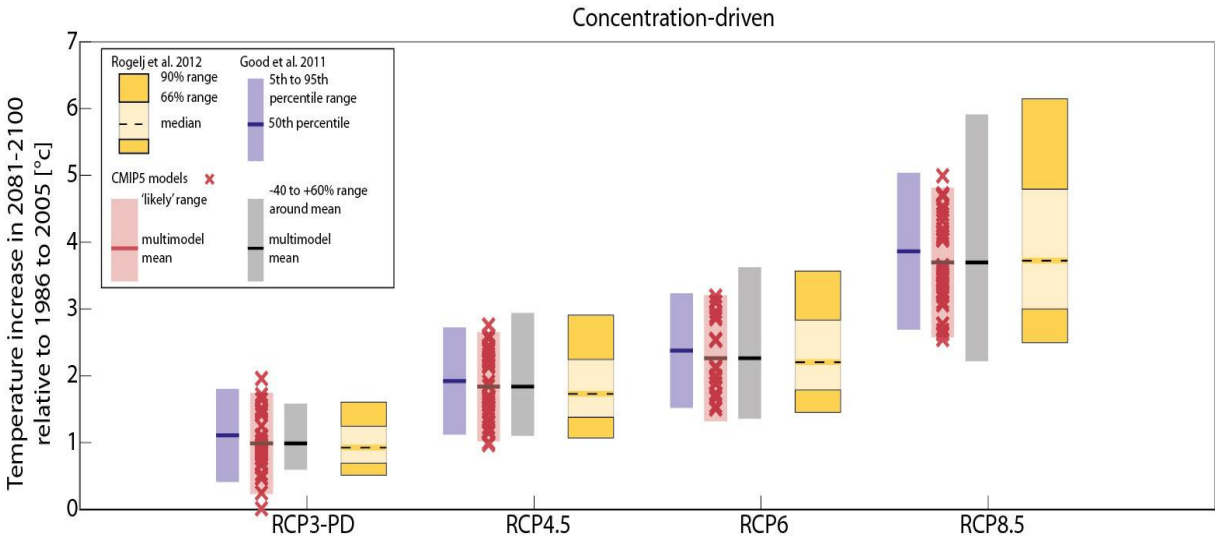

Box TS.4, Figure 1: Uncertainty estimates for global mean temperature change in 2081–2100 with respect to 1986–2005. Red crosses mark projections from individual CMIP5 models. Red bars indicate mean and 5–95% ranges based on CMIP5 (1.64 standard deviations), which are considered as a *likely range*. Blue bars indicate 5–95% ranges from the pulse response emulation of 18 models . Grey bars mark the range from the mean of CMIP5 minus 40% mean to the mean +60%, assessed as *likely* in AR4 for the SRES scenarios. The yellow bars show the median, 33–66% range and 10–90% range. {Figure 12.8}

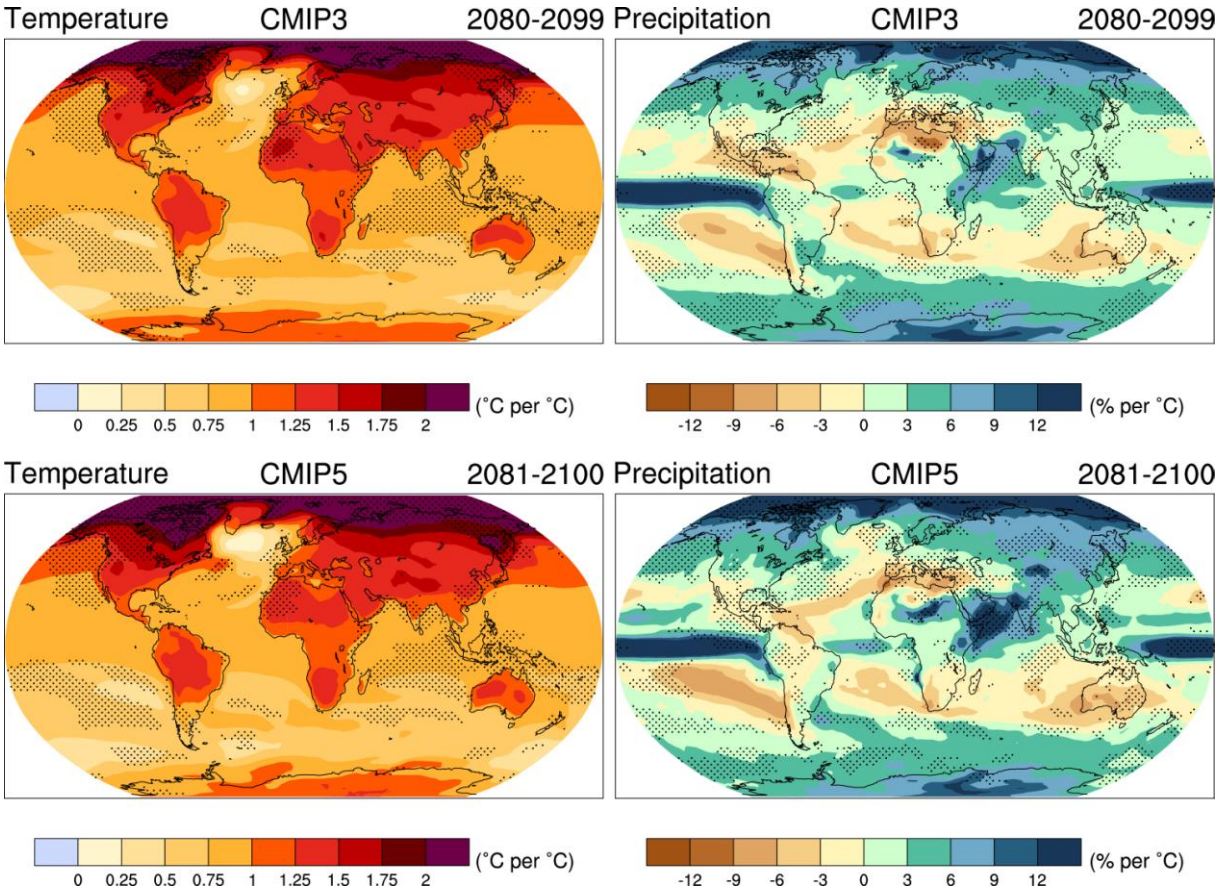

Box TS.4, Figure 2: Patterns of temperature (left column) and percent precipitation change (right column) by the end of the 21st century (2081–2100 vs 1986–2005), for the CMIP3 models average (first row) and CMIP5 models average (second row), scaled by the corresponding global average temperature changes. {Figure 12.41}

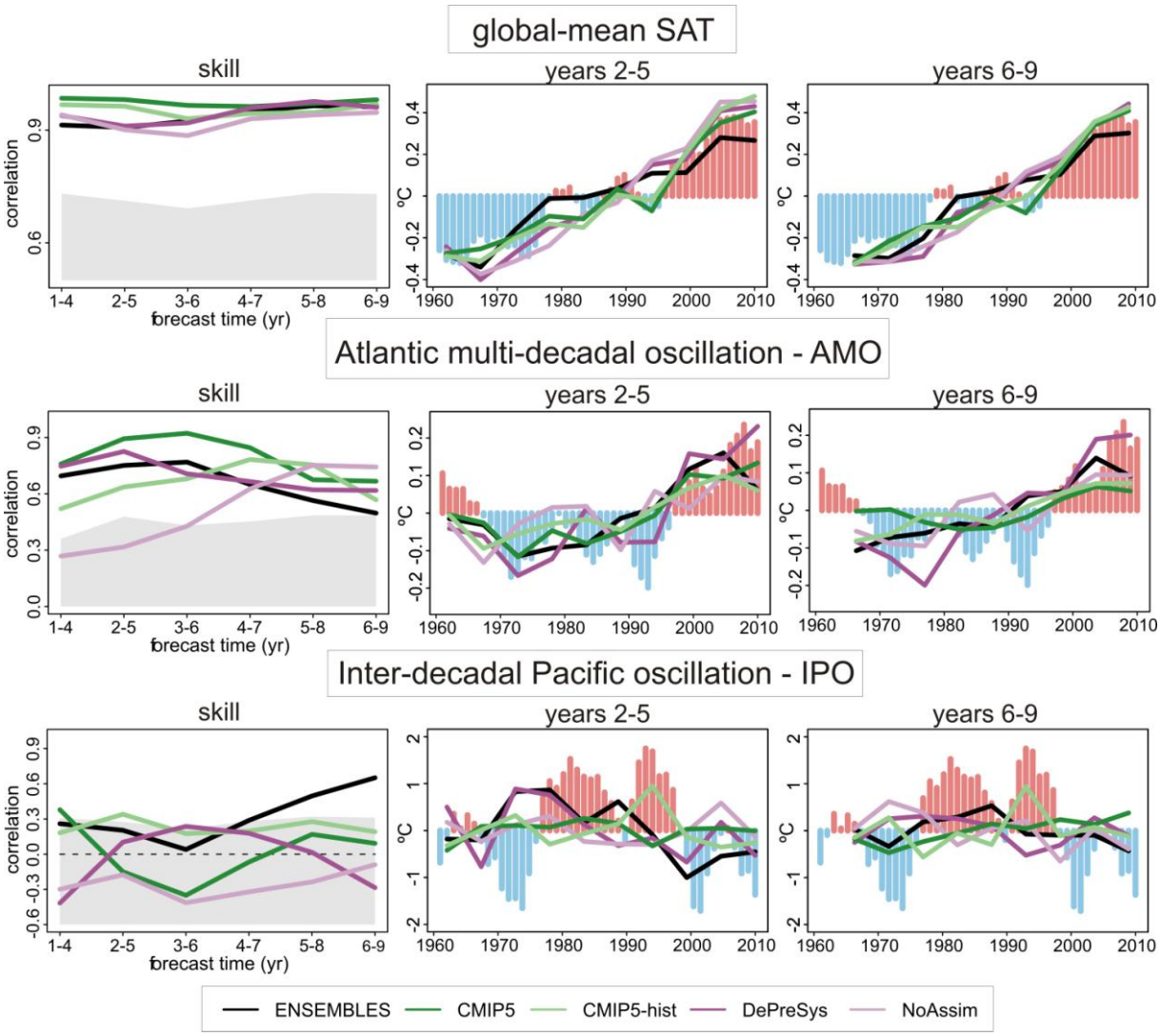

Figure TS.11: Examples of ensemble-mean correlation with the observations (left column) and time series of 2–5 (middle column) and 6–9 (right column) year average predictions of the global-mean temperature (top row), and AMV (bottom row) from the ENSEMBLES (black), CMIP5 Assim (dark green) and NoAssim (light green) and DePreSys Assim (dark purple) and NoAssim (light purple) forecast systems. The AMV index was computed as the SST anomalies averaged over the region Equator-60ºN and 80ºW–0ºW minus the SST anomalies averaged over 60ºS–60ºN. Predictions initialized once every five years over the period 1960–2005 have been used. The CMIP5 multi-model includes experiments from the HadCM3, MIROC5, MIROC4h and MRI-CGCM3 systems. The one-side 95% confidence level is represented in grey, where the number of degrees of freedom has been computed taking into account the autocorrelation of the observational time series. The observational time series, GISS global-mean temperature and ERSST for the AMV and IPO, are represented with red (positive anomalies) and blue (negative anomalies) vertical bars, where a four-year running mean has been applied for consistency with the time averaging of the predictions. {adapted from Figure 11.6}

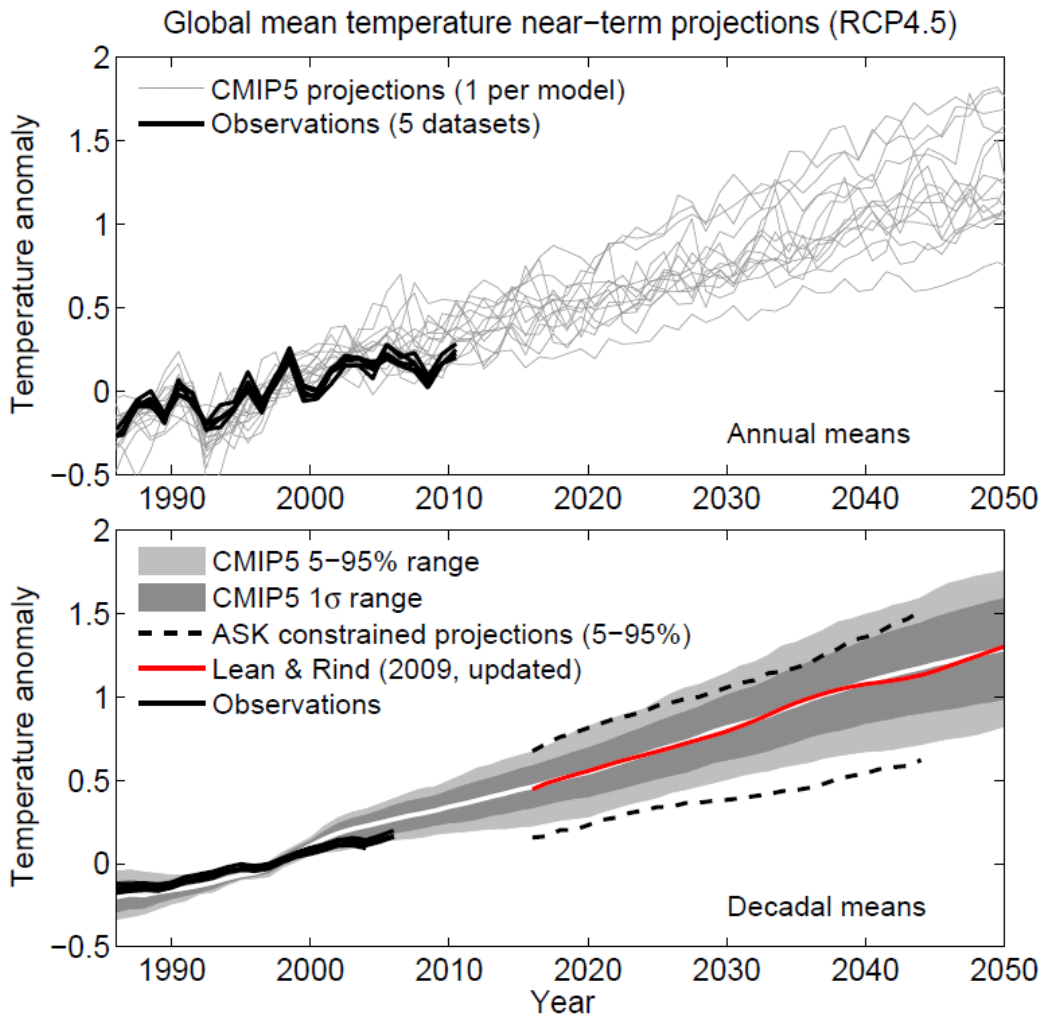

Figure TS.12: a) Projections of global mean, annual mean surface air temperature 1986–2050 (anomalies relative to 1986–2005) under RCP4.5 from CMIP5 models (grey lines, one ensemble member per model), with five observational estimates for the period 1986–2010 (black lines); b) as a) but showing the range (grey shades, with the multi-model mean in white) of decadal mean CMIP5 projections using (where relevant) the ensemble mean from each model, and decadal mean observational estimates (black lines). An estimate of the projected 5–95% range for decadal mean global mean surface air temperature for the period 2016–2040 derived using the ASK methodology applied to simulations with the HadGEM2ES climate model is also shown (dashed black lines). The red line shows a statistical prediction. {Figure 11.33}

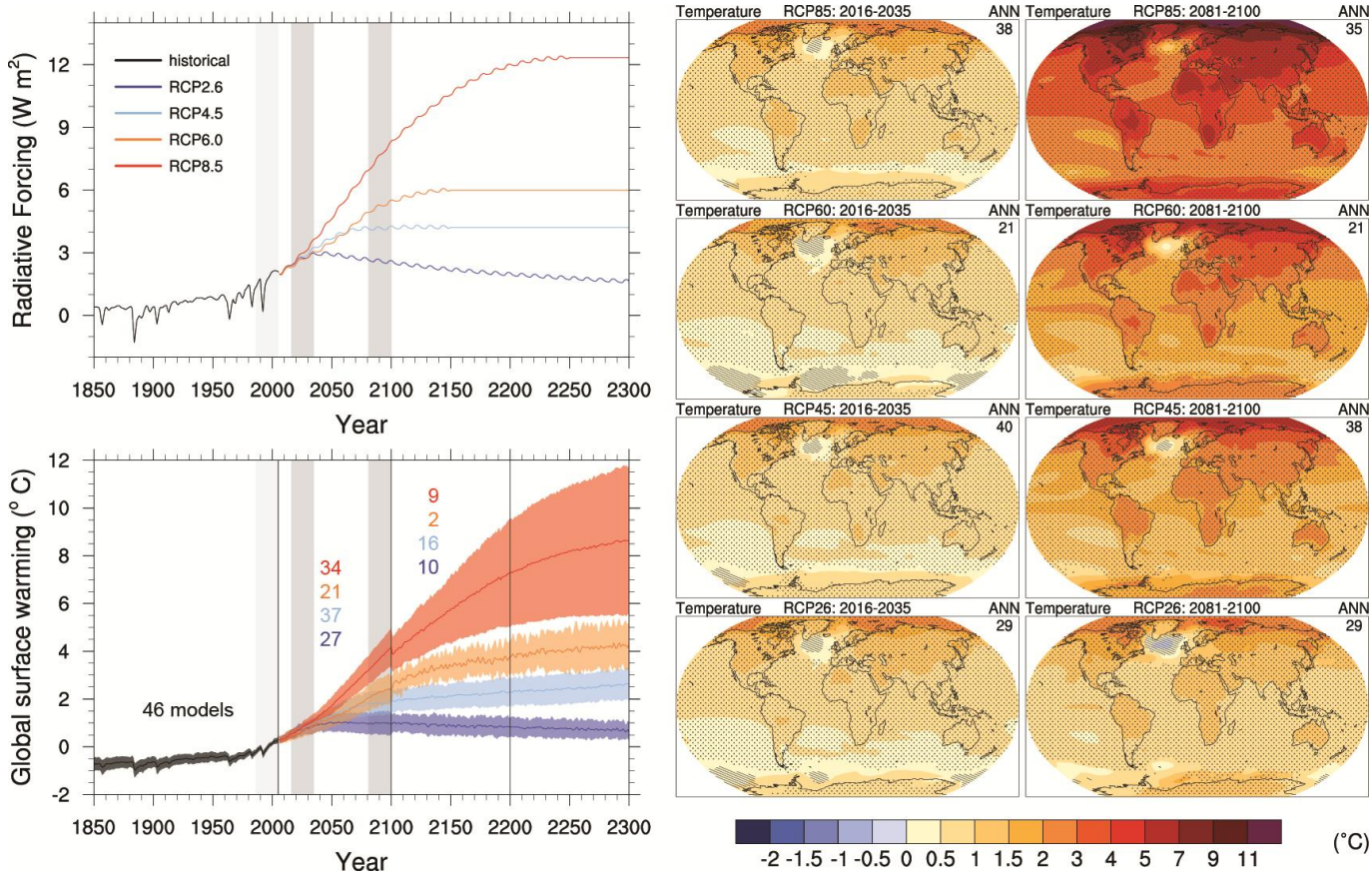

Figure TS.13: Top left: Total global mean radiative forcing for the 4RCP scenarios based on the MAGICC energy balance model (light grey: base period 1986–2005, grey: 2016–2035 and 2081–2100 periods used in maps to the right). Note that the actual forcing simulated by the CMIP5 models differs slightly between models. Global mean near surface temperature change. Bottom left: Time series of global and annual mean surface air temperature anomalies (relative to 1986–2005) from CMIP5 concentration-driven experiments. Projections are shown for each RCP for the multimodel mean (solid lines) and ±1 standard deviation across the distribution of individual models (shading). Discontinuities at 2100 are due to different numbers of models performing the extension runs beyond the 21st century and have no physical meaning. Numbers in the figure indicate the number of different models contributing to the different time periods. Maps: Multimodel ensemble average of annual mean surface air temperature change (compared to 1986–2005 base period) for 2016–2035 and 2081–2100, for RCP2.6, 4.5, 6.0 and 8.5. Hatching indicates regions where the multi model mean is less than one standard deviation of internal variability. Stippling indicates regions where the multi model mean is greater than two standard deviations of internal variability and where 90% of the models agree on the sign of change. {Box 12.1} The number of CMIP5 models used is indicated in the upper right corner of each panel. {adapted from Figure 12.4, Figure 12.5, Annex I}

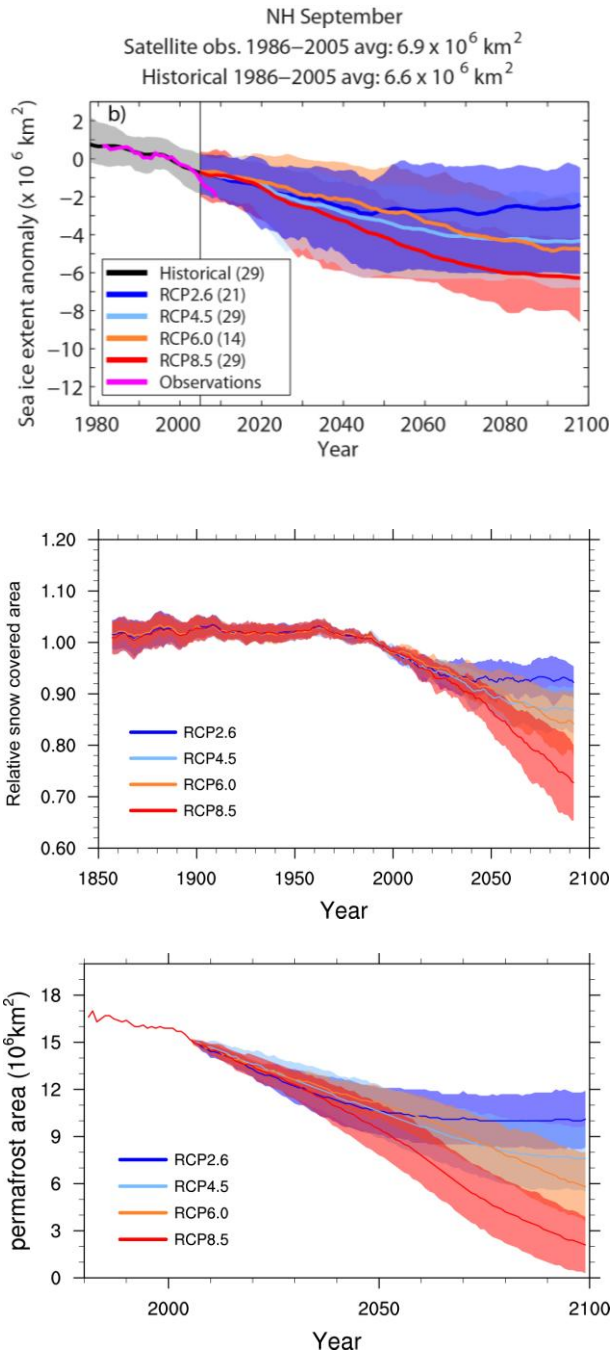

Figure TS.14: Anomalies in sea ice extent (5-year running mean) as simulated by CMIP5 models over the late 20th century and the whole 21st century under RCP2.6, RCP4.5, RCP6.0 and RCP8.5 for Northern Hemisphere September. Northern Hemisphere spring (March to April average) relative snow covered area (RSCA) in the CMIP5 MMD, obtained through dividing the simulated 5-year box smoothed spring snow covered area (SCA) by the simulated average spring SCA of 1986–2005 reference period. Blue: RCP2.6; Light blue: RCP4.5; Orange: RCP6.0; Red: RCP8.5. Thick lines: MMD average. Shading and thin dotted lines indicate the inter-model spread (one standard deviation). Northern hemisphere diagnosed near-surface permafrost area in the CMIP5 MMD and using 20-year average monthly surface air temperatures and snow depths. Blue: RCP2.6; Light blue: RCP4.5; Orange: RCP6.0; Red: RCP8.5. Thick lines: MMD average. Shading and thin lines indicate the inter-model spread (one standard deviation). {Figures 12.28, 12.32, 12.33}

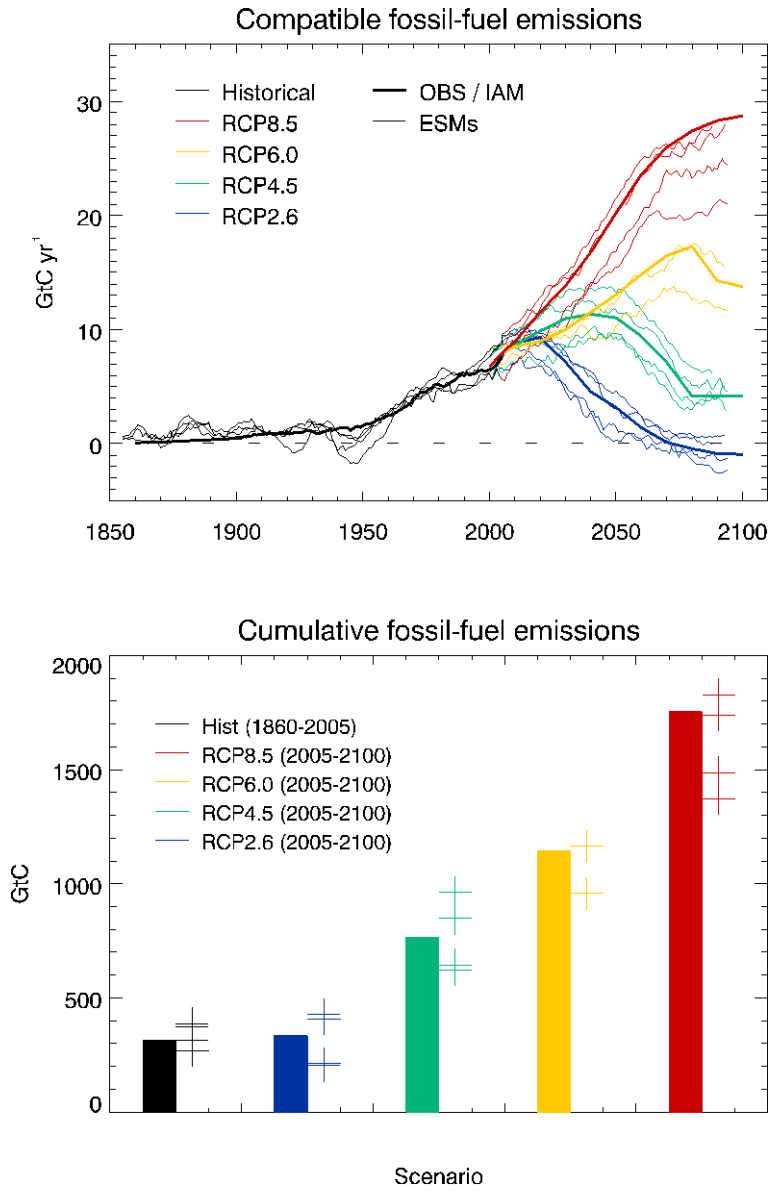

TFE.7, Figure 1: Compatible fossil fuel emissions simulated by the CMIP5 models for the 4 RCP scenarios. Top: timeseries of instantaneous emission rate. Thick lines represent the historical estimates and emissions calculated by the integrated assessment models (IAM) used to define the RCP scenarios, thin lines show results from CMIP5 ESMs. Bottom: cumulative emissions for the historical period (1860–2005) and 21st century (defined in CMIP5 as 2005–2100) for historical estimates and RCP scenarios (bars) and ESMs (symbols). In the CMIP5 model results, total carbon in the land-atmosphere-ocean system can be tracked and changes in this total must equal fossil fuel emissions to the system (see also Table 6.13). Other sources and sinks of CO_2 such as from volcanism, sedimentation or rock weathering, which are very small on centennial timescales, are not considered here. Hence the compatible emissions are given by cumulative-Emissions = $\Delta C_A + \Delta C_L + \Delta C_O$ remission rate = d/dt $[C_A + C_L + C_O]$, where C_A, C_L, C_O are carbon stored in atmosphere, land and ocean respectively. {adapted from Figure 6.25}

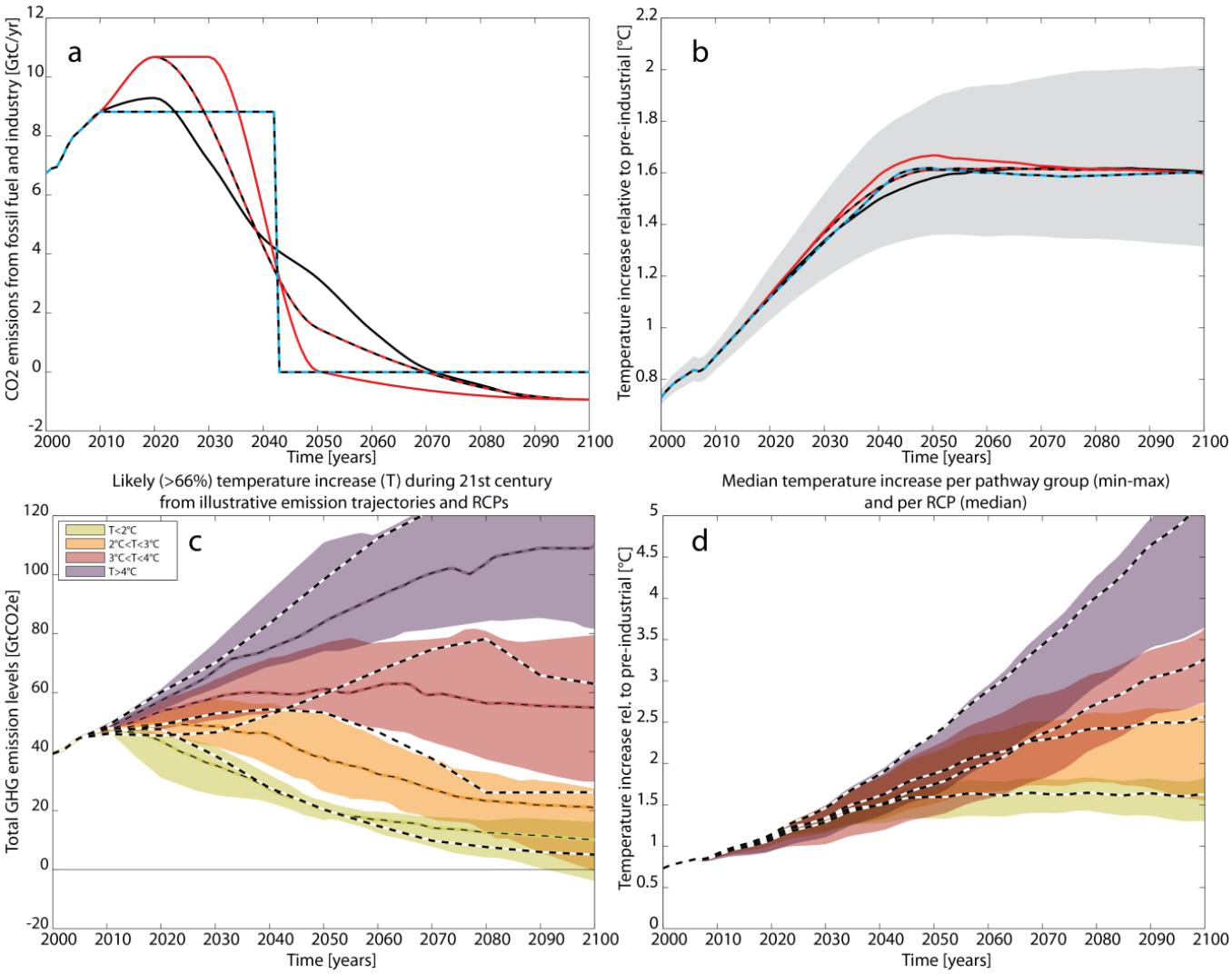

TFE.8, Figure 1: a) CO_2 emissions for the RCP3PD scenario (black) and three illustrative modified emission pathways leading to the same warming, b) global temperature change relative to preindustrial for the pathways shown in panel a. c) Coloured bands show IAM emission pathways over the twenty-first century. The pathways were grouped based on ranges of *likely* avoided temperature increase in the twenty-first century. Pathways in the yellow, orange and red bands *likely* stay below 2°C, 3°C, 4°C by 2100, respectively, while those in the purple band are higher than that. Emission corridors were defined by, at each year, identifying the 20th to 80th percentile range of emissions and drawing the corresponding coloured bands across the range. Individual scenarios that follow the upper edge of the bands early on tend to follow the lower edge of the band later on, d) global temperature relative to preindustrial for the pathways in panel a. {Figure 12.47}

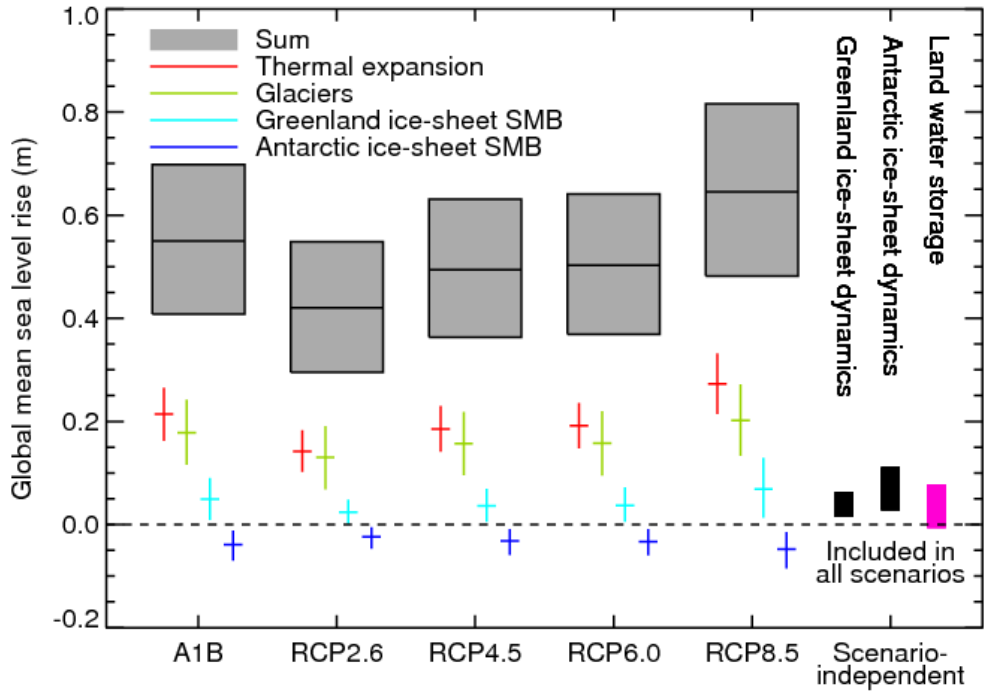

Figure TS.15: Projections from process-based models with *likely* ranges and median values for global-mean sea-level rise and its contributions in 2081–2100 relative to 1986–2005 for the four RCP scenarios and scenario SRES A1B used in the AR4. Contributions from ice-sheet dynamical change and anthropogenic land water storage are included in the sum; they are independent of scenario, and are treated as having uniform probability distributions. See discussion in Sections 13.5.1.1 and 13.5.1.3 and Appendix 13.A for methods. {Figure 13.8}

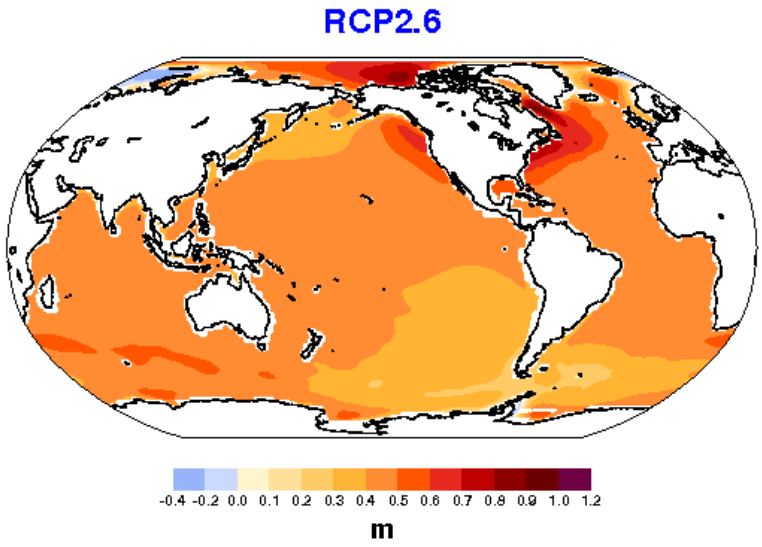

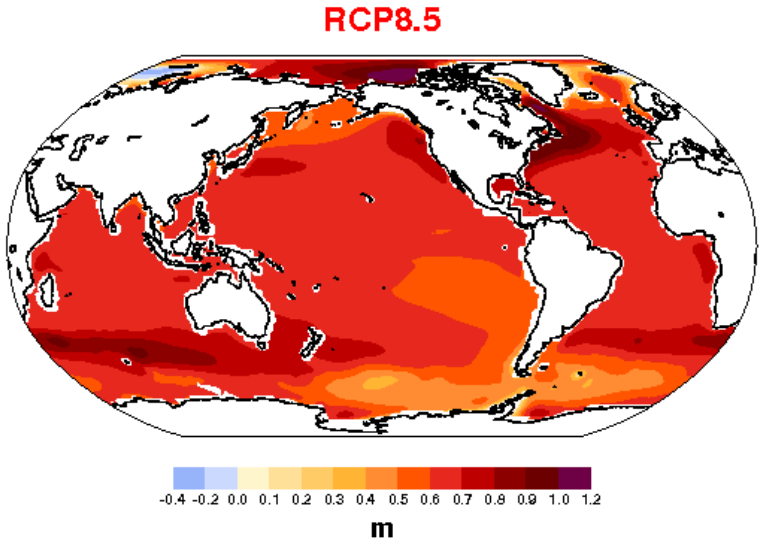

Figure TS.16: Ensemble mean regional sea-level change (m) evaluated from CMIP5 models for scenarios RCP2.6 and RCP8.5 between 1986–2005 and 2081–2100. [PLACEHOLDER FOR FINAL DRAFT: this figure is derived by related methods to those used for Figure 13.15a, but is not entirely consistent; this will be resolved in the final draft.]

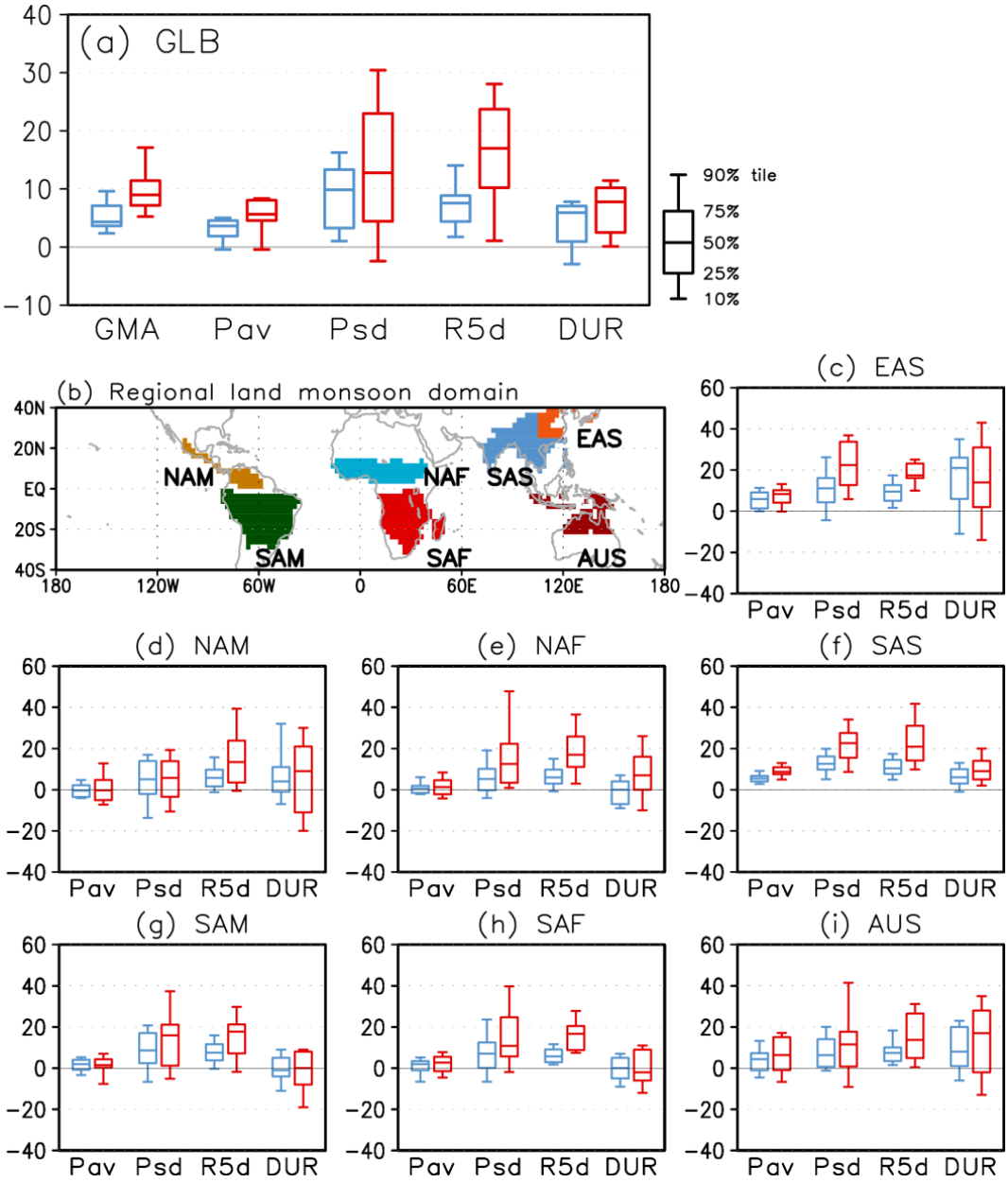

Figure TS.17: (a) Future change in global monsoon statistics between the present-day (1986–2005) and the future (2080–2099) based on 21 CMIP5 models: area (GMA), seasonal average precipitation (Pav), standard deviation of inter-annual variability in seasonal precipitation (Psd), seasonal maximum 5-day precipitation total (R5d), and monsoon season duration (DUR). Units are % for GMA, Pav, Psd and R5d, and days for DUR. (b) Regional land monsoon domain determined by multi-model mean precipitation in the present-day. (c)-(i) Future change in regional land monsoon statistics: (c) East Asia (EAS), (d) North America (NAM), (e) North Africa (NAF), (f) South Asia (SAS), (g) South America (SAM), (h) South Africa (SAF), and (i) Australia (AUS). Box-whisker plots in blue (red) color are for the RCP4.5 (RCP8.5) scenario. The 10th, 25th, 50th, 75th, and 90th percentiles refer to 3th, 6th, 11th, 16th, and 19th values in ascending order among the 21 models, respectively. All the indices are calculated for the summer season (May-September (MJJAS) for the Northern Hemisphere (NH), November-March (NDJFM) for the Southern Hemisphere (SH) over monsoon domains which are determined in each model and each scenario. The monsoon domains are defined where the annual range of precipitation (difference between MJJAS and NDJFM means) exceeds 2.5 mm per day. {adapted from Figure 14.4}

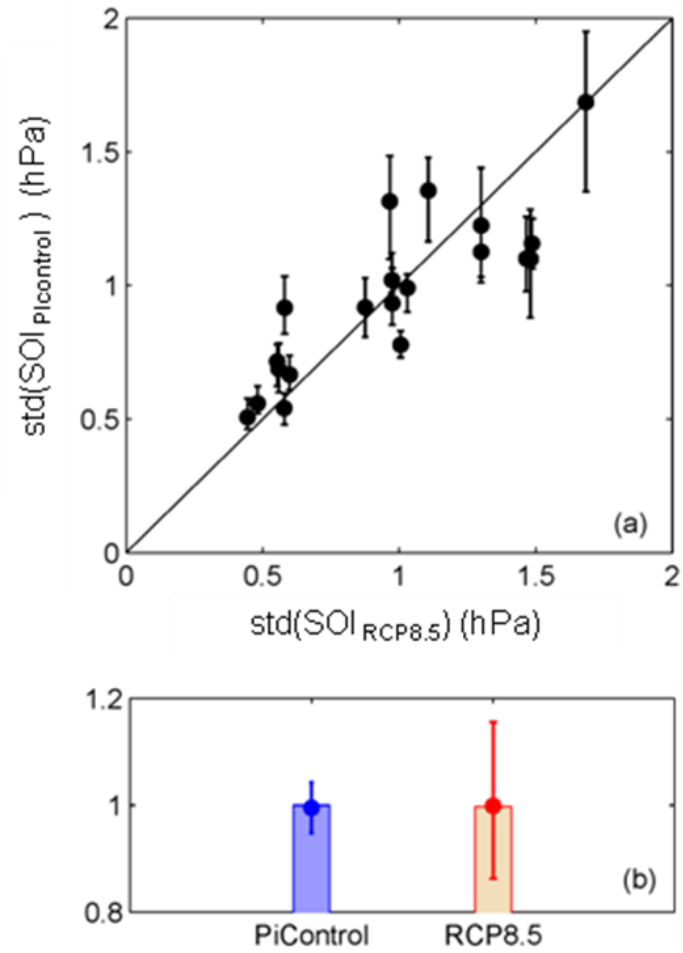

Figure TS.18: Comparison of Southern Oscillation index (SOI) standard deviation between the pre-industrial (PiControl) run and RCP8.5 projection (2050–2099). (a) Scatter plot (Unit: hPa) in 20 CMIP5 models. The error bars denote the 95th and 5th percentiles in 50-year windows of PiControl. (b) Ensemble mean standard deviation of SOI in PiControl (blue bar) and RCP8.5 (red), normalized by PiControl value in each model. The dot and error bars denote the 50th, 75th and 25th percentiles in 50-year windows for PiControl, and for inter-model variability for RCP8.5.

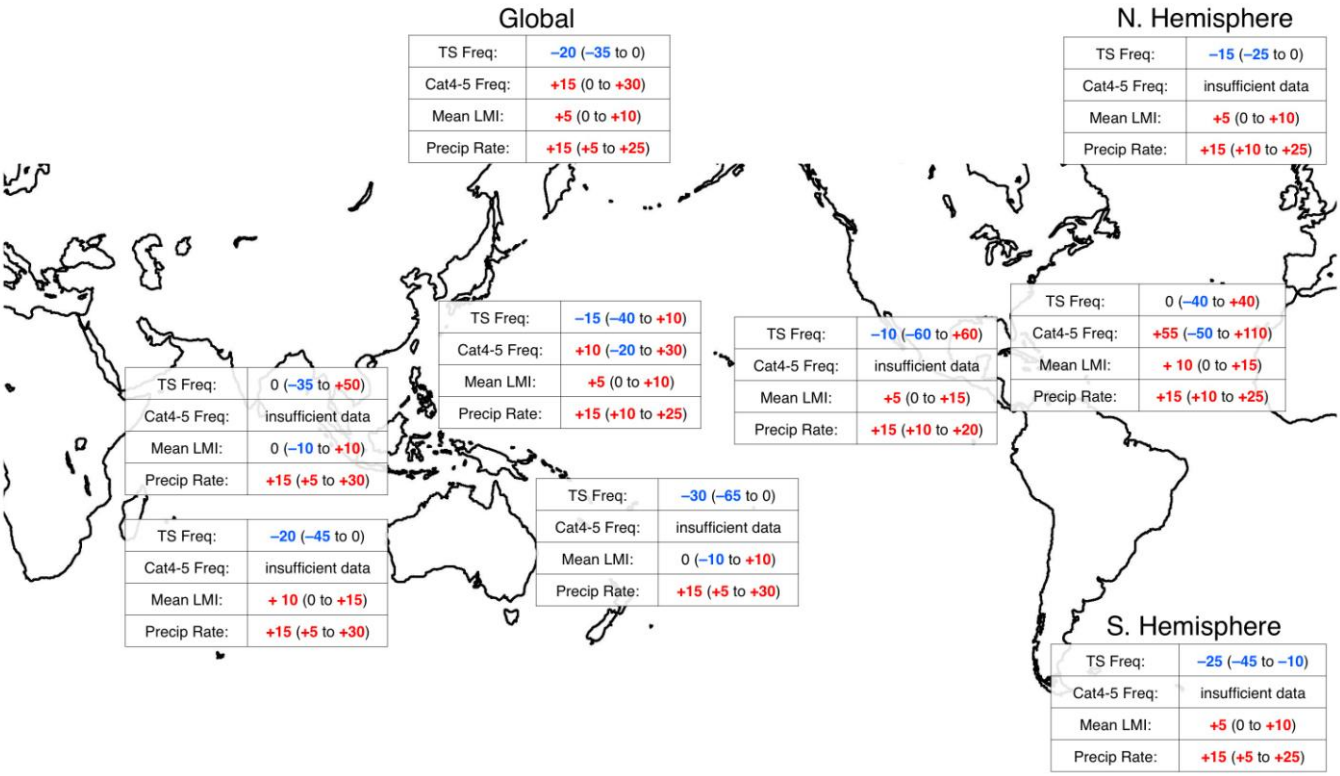

Figure TS.19: Tropical Cyclone Characteristics: General consensus assessment of the numerical experiments described in Box 14.2, Tables 1–4. All values represent expected percent change (year 2100 relative to 2000) under an A1B-like scenario, based on expert judgment after subjective normalization of the model projections. Four metrics were considered: the percent change in 1) the total annual frequency of tropical storms, 2) the annual frequency of Category 4 and 5 storms, 3) the mean Lifetime Maximum Intensity (LMI; the maximum intensity achieved during a storm's lifetime), and 4) the precipitation rate within 200 km of storm center at the time of LMI. For each metric, the first numeric value is the best guess of the expected percent change, and the range in parentheses is the 67% (*likely*) confidence interval for this value. Nine regions were considered: Global, Northern Hemisphere, Southern Hemisphere, Eastern North Pacific, North Atlantic, Northern Indian, Southern Indian, Western North Pacific, and South Pacific. {Box 14.2, Figure 1}

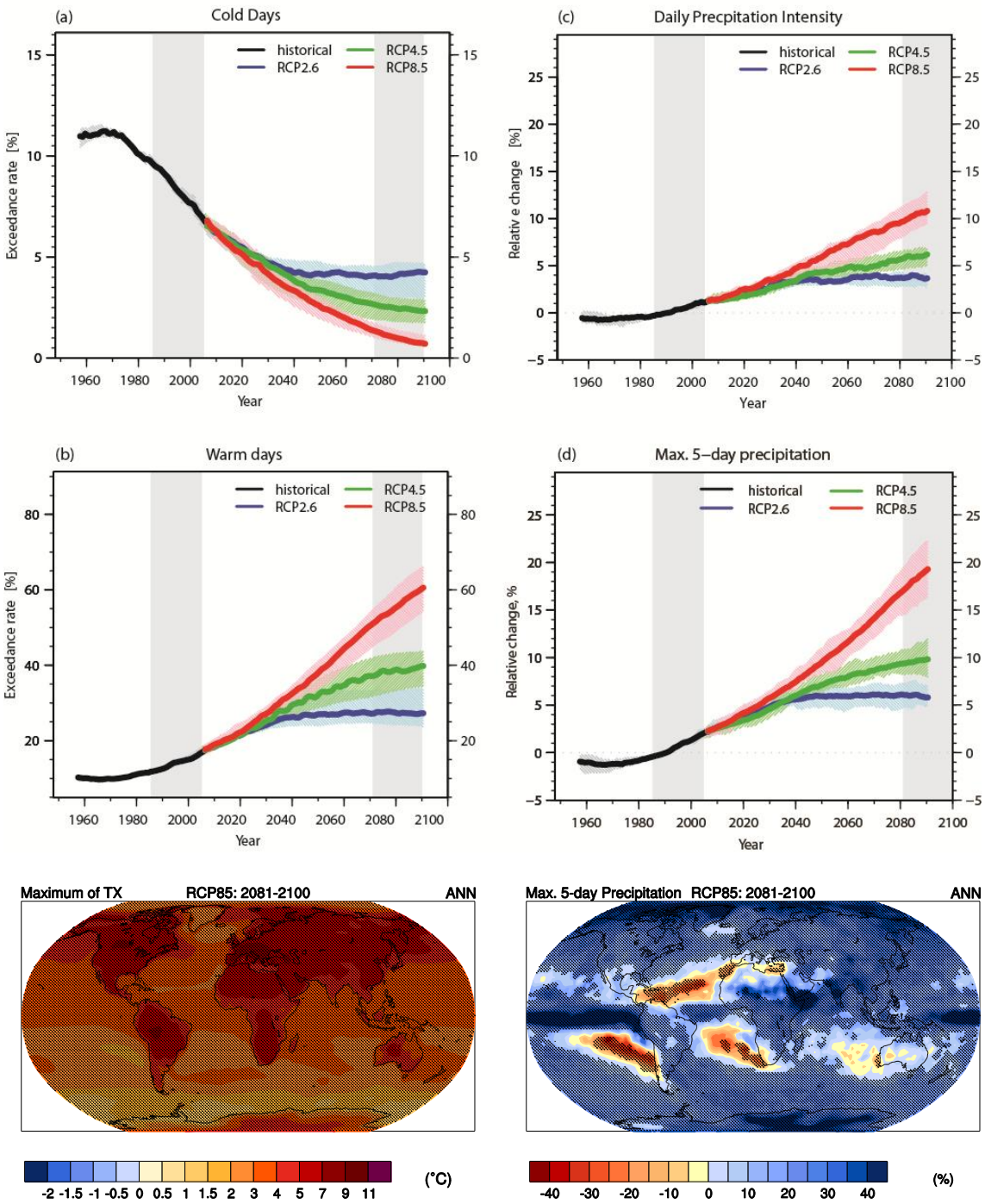

TFE.9, Figure 1: Maps indicate the CMIP5 multi-model ensemble of (a) annual maximum of maximum daily temperature and (c) annual maximum five-day precipitation accumulation as percent change over the 2081–2100 period relative to 1986–2005 in the RCP8.5 experiments. Timeseries plots show global mean projections for the occurrence of (b) annual maximum of maximum daily temperature (c) precipitation intensity, and (d) annual maximum five-day precipitation accumulation from CMIP5 for the RCP2.6, RCP4.5 and RCP8.5 scenarios relative to 1986–2005. Panel (a) shows percentage of cold days (tx10p: Tmax below the 10th percentile), panel (b) shows percentage of warm days (tx90p: Tmax exceeds the 90th percentile), panel (c) shows relative change of simple precipitation intensity (sdii: average daily wet-day precipitation amount) and panel (d) shows relative changes of annual maximum consecutive 5-day precipitation amounts. Map (left hand side) show the CMIP5 multi-model median change in 20-year return values of annual warm temperature extremes as simulated by CMIP5 models in 2081–2100 relative to 1986–2005 in the RCP8.5 experiments; and map (right hand side) indicates CMIP5 multi-model ensemble R5dmax, the annual maximum five-day precipitation accumulation as percent change over the 2081–2100 period relative to 1986–2005 in the RCP8.5 experiments. {Figure 12.26, 12.13}